

Design optimization of two-way spanning concrete systems for low-carbon, context-informed construction

by

Ashley J. Hartwell

B.S. Mechanical Engineering
Stanford University, 2016

S.M. in Mechanical Engineering
Massachusetts Institute of Technology, 2018

Submitted to the Department of Mechanical Engineering
in Partial Fulfillment of the Requirements for the Degree of
Doctor of Philosophy in Mechanical Engineering
at the

Massachusetts Institute of Technology
June 2023

© 2023 Ashley Hartwell. All rights reserved.

The author hereby grants to MIT a nonexclusive, worldwide, irrevocable, royalty-free license to exercise any and all rights under copyright, including to reproduce, preserve, distribute and publicly display copies of the thesis, or release the thesis under an open-access license.

Signature of Author:

Department of Mechanical Engineering
May 9, 2023

Certified by:

Caitlin T. Mueller
Associate Professor of Architecture and Civil and Environmental Engineering
Thesis Supervisor

Accepted by:

Nicolas G. Hadjiconstantinou
Professor of Mechanical Engineering
Graduate Officer

Dissertation Committee

Caitlin T. Mueller, PhD

Associate Professor of Architecture
Associate Professor of Civil and Environmental Engineering
Massachusetts Institute of Technology
Thesis Supervisor

Leon Glicksman, PhD

Professor of Building Technology and Mechanical Engineering
Massachusetts Institute of Technology
Thesis Committee Chair

Maria Yang, PhD

Gail E. Kendall (1978) Professor of Mechanical Engineering
Massachusetts Institute of Technology
Thesis Reader

Design optimization of two-way spanning concrete systems for low-carbon, context-informed construction

by
Ashley Hartwell

Submitted to the Department of Mechanical Engineering
on May 12, 2023, in Partial Fulfillment of the
Requirements for the Degree of

Doctor of Philosophy in Mechanical Engineering

Abstract

The built environment is one key sector that can be readily targeted for sustainable design intervention as it accounts for approximately 40% of global CO₂ emissions. Within these emissions, embodied carbon of construction materials is substantial. Two broad strategies to reduce embodied carbon are materials substitution and geometric optimization. This dissertation focuses on the latter, presenting strategies to reduce embodied carbon in floors systems that are generally characterized by inefficiently shaped sections, typically designed with little consideration for carbon impacts, and optimized for conditions that favor western construction economics.

This dissertation addresses these challenges in several ways. The first is by employing structural analysis and design space exploration techniques to rapidly locate feasible concrete slab designs for flat and waffle typologies solutions that outperform code-prescribed rules of thumb with respect to carbon, mass and material cost. Second, this work integrates first-principle structural engineering and building physics knowledge into multi-objective optimization workflows to formalize the study of filler slabs, a lost formwork two-way spanning concrete typology with the potential to reduce both the embodied carbon and energy use of a building. Finally, this work considers context-informed fabrication of waffle and filler slabs, evaluating the tradeoffs between mass customization and manufacturability in waffle and filler slab systems with emerging and scalable digital fabrication techniques for concrete construction.

Research outcomes of thesis include generalized knowledge about how to achieve carbon efficiency in two-way spanning floor systems and a demonstration of how computational tools can be leveraged to discover high performing design typologies. Results indicate that with accessible changes in construction practices and utilization of computation, savings as large as 35% of embodied carbon for a residential building of average span can be achieved with minimal additional capital expenditure and optimally designed typologies.

Thesis Supervisor: Caitlin T. Mueller

Title: Associate Professor of Architecture and Civil and Environmental Engineering

Acknowledgements

This dissertation, the research enclosed, and the completion of my journey here at MIT would not be possible without a robust community of support and nurturing during the nearly 7 years I've spent here at MIT. I want to thank first and foremost my Ph.D advisor, Professor Caitlin Mueller. To simply say that Caitlin completely changed my trajectory when I joined her group 4 years ago would be an understatement. She has encouraged me during periods of frustration, shown me the value in meticulous and detail-oriented approaches, and inspires me daily with the passion and expertise she has not just for architectural design and computational engineering, but also for education and mentorship. I hope to continue to grow into the type of researcher she's proven to me can exist.

I am also grateful for members of my thesis committee Professor Leon Glicksman and Professor Maria Yang. Your questions have helped me stretch my imagination about the impact my work could have, and your guidance, especially our conversations about larger career trajectories, have been filled with nuggets of wisdom I'll carry with me beyond this time at MIT. You have truly shown me the utility of a variety of approaches in tackling a huge problem, such as climate change and physics-informed design. I also want to thank the Building Technology faculty that I've been able to interact with both in the classroom and informally, Professors Christoph Reinhart, John Ochsendorf, and Les Norford.

During my time at MIT, I was fortunate enough to have MANY informal advisors ranging from faculty, technical instructors, and members of the broader MIT community. They include Mechanical Engineering instructors who I have taught with and have helped me build a toolkit on how to effectively engage students in the classroom, how to be a member of a vibrant academic community, and effectively improve said community for the better such as Dr. Dawn Wendell and Dr. Benita Comeau. This group of mentors also includes Professor Leslie Kolodziejwski, who has been a constant ray of support and understanding. I'm so appreciative for the work she and many others (Gloria Anglón, Zoe Lemon) have done in building our community of UCEM scholars, which was the first interdepartmental community I had of graduate scholars of color here at MIT. My time as a UCEM scholar has been pivotal in my professional and personal development and has made MIT a much less lonely place.

I have had the great privilege to collaborate directly with many experts in the world of concrete, computational design and digital fabrication who have made the work in this dissertation and other publications possible during my time as a graduate student including Professor Mohamed Ismail, Eduardo Gascón Alvarez, Alexander Curth, Jonathan Broyles and Professor Nathan Brown. More broadly, I would like to thank other members my research group including Dr. Paul Mayencourt, Dr. Renaud Danhaive, Dr. Yijiang Huang, Eamon Whalen, Bryan Ong, Eduardo Gascón Alvarez, Kiley Feickert, Alexander Curth, Keith Lee, Demi Fang, Ramon Weber, Sarah Mokhtar, Leilah Sory, Lauren Moore, and Jaya Manideep Rebbagondla. My lab mates possess admirable work ethic, deep enthusiasm and domain knowledge, and incredible kindness. I have been so lucky to have them be a part of my intellectual journey. In the broader community BT and architectural community, I'd like to thank Juliana Berglund-Brown and Nada Tarkhan, for their insightful discussions and feedback.

I have many friends who have helped cheer for my successes small and large, have given me care during the disappointments that are so common to this period personally and professionally. I'd like to thank Karlia Brown, Leia Brown and Ida Kassa, my oldest friends from childhood who have always made me feel incredibly special, understood, and loved. I'd like to thank my Boston and Cambridge friends who in addition to being amazing scientists, have encouraged me to be more courageous and open-minded including Candace Ross, Alex Berry, Beck Holden, Lindsey Backman, Sheena Vasquez, and Chad Sauvola. In addition, I want to thank Isabel Crystal, Shayna Hilburg, Kendall Fawcett, Dara Cuffe, Corinna MacIsaac, Alex Rigobon, for all the laughter and joy you've brought to me over shared meals, TV nights, trivia and a variety of outdoor activities.

From my Stanford community that has continued beyond undergrad, I want to thank you for the familiarity in this transitional period of life. Specifically, I'd like to thank Shelby Sinclair, my assigned "big sib" who has grown into one of my best friends and has been hugely instrumental in my personal growth. I also am so appreciative of my SSEA friends who have given me a family and lent me theirs when I couldn't be physically close to my own, Nicole Crawford, Ariel Reid and Jotthe Kannappan. As the four of you may remember there was a pretty significant consequence for not getting a Ph.D after participating in SSEA, so I decided to take one for the team 😊. Last, but not least, I'd like to thank my sorority sisters who ended up here in Boston and the east coast such as Khiana Lowe and Ufuoma Oveinmhada. Your support has been unconditional and I'm so happy our friendship has persisted.

To my parents, Mom, Dad and Mama Rose, thank you for the love you've always bestowed on me, for your belief that accomplishing this Ph.D. and dissertation work was possible even when I didn't, thank you for the company you've provided on the phone while walking home from lab at various hours in the day, and the sounding board you've provided for all issues big and small. I'm so proud to be your daughter. To my sister, Anne and brother-in-law Gregory, thank you for the perspective and the love that has come.

Finally, I'd like to thank sources of funding that has made this work as well as a variety of professional endeavors possible during my time as a Ph.D. student including the Dar Group Urban Seed Fund, Norman B. Leventhal Center for Advanced Urbanism (LCAU), The Martin Family Fellowship and The Alfred P. Sloan Foundation.

Table of Contents

1. Introduction.....	19
1.1 Motivation	19
1.2 Environmental impact metrics for structural design	20
1.3 Concrete: An omni-present structural material	21
1.3.1 History of concrete use and prevalence in modern construction	21
1.3.2 Structural behavior of reinforced concrete	22
1.4 Thesis foundation and scope	23
1.5 Organization of dissertation	23
2. Literature Review	25
2.1 Towards computational and non-serialized design processes in architecture and structural engineering.....	25
2.1.1 Separation of architecture and structural engineering disciplines	25
2.1.2 Enabling creativity in computational structural design	26
2.1.3 Parametric design and structural optimization.....	27
2.1.4 Critiques and reframing of computational design processes	28
2.2 Materially efficient concrete spanning systems	29
2.2.1 Shells and Plates	29
2.2.2 Ribbed slabs and non-rectangular cross section systems.....	33
2.3 Lost formwork construction.....	36
2.4 Filler slabs	37
2.5 Materially and global context-informed fabrication	38
3. Data-driven design of standard two-way concrete systems	41
3.1 Background and state of the art.....	42
3.1.1 Two-way flat slabs and waffle slab analysis methods	42
3.1.2 Critique of rule of thumb approaches in architectural and structural engineering .	43
3.1.3 Parametric design of flat concrete slabs and waffle slabs.....	44
3.2 Methods for design parameterization, analysis, and data collection.....	45
3.2.1 Parametric model definition and design space sampling.....	46
3.2.2 Slab design performance metrics and evaluations	48
3.2.3 Moment analysis with the Direct Design Method (DDM)	49

3.2.4	Reinforcing steel calculations and ductility constraints.....	49
3.2.5	Shear design of two-way concrete slabs and preliminary column sizing	50
3.2.6	Serviceability and prescribed minimum depth	51
3.2.7	Moment of inertia and section properties	52
3.2.8	Deflection of a rectangular panel and maximum possible deflection.....	54
3.2.9	Post-processing of data for feasibility: direct and indirect constrain application...	54
3.3	Results	55
3.3.1	Flat square concrete slab studies.....	55
3.3.2	Design solution space for flat and waffle slab typologies	57
3.3.3	Performance evaluation based on a programmatic need and slab typology	58
3.3.4	Potential impact of policy and carbon intervention strategies	60
3.4	Conclusions	64
3.4.1	Future work and remarks	64
3.4.2	Summary of intellectual contributions.....	64
4.	Multi-objective optimization of thermally and materially efficient filler slabs	65
4.1	Background	66
4.1.1	Filler slabs in context	66
4.1.2	Agricultural waste as formwork.....	66
4.1.3	Building performance metrics for filler slabs	67
4.2	Methodology	67
4.2.1	Material analysis	68
4.2.2	Structural design and validation.....	71
4.2.3	Thermal design, validation, and structure-property relationships	73
4.2.4	Computational integration and filler module parameterization	78
4.3	Results	81
4.3.1	Span and filler material variation.....	81
4.3.2	Filler module number variation	84
4.3.3	Uniform versus non-uniform module sizes.....	84
4.4	Scaled prototype of filler slab with agricultural formwork.....	85
4.5	Discussion	86
4.6	Conclusions	87
4.6.1	Future work and remarks	87
4.6.2	Summary of intellectual contributions.....	87
5.	Parametric customization of waffle and filler slab systems	89

5.1	Background and state of the art.....	90
5.1.1	The intention of structural logic in architecture.....	90
5.1.2	Mechanics of reinforced concrete section.....	93
5.1.3	Shape optimization and customization in waffle spanning structures	95
5.2	Methodology	96
5.2.1	Parameterization of waffle slab typology	96
5.2.2	Hybrid structural modeling and analysis	97
5.2.3	Grid sampling and local optimization.....	98
5.2.4	Case study: Roof for a 3D printed utility shed	99
5.2.5	Additively manufactured formwork for filler slab customization	99
5.3	Results	100
5.3.1	Structural demand forecasting highlights problems suited for customization.....	100
5.3.2	Design of size customized waffle slab roof improves utilization.	101
5.3.3	Structural efficiency is limited by geometric and manufacturing constraints.	103
5.3.4	A prototype of a filler slab with additively manufactured shell formwork	105
5.4	Discussion	105
5.5	Conclusions	106
5.5.1	Future work and remarks	106
5.5.2	Summary of intellectual contributions.....	106
6.	Conclusions.....	109
6.1	Summary of contributions.....	109
6.1.1	Parametric design and closed form analysis methods of traditional structures reveal new opportunities for efficiency in the early design stage	109
6.1.2	Filler slabs are a promising solution that now have a computational framework for integrated building energy needs	110
6.1.3	Parametric customization of waffle slabs can be achieved but manufacturing tradeoffs limit full carbon savings potential	110
6.2	Potential applications and broader impact	111
6.2.1	In research.....	111
6.2.2	In practice.....	111
6.3	Remaining questions and future research directions.....	112
6.3.1	Accommodation of organic and non-orthogonal ribbing and framing	112
6.3.2	Economic analysis for implementation of waffle and filler slabs.....	112
6.3.3	Repurposing of agricultural waste streams	112
6.4	Concluding remarks and outlook	113

References..... 114

List of Figures

Figure 1-1: Cement and steel demand by region from 2000 – 2020. Note: 2020 decline correlates with Covid-19 Pandemic (United Nations Environment Programme, 2021)	21
Figure 1-2: Left: Representation of the structurally acting materiality in a rectangular reinforced concrete beam as well as the distribution of compressive and tensile stress adapted from (ACI Committee 318 et al., 2016). Right: Illustration of the primary directions for load transfer with black arrows on one-way and two-way slab as well as their efficiently ribbed counterparts (dimensions.com).....	22
Figure 2-1: Example of Environmental Tradeoff Diagrams proposed by Radford and Gero as a design aid for the built environment.	28
Figure 2-2: Image of a) Zarzuela Hippodrome and b) Algeciras Market by Eduardo Torroja and c) Chapel Lomas de Cuenavaca and d) Restaurante Los Manantiales by Felix Candela	30
Figure 2-3: Isler’s Deitingen Service Station, Switzerland completed in 1968.....	30
Figure 2-4: a) UNESCO Conference hall, Paris, France by Pier Luigi Nervi, Bernard Zehrufuss, Marcel Bruer, b) American Concrete Institute Headquarters, Detroit, Michigan by Minoru Yamasaki, c) Aerial view of concrete folded plate roof of the Arkansas Museum of Fine Arts, Little Rock Arkansas d) Interior cast of connecting corridor	32
Figure 2-5: Images of the fabrication and deployment of a folded plate structure made with the ORICRETE design method.....	32
Figure 2-6: Plan and section view of a two-way flat slab with drop panels system (left) and a two-way waffle slab system (right). © 2004 John Wiley and Son, Inc.	34
Figure 2-7: Images of Pier Luigi Nervi’s famous floor concrete ribbed floor systems, a) Gatti Wool Factory, Rome 1953, b) Tobacco Factory, Bologna 1952, c) The Palace of Labor, Turin 1959.....	35
Figure 2-8: Renown built examples in the United States of waffle slabs, a key spanning system in many brutalist structures. Examples featured include a) The Yale University Art Gallery and b) Washington D.C. Metro Train Stations	35
Figure 2-9: Casting of a concrete slab utilizing BubbleDeck technology for Western Michigan University.....	36
Figure 2-10: Acclaimed examples of Filler Slab construction in India. Structures highlighted include a) SEWA Building by Laurie Baker, Trivandrum, 2004 and b) Wall House by Anupama Kundoo, Auroville, 2000	37
Figure 3-1: View of test structure from Gamble, Sozen and Siess experimental study of a two-way floor slab.....	42
Figure 3-2: Diagram of computational workflow used to design, evaluate and select optimal flat and waffle slabs.....	46

Figure 3-3: Illustration of plan view of 3x3 bay (left) and single concrete slab models for analysis (right).	46
Figure 3-4: Variation with structural depth in embodied carbon (left) and material cost (right) of a square flat slab under residential loading conditions. Infeasible designs do not meet constraints given in Table 3-2.	56
Figure 3-5: Optimal depth for a given span of a flat concrete slab with 1:1 aspect ratio. Application of a typical residential live load of 2 kN/m ² (left) and assembly live load of 7 kN/m ² (right) are presented.	57
Figure 3-6: Optimal depth across given Lx and Ly dimensions for both flat slabs (top) and a 70% voided waffle slab (bottom). Geometric infeasibility are aspect ratios not permitted for analysis by DDM and load ratio infeasibility regions are those where the live load to self-weight ratio exceeds the boundaries set for DDM.	58
Figure 3-7: Optimal solution sets for depth, mass, carbon and cost across square flat waffle slab typologies, and three selected spans.	59
Figure 3-8: Average ratio of optimal slab typology to optimal flat slab for embodied carbon, mass and cost for 8m spans.....	60
Figure 3-9: Carbon reduction strategy matrix for 8m square slabs, subject to residential live loading (2 kN/m ²)	62
Figure 4-1: Filler material comparison plots. Light blue refers to natural materials in early investigation stages, medium blue highlights traditional structural materials in the region of interest, India, and dark blue corresponds to traditional insulation materials.	70
Figure 4-2: Comparison of the moment (left) and shear (right) demand found from the closed-form code-based approach and a FEA model.	73
Figure 4-3: Drawing of thermal circuits for both the infinite lateral conduction and zero lateral conduction heat transfer model of the filler slabs.	74
Figure 4-4: Comparison of 1D (closed form analytical) and 2D (THERM) conduction models for filler slabs.....	75
Figure 4-5: Comparison of 1D and 2D models with respect to the ranking of the solutions by U-Value	77
Figure 4-6: Overview of computational work flow for multi-objective optimization of filler slab	78
Figure 4-7: Section drawing of parameterized filler slab, with n = 4 modules and straw filler material	78
Figure 4-8: Examples of module size distribution in plan (top), based on a representative width scaling surface (bottom).....	79
Figure 4-9: Parallel coordinate plot of 6m span designs generated with the three filler materials and the benchmark	82
Figure 4-10: Drawing of the best performing solution for 6m – straw filler slab. Scaling surface has 1 control point.....	82

Figure 4-11: Feasible but non-optimal performing solution designed with 4 point-controlled scaling surface for a 6m span with $n = 10$ straw filler with a 53% increase in embodied energy, 65% reduction in thermal conductance and 3% reduction in mass.	84
Figure 4-12: Left - Image of the straw bale formwork and scaled conventional construction materials for a concrete filler slab (left), Right- image of the bottom of the filler slab with straw bales integral to slab and concrete waffle.	86
Figure 5-1: Images of shaped and twisted columns that respond to loading demands by Pier Luigi Nervi (left) and shaped column and folded plate structural system of Tagore Hall by Mahendra Raj (right).....	90
Figure 5-2: Topology optimized floor slabs from ETH Zurich with cast-in-place additively manufactured formwork.....	91
Figure 5-3: Examples of work expanding the fields of structural patterning of shell structures a) Footbridge TRUMPF in Ditzingen, Germany (2018), b) adaptive framework to reduce computational time in the design process of perforated shell structures (Rivera et al., 2020)	92
Figure 5-4: Images of systems evoking structural logic and expression but realized via conventional systems and cladding. Left: Chhatrapati Shivaji International Airport, Right: Qatar National Convention Center	93
Figure 5-5: Design variable highlighted in blue and with * correlated to visual impact and fabrication complexity for waffle and filler slabs.....	94
Figure 5-6: Sample of standard sized waffle slab formwork available for purchase or rent for slab construction (Fercanorte - Structures, Slabs and Formworks Ltd.).....	95
Figure 5-7: Left - ShriRam Centre for Arts and Culture, New Delhi, India, middle – close up shop of shaped waffle slab ribs for cantilevered roof element and right – roof framing drawing.....	95
Figure 5-8: Demonstration of the variation in void widths that can be achieved with the manipulation of control point heights on a scaling surface	97
Figure 5-9: Sample waffle slab with standard void sizing and blue lines to illustrate the locations of the T sections used for analysis	98
Figure 5-10: Plan image utility shed roof with 3 overhanging spans. Squares indicate column locations	99
Figure 5-11: Moment and shear demand for every point of analysis in the waffle slab for 3 different aspect ratios and support condition. The darker the point, the more times that combination of demands appears in a slab.	100
Figure 5-12: Moment and shear utilization histograms for the shape optimized waffle slab example.	102
Figure 5-13: (Top row) Moment capacity of sampled t-section vs. embodied carbon (Bottom row) Shear Capacity of sampled T-sections vs. embodied carbon. Figures are colored by structural depth in the left column and web ratio in the right column.....	104
Figure 5-14: Proof of concept for fabrication of flat concrete element with conventional rebar and fabrication methods, and additively manufactured formwork that can be sized according to optimal dimensions for slab	105

List of Tables

Table 3-1: Design variable and bounds for flat and waffle concrete slabs	47
Table 3-2: General structural and geometric constraints for concrete slab design	54
Table 3-3: Updated material property values for structural analysis with carbon intervention strategies	62
Table 4-1 Material properties used for analysis and optimization in Chapter 4.....	68
Table 4-2 Qualitative error measures for thermal modeling.....	77
Table 4-3: Design variable vector for filler slab with associated bounds and values.....	79
Table 4-4: Performance savings of optimal designs compared to minimum depth flat slab benchmarks	83
Table 4-5: Comparison of reductions achieved with different number of filler modules	84
Table 4-6: Thermal transmittance ranges for optimal 6m slabs design with this chapter's method	86
Table 5-1: Design vector variables for parametric waffle slabs, with multiple scaling surfaces .	97
Table 5-2: Performance metrics for parametric slab with standard void sizes, vs with a size distribution.	101

1. Introduction

1.1 Motivation

Given the climate crisis, it is important to reconsider the way we approach design in every aspect of life. This of course includes design of the built environment as buildings account for 40% of emissions globally, with this on track to keep increasing if business as usual design and construction practice continues (United Nations Environment Programme, 2021). In fact, it is estimated that in 2023 alone, 13.8 trillion dollars USD will be spent globally on construction (McKinsey & Company, 2020).

This demand for new construction in a rapidly urbanizing world has been sharply marked by an increase in the use of concrete construction – one of the most widely used substances on the planet. There are many attractive qualities that make concrete the material of choice in modern construction, including but not limited to its low cost and widespread knowledge of its workability. However, the use of concrete also has a significant impact on the environment at almost every stage of its life, from the mining of stone to produce the aggregate to its lack of recyclability at the end of a building’s structural life. Many studies have already quantified the impact of concrete in buildings and have found that concrete horizontal spanning systems – i.e. floors and roofs –are the key contributors to embodied carbon emissions with the 50% – 60% of a structures carbon footprint resulting from these elements (Huberman et al., 2015; Mata-Falcón et al., 2022). These floors and roofs are particularly important as their design has downstream effects on structural material needs for the gravity and lateral systems and foundations.

In parallel to this carbon challenge and the imperative we have as structural engineers and designers to offer the world actionable solutions and carbon mitigation strategies, there has been an increasing excitement about data-driven or performance-based design and the influence that computation can have on shifting the tides towards low-carbon, energy-efficient structural solutions (Kocaturk, 2017). Despite advances in methods, technologies, and pushes towards interdisciplinary education of structural engineers and architects, adoption has not kept this same pace. There exists a research gap that computation can fill in the acquisition of new, generalized knowledge about existing and scalable structural systems as it pertains to carbon reduction objectives. Furthermore, there exists an opportunity to evaluate successful, localized structural design strategies and create flexible design methods that can be honed to wider context, fabrication methods, secondary design objectives etc.

The motivation for this work is two-fold. First, to empower the proliferation of low-carbon concrete spanning systems with accessible computational design strategies for common spanning typologies. Second, this work aims to formalize and provide a comprehensive methodology to design and quantify the performance of an integrated spanning system most popular in India, the filler slab, for wider contexts.

1.2 Environmental impact metrics for structural design

There are two key and deeply related metrics for how the environmental impact of a building can be quantified: operational carbon and embodied carbon. The operational carbon contributions of a building comprise all of the emissions associated from the use of a structure during its life, while embodied carbon focuses on the carbon emissions emitted during the manufacture, transport and construction of a new building (De Wolf et al., 2015). In other words, operational carbon measures building use, while embodied carbon addresses with material quantities and properties derived from the form of a structure. Engineers can quantify this impact directly from the material quantities with the use of embodied carbon coefficients, a concept that has been heavily researched and developed in building computational science since 2004 (Dias & Pooliyadda, 2004). A huge barrier to the use of embodied carbon coefficients and accounting in engineering is a universal method for calculating these coefficients and benchmarking structural projects at scale. This has begun to be tackled by many researchers in the built environment (De Wolf et al., 2020; Hammond & Jones, 2008), but crucial data gaps still exist in non-western parts of the world. In addition to the benchmarking of built projects, parametric modeling and optimization (Section 2.1.3) been identified as influential strategies to create generalizable knowledge about the embodied carbon content of structures and a key parallel step that can work in conjunction with other embodied carbon reduction strategies (Fang et al., 2023).

This thesis also refers to the metric embodied energy which instead refers to the energy expended to manufacture, transport and construct a new building. Though typically positively correlated to embodied carbon, embodied energy refers to a manufacturing need and not the resulting emissions. Thus, depending on fuel source and efficiency of the process, it is possible for a material to have a high embodied energy but a low embodied carbon (M. Hu, 2020). Nevertheless, in this dissertation, embodied carbon and energy are used in a similar way and are assumed to be correlated.

1.3 Concrete: An omni-present structural material

1.3.1 History of concrete use and prevalence in modern construction

Reinforced concrete use is particularly environmentally impactful, not just because of the high embodied carbon coefficients of both the cement as well as the steel rebar, but also the sheer volume being used globally (Figure 1-1). Furthermore, a substantial amount of the concrete is wasted in inefficiently design sections, optimized for manufacturing cost and not sustainability.

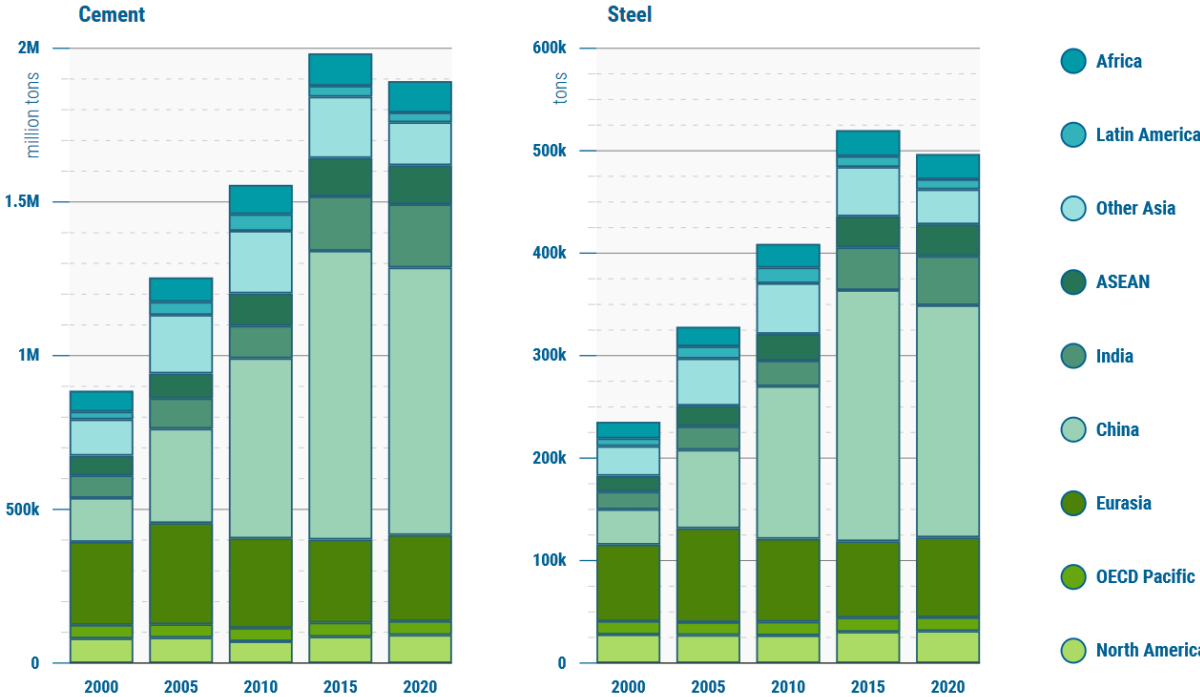


Figure 1-1: Cement and steel demand by region from 2000 – 2020. Note: 2020 decline correlates with Covid-19 Pandemic (United Nations Environment Programme, 2021)

Modern concrete is owed in large part to the invention of Portland cement by Joseph Aspdin, the binding agent in concrete and the main contributions to the emissions associated with this material (Crow, 2008). It is a desired material because of its versatility and ease of use, especially in regions with a large amount of informal or self-built construction. It is viewed as a symbol of strength and longevity and in fact the first reinforced concrete home was built in 1875 by William Ward, who selected the material due to a fear of fire (Ward House, 2023). That building still stands. Huge quantities of concrete were utilized to rebuild quickly and cheaply after WWII (Watts, 2019). During this same time period, reinforced concrete was the material of choice for countries in the Global South as they gained independence from colonial rule and brought forth numerous works of material efficiency as well as helped cement a national identity (M. A. Ismail & Mueller, 2022).

1.3.2 Structural behavior of reinforced concrete

Concrete itself is strong in compression, but performs very poorly in tension, hence the addition of the reinforcement in the tensile regions of the structure (Darwin et al., 2010). This makes efficient design of reinforced concrete structures a complex issue with non-linear performance relationships hindering the development of constitutive relationships. Thus, performance assurances and prediction, especially for novel forms, rely heavily of experimental verification and semi-empirical expressions.

Let’s consider a rectangular beam undergoing flexure, or bending, a behavior that combines both compression and tension behavior to support a load. In the image shown in Figure 1-2 below, the region above the neutral axis is in compression while the region below the neutral axis is the tensile region, where concrete material is structurally useless aside from the rebar. Only the highlighted regions in blue are needed to carry the flexural load and the other material is functionally wasted (aside from shear capacity, which may consider the full section). A one-way flat slab could be thought of as an array of these inefficient structures, repeated over and over, proliferating material inefficiency in the billions of square meters of floor area (United Nations Environment Programme, 2021) to be designed globally. It may make more sense to carve away material that is not behaving structurally to minimize the amount of waste, which is exactly the intuition behind these T-beams or ribbed joist systems that take advantage of concentrating material to reduce this waste (Allen & Iano, 2004).

Another option, which is where this dissertation focuses, is to consider two-way slab behavior, which is a statically indeterminate scenario where the loads can be carried in both spanning directions to the supports. This represents a larger amount of construction scenarios, and similarly can be thought of two sets of these beams’ arrays linked orthogonally. Waffle slabs, which are discussed in Section 2.2.2 are the orthogonally ribbed version of this case.

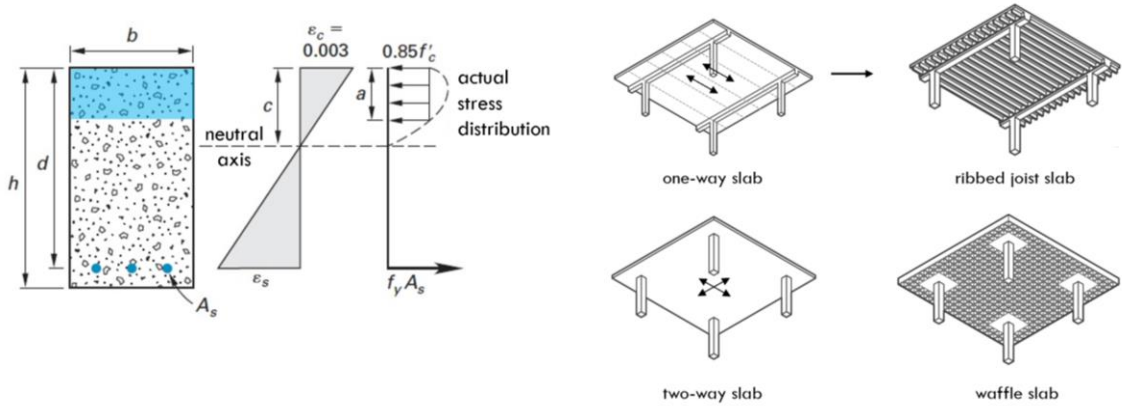


Figure 1-2: Left: Representation of the structurally acting material in a rectangular reinforced concrete beam as well as the distribution of compressive and tensile stress adapted from (ACI Committee 318 et al., 2016). Right: Illustration of the primary directions for load transfer with black arrows on one-way and two-way slab as well as their efficiently ribbed counterparts (dimensions.com).

The design task of carbon-efficient, reinforced concrete spanning structures is still not simple, especially when considering the carbon contributions of the individual materials in reinforced

concrete systems. Concrete has an embodied carbon coefficient of 0.15 kgCO₂/kg, while steel has one of 2.00 kgCO₂/kg (Jones & Hammond, 2019). The order of magnitude difference between the two means that even smallest increase in mass percentage of steel can have significant impacts on total embodied carbon of an element, even as it may allow for a thinner slab and less concrete material overall. This problem persists even when switching to more efficient ribbed typologies as other design constraints such as cover requirements, rib spacing, and manufacturing are added.

1.4 Thesis foundation and scope

This thesis is not written to propose the omission of concrete in its entirety, as it is a material with a significant utility and cultural legacy. The hope instead is to present methods that can equip those who choose to use concrete structurally, with the nuanced understanding to make as efficient use of it as possible for widely used typologies. Furthermore, this work aims to bridge a gap between boutique methods for concrete reduction in other contexts, particularly the filler slab system, popular in cost-conscious Indian construction, to more formalized design methods that can be applied successfully in other regions.

Successful application with respect to this work would mean the early-stage design and performance assessment of concrete spanning systems that are materially efficient compared to current benchmarks under the same loading conditions and spans. With respect to the filler slabs, this be the improvement in design in thermal performance objectives compared to flat roof construction, as well as the creation of generalized knowledge correlating the systems geometry to its environmental and thermal performance. Lastly, this thesis will propose and evaluate alternative fabrication methods for filler slabs that are broadly applicable to lost formwork concrete systems.

1.5 Organization of dissertation

This dissertation is divided into 6 chapters. The first chapter serves as the introduction and provides relevant context on the environmental and cultural imperatives that motivate this work.

Chapter 2 provides a literature review on computational design in structural engineering and architecture and the acceptance of interdisciplinary methods and approaches. It highlights key methods such as parametric design and optimization and also reviews materially efficient concrete structural systems that are either predecessors to the typologies discussed in this thesis (flat, waffle slabs and filler slabs) or can be used as benchmarks (shells, folded plates). This section concludes with a discussion on context-informed fabrication and highlights how additive manufacturing may be leveraged for low carbon custom formwork, which is particularly relevant to Chapter 5

Chapter 3 presents the results of a comprehensive parametric study on the design of widely deployed two-way spanning systems and assesses the resulting design space with respect to metrics of embodied carbon, mass, cost. This chapter presents additional background on the current design methods for flat and waffle slabs, as well as provides evidence to critique serial design processes and the use of rules of thumb for early-stage concrete slab design.

Chapter 4 proposes a computational methodology for the design and optimization of filler slabs for minimum embodied emissions as well as minimum thermal transmittance. It presents a new way to evaluate filler materials based on their material properties in the spirit of the Ashby plot and presents a key finding about the optimal depth of filler slab systems that adds nuance to one widely accepted rule of thumb for the design of these systems. It also presents a scale model fabricated with one of the options studied as a viable agricultural formwork alternative.

Chapter 5 presents a case study for a roof which has non-standard boundary conditions for the to determine if the customization of the filler and waffle slab voids provide structural and embodied carbon benefit when compared to the benchmarks. It also shows a prototype of 3D printed formwork that could enable customization of a filler/waffle slab system.

Chapter 6 summarizes the intellectual contributions of this thesis, its potential impact as well open questions and future research directions.

2. Literature Review

2.1 Towards computational and non-serialized design processes in architecture and structural engineering

With the advent of computational design and increasingly intuitive design and visualization tools for engineers and architects, the field of structural engineering has recently seen a revolution in the way that engineering design is taught, aiming towards a widespread transformation of how buildings are conceptualized and built.

2.1.1 Separation of architecture and structural engineering disciplines

In the early 16th century, Michelangelo stated “a bridge should be thought out and built the same as a cathedral, with the same attention and same materials”, harkening to the cultural relationship that structural design can have in shaping society. Physical reasoning and mathematical basis for structural design followed subsequently in the 17th century by the likes of Galileo and Newton led to greater scientific understanding of underlying structural mechanics and interest in more correctly understanding the strength of building elements such as beams. This allowed for the increased scale of structures. Next came the establishment of engineering educational programs in the mid to late 18th century which is thought to have been the beginnings of the present division between the disciplines of architecture and structural engineering (N. Hu & Dai, 2010).

Presently, this separation is marked by separate training for architects and structural engineers, as well as reinforced beliefs that aesthetically-desirable and well-accepted novel designs are not correlative to high performing ones. Despite firmly disagreeing with the belief that structural efficiency cannot beget beauty, Billington does give merit to this dichotomy and classifies structural designers as those who give form to objects large in scale and of single use, such as a public bridge, while considers architectural designers, as those who give form to objects that are relatively smaller and for complex human use, such as a home. In *The Tower and the Bridge*, he states that it is structural designers that have given rise to materially efficient and structurally rational forms, not architects (Billington, 1985). Antonsson and Cagan also make a distinction in their work in design synthesis, stating that “engineering design” is concerned with the technical performance aspects rather than the aesthetic, and is done in support of the architect (Antonsson & Cagan, 2001). More recently these beliefs have been met with pushback from scholars in the spatial structure community who have highlighted numerous fruitful collaborations between architects and engineers that have led to the creation of “structural art”, but also the ability of interdisciplinary design processes to find new ways to utilize available and often constrained resources (Herr, 2019). This ability is largely owed to the development of integrated design tools and methods for conceptualization and analysis as well as interdisciplinary design instruction.

2.1.2 Enabling creativity in computational structural design

Computation allows for the synthesis of both structural engineering and architectural design, the performance of a structure, with visual and other subjective and context dependent characteristics. Radford and Gero posed three following advantages that computation could add to architectural design (Radford & Gero, 1980a):

- 1) Automating “manual” analysis for speed and accuracy
- 2) Access to previously inaccessible methods that required huge quantities of computation
- 3) New approaches to design, such as parametric modeling and other generative methods

This was in response to the revolution of the field of architecture and structural engineering with the invention of Computer-Aided Design (CAD) (Sutherland, 1963) and building information modeling (BIM) (Eastman, 1975). With respect to CAD tools, one of the most widely used commercial tools at present is Rhinoceros 3D (Rhino) which launched in 1998 by Robert McNeel & Associates and has evolved to include Grasshopper, a visual programming tool that enables complex parametric models the couple directly with the 3D model definition in Rhino. Furthermore, Grasshopper allows the addition of open sources plug-ins to supplement its core design functions and have been leveraged by architects and structural engineers to create architecturally striking and high performing designs (Caetano & Leitão, 2020).

Especially relevant to the subsequent work in Chapters 4 and 5, is the development of the Design Space Exploration toolbox, which is a suite of open-source plugins to enable both exhaustive search methods as well as single and multi-objective optimization of structures in Rhino (Brown et al., 2020). Chapter 4 also takes advantage of Ladybug Tools, a set of plugins that allow designers to measure various aspects about the energy consumption, thermal and visual comfort of building designs (Roudsari et al., 2013) , while Chapter 5 introduces a hybrid structural

analysis method made possible with the use of Karamba, a Finite Element Modeling plugin for Grasshopper (Presinger & Bollinger+Grohmann, 2018).

There has also been a recent emphasis on generative design tools and models in structural engineering and architecture, which can be used to widen access to design generally and promote high-performing, creative structural design. This includes methods such as shape grammars, or rule-based design generation (Stiny, 1980) or interactive evolutionary optimization tools such as StructureFit and StormCloud (C. T. Mueller & Ochsendorf, 2015; C. Mueller, 2017). Machine learning has also led to an abundance of applied generative modeling research in architecture and highlighted the value of performance-based data for visual representations as large quantities are needed to supervise and train machine learning models. One type of generative model, a variational autoencoder, which at a very high level can be thought of as a method to train a low dimensional design space to generate quality data from one of higher dimensions and complexity have also shown great promise in enable creativity and exploration for structural designers. Performance-conditioned Variation Autoencoders (PVAEs) (Sohn et al., 2015) have been leveraged by Danhaive and Mueller to aid in intuitive exploration of high dimensional design spaces by re-mapping them to 2-dimensional design latent spaces that can be explored continuously based on the desired final design performance (Danhaive & Mueller, 2021). In addition, VAEs have been used to generate latent space representations of hand drawn sketches and subsequently train a surrogate model to provide real time performance predictions at what is often the earliest stage of design (Ong et al., 2021). Methods such as this bring together the harmony of organic and analog design representation with performance, and truly show how the computer can aid and not replace designer intent for structural problems.

2.1.3 Parametric design and structural optimization

Of great importance to this work, is the field of computational structural optimization, whose purpose is to define a structure's geometry to meet a specific need, (i.e. a roof that can support high snow loads, and also provide insulation), while meeting a set of structural constraints (i.e. static equilibrium, small deflections under loading, etc.). Its modern roots can be traced back to the 1960s work of Schmit whose demonstrative example featured the mass optimization of a three-bar truss (Schmit, 1960) and has grown immensely to include a variety of complex structures and loading conditions. Structural optimization generally starts with a parametric model, which in this dissertation is a digital representation of an engineered object, where a set number of critical features (some set as variable parameters) and geometric relationships are used to define its full form (Davis, 2013). After defining the geometric model, structural analysis can be performed based on loading, material properties, etc. Resultants of this analysis include a quantification of the behavior of the system and of key constraints that may be important to consider given designer intention or building code. Finally, the variables that will be tuned, the objective function or goal, and constraints, can be fed into an optimization algorithm to find the "best solution".

It is also possible and more than likely that there are multiple objectives of importance for a structural design and the engineer may want to pursue a multi-objective optimization method. Multi-objective optimization has its roots in economic theory, with one of its key concepts, the Pareto front, first published in 1906, defines a region of the objective function space, where one

design solution cannot be chosen without sacrificing the performance of another (Pareto, 2007). Stadler was the first to mathematically formalize multi-objective optimization for structural design with his work on minimizing mass and stored energy of shallow arches (Stadler, 1977), while shortly after Radford and Gero introduced “environmental tradeoff diagrams” which utilized Pareto optimality principles to demonstrate how building designs could be evaluated and optimized for multiple objectives (Radford & Gero, 1980b)

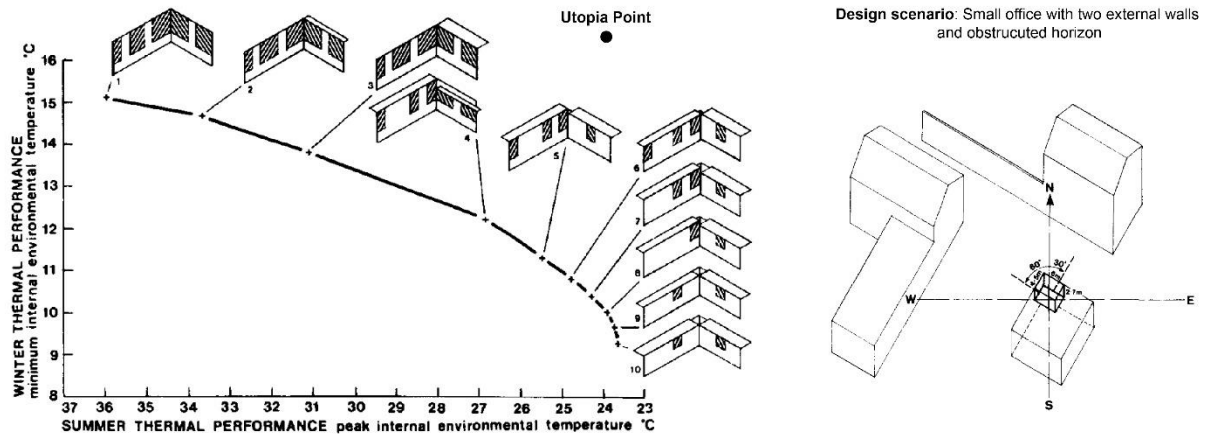


Figure 2-1: Example of Environmental Tradeoff Diagrams proposed by Radford and Gero as a design aid for the built environment.

Another work germane to Chapter 3, is that of Marks who utilized multi-objective optimization of the shape of a building for initial building and operational costs. The goal of that particular study wasn’t necessarily one of direct design, but in the creation of generalized knowledge of wall length proportions, glazing design etc. (Marks, 1997). With respect to concrete structural design in particular, several researchers have used parametric design and optimization to design standard and novel concrete systems, this is described in further detail in Section 3.1.3

2.1.4 Critiques and reframing of computational design processes

Critiques of computational design can be broadly placed into categories of critiques of the methods themselves and critiques of the design tools. For example, parametric modeling, a popular method to generate designs, can require a significant amount of upfront labor (Davis, 2013) or can result in solutions with much self-similarity in the design space (A. Hartwell et al., 2023). The overhead to begin the computational design model applies to a broad range of generative methods and can partially be attributed to available tools for architects, structural engineers and designers, that they are non-intuitive or result in over formulization that is not truly representative of organic design (Mitchell, 2001).

Mueller’s work in the creation of intuitive and flexible design tools and methods for structural engineers highlights that analysis software decoupled from generation capabilities, limits engineering participation (or performance-based consideration) in early design stage. Furthermore, many computational design tools without these features simply exist to reinforce existing, linear design strategies. Mueller also suggests that computational design tools and the

process requires real-time feedback, and guidance in order to promote successful exploration of a design space and selection of high performing designs (C. T. Mueller, 2014).

This dissertation not only acknowledges these critiques, but adds that computational design, and the advent of “data-driven design” especially in architecture and the built environment, can hold a more powerful role than just the sizing and geometric specification of building for one environmental context or design case study. Advances in computational power and the development of context-inclusive design methodologies lead to the production and revision of generalized design knowledge for traditional and novel structural systems and enables immediate impact on performance in the stage where it matters most (early design stage/concept generation). This is increasingly important as we aim to meet incredibly ambitious performance goals as it relates to carbon use reduction in the built environment.

2.2 Materially efficient concrete spanning systems

The wide acceptance and ubiquity in structural materials such as concrete and steel ensures their use will not be stymied, despite the carbon implications of the production volume necessary to meet building demand. As many objectives of designing and fabricating floor systems such as form, cost, and construction ease coalesce, historic precedent and renewed application via computational design and digital fabrication have proven key in the balance desires of creativity and economy in the modern age. With respect to concrete spanning structures, there are several examples that can be key reference points for emerging structural design talent and can push us into a materially efficient and low carbon future.

2.2.1 Shells and Plates

Of particular interest for efficient concrete spanning structures are shells and folded plate systems which are self-supporting structures that distribute loads via compressive only action. The first realizations of these structures were built in concrete, focused on forms that could be analyzed with simple manual and hand calculation, as these were the only methods available at the time.

Famous structural pioneers of these structures include figures such as Eduardo Torroja, a Spanish structural engineer whose is well known for his linked and repeating parabolic roof structures as illustrated by the Zarzuela Hippodrome (Figure 2-2a) and adaptation of indigenous structural forms such as the Catalonian vault which inspires Market Hall in Algeciras (Figure 2-2b) (Tippey, 2018). In addition, there was Felix Candela, whose work is synonymous with the hyperbolic paraboloid or *hypar* shape and produced a series of prolific shell structures in Mexico such as Chapel Lomas de Cuernavaca and Restaurante Los Manantiales (Figure 2-2 c, d) (Chilton & Chuang, 2017).



Figure 2-2: Image of a) Zarzuela Hippodrome and b) Algeciras Market by Eduardo Torroja and c) Chapel Lomas de Cuenavaca and d) Restaurante Los Manantiales by Felix Candela

Heinz Isler, who believed that for shell systems, “the task of architectural and structural design are one in the same” as the logic of the shells form directly influences its static design (Isler, 1994), is credited to introducing a variety of alternative form-finding methods to shell structural design via physical experimentation such as the use of hanging membrane and cloth for equilibrium shapes. These experimental methods have led to the design and construction of structures with less “straightforward” and mathematically defined forms, such as Deitingen Service Station.



Figure 2-3: Isler’s Deitingen Service Station, Switzerland completed in 1968.

The emergence of design tools that integrate and can stand in for physical form-finding methods such as the force density method (Schek, 1974; Veenendaal, 2017) or particle-spring methods (Kilian & Ochsendorf, 2005) or can ensure equilibrium behavior such as thrust-network analysis (Block & Ochsendorf, 2007) or linear finite element analysis, have renewed interest in these efficient systems. In parallel to the introduction of these methods, recent built works in shell architecture for roofs and floor systems have highlighted sustainability as driving performance metric. The South African National Parks Mapungubwe Interpretive Center which utilized stabilized soil cement tiles (Ramage et al., 2010) or thin shell prototype floor systems introduced by Hawkins et al. which demonstrated up to 58% reduction in embodied carbon for a variety of spans as compared to conventional flat slab construction (Hawkins et al., 2020).

Similarly, folded plates, which feature successive flat structural elements are also thin structures capable long spanning with material efficiency and relative fabrication simplicity when compared to some organic shell structures (Dowrick, 1967). For folded plates, gravity loads are resolved not across the thickness of the plate element itself, but through the inclined surfaces to the supports (membrane action) as well as bending forces across the depth of the folded section (Garcia, 2018). Design generation of folded plate structures has its roots in the Japanese art of origami, and has seen its extension as a form finding method for structures with the work of architect-educators such as Joseph Albers and Heino Engel (Lebée, 2015).

Prominent and acclaimed examples of folded plate spanning structures include the UNESCO conference hall (Figure 2-4a) which at the time of its completion in 1958 was the longest spanning folded plate structure (Calvo-Salve, 2018). During the same year in America, there was the construction of the American Concrete Institute headquarters by Yamasaki (Figure 2-4b) which won the Progressive Architecture Award. When tasked with showing off the capabilities of concrete as a building material, he designed a folded plate roof that cantilevers, bidirectionally off a single central corridor (Wilde, 2004). More recent works could point to a revival in popularity of this structural system such as the remodel and expansion of the Arkansas Museum of Fine Arts completed in 2023 by Studio Gang which features a sinuous folded concrete cover connecting the museums various spaces (Figure 2-4c, d).

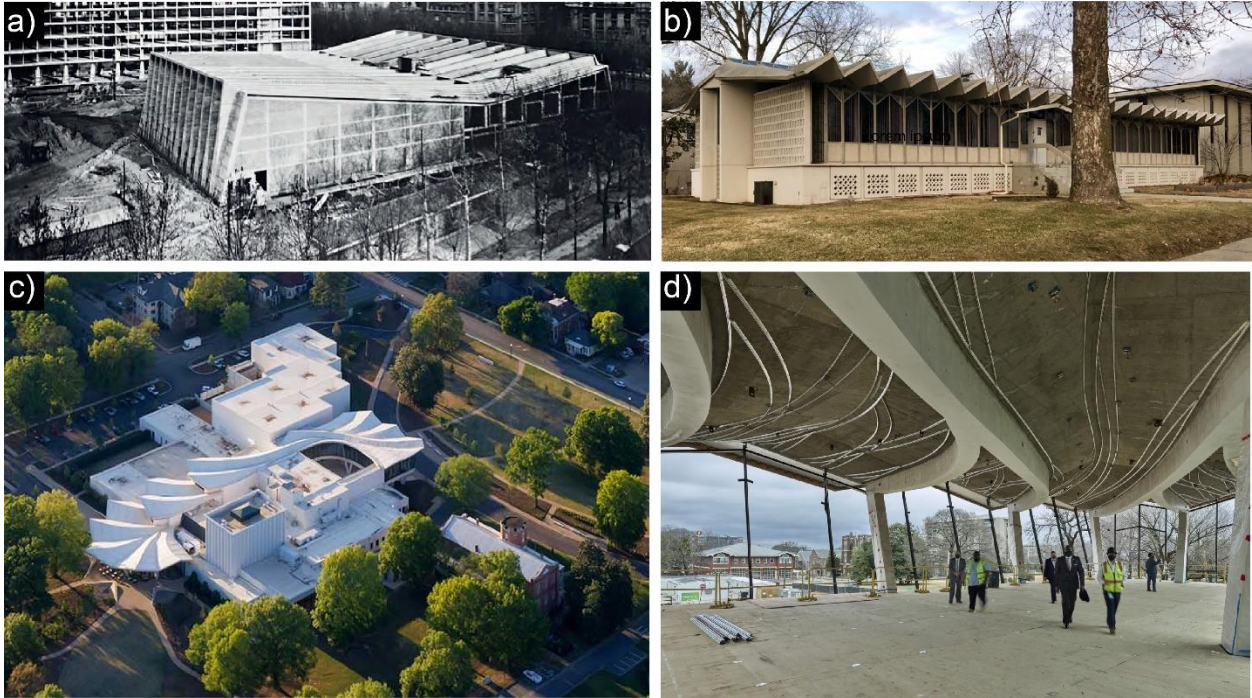


Figure 2-4: a) UNESCO Conference hall, Paris, France by Pier Luigi Nervi, Bernard Zehrjuss, Marcel Bruer, b) American Concrete Institute Headquarters, Detroit, Michigan by Minoru Yamasaki, c) Aerial view of concrete folded plate roof of the Arkansas Museum of Fine Arts, Little Rock Arkansas d) Interior cast of connecting corridor

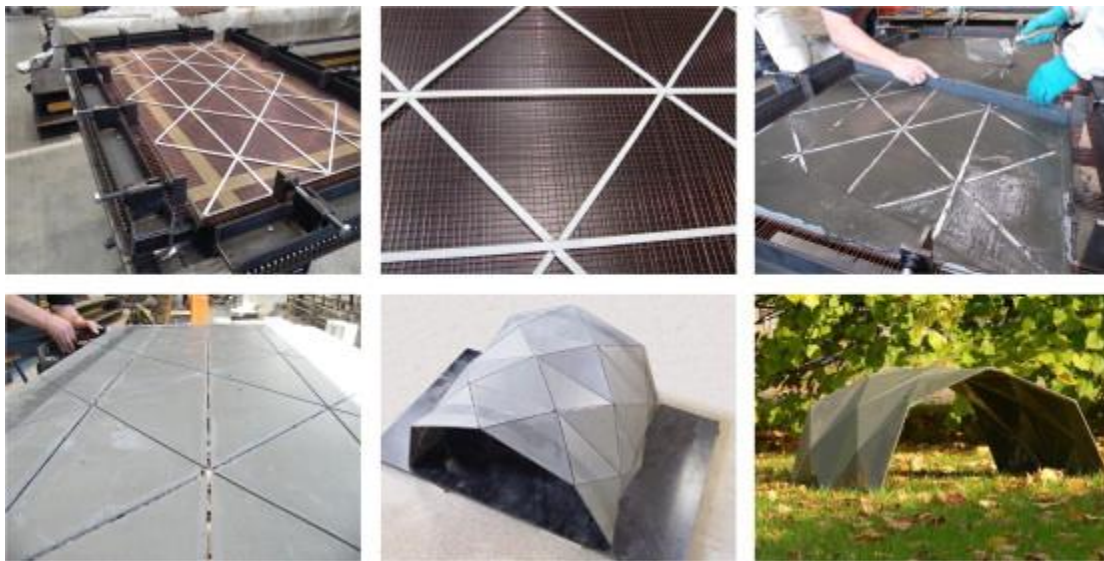


Figure 2-5: Images of the fabrication and deployment of a folded plate structure made with the ORICRETE design method

Two major research areas have created a regenerated interest in folded structures generally: digital fabrication and deployable surface structures (Lebée, 2015; Samuelsson & Vestlund,

2015). While a lot of this work has focused on fabric membranes and truss construction, concrete folded plate systems have also been considered. One recent development at the research scale is that of Oricrete, a design and fabrication method that casts concrete plates with fabric reinforcement and gaps that make up the location of the creases for folding. The plates can then be folded, hoisted and fasted (grouting or with mechanical bolts) into its final configuration on site (Chudoba et al., 2014).

While shells and folded plate systems are proven structural spanning typologies and have been critical in concrete design and the structural identity of several cities and regions, construction of these systems under current economic conditions remains challenging when compared to traditional typologies such as flat slabs. Furthermore, it is not clear how they could function as floor systems, as they have primarily been proposed as deep or highly shaped roof and canopy structures.

2.2.2 Ribbed slabs and non-rectangular cross section systems

It is well established that the flat slab typology, common in cast-in-place construction, is the one of the least materially efficient ways to support gravity loads and resist bending moments. This is due to the significant portions of the slab being filled with concrete that does not perform well under tensile loading. Waffle slabs are one alternative structural solution that addresses this problem. They are horizontal spanning elements with a flat deck (or flange) on top and ribs running in two perpendicular directions, resembling a waffle when looked at from below as shown in Fig. 2-6. This shaping removes most concrete material placed in the tensile region of the element and allows for two-way distribution of loads to the supports and foundations via the interlocked ribs. Waffles slabs are an often-suggested solution for building programs requiring long clear spans that cannot always be achieved with flat concrete slab systems, due to issues supporting the dead load of a slab as the span lengths increase (Allen & Iano, 2004).

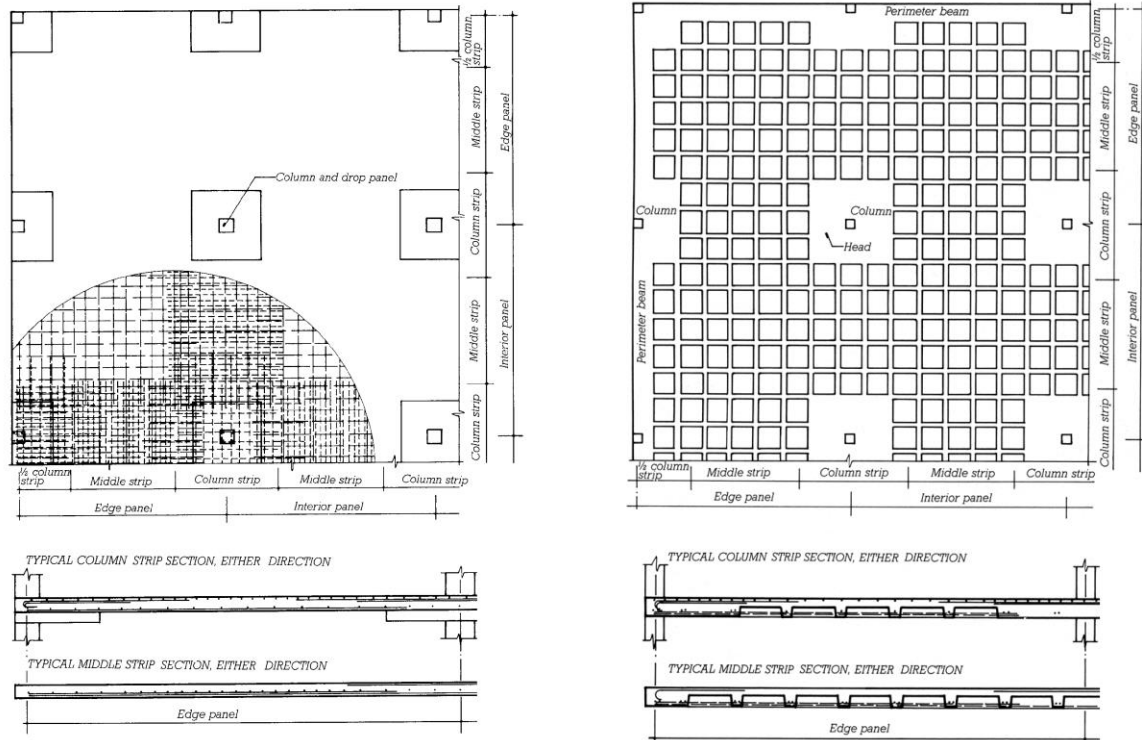


Figure 2-6: Plan and section view of a two-way flat slab with drop panels system (left) and a two-way waffle slab system (right). © 2004 John Wiley and Son, Inc.

Ribbed concrete floor slabs are often credited to Francois Hennebique whose 1892 patent featured the Béton Armé system or System Hennebique, a reinforced concrete floor and framing system with orthogonal ribs and beams cast monolithically with the slab, and iron reinforcement only in the rib region (Wang, 2013). Ribbed systems continued to rise in popularity, especially as designers such as Pier Luigi Nervi were able to introduce fluid and curved rib configurations that were structurally and economically efficient as well as aesthetically interesting (Halpern et al., 2013). One of the most interesting facts about Nervi's work was that most originated from successful competition proposals, where it was necessary for him to consider economy, or as he states, "the method of bringing dead and live loads down to the foundations with the minimum use of materials." In other words, it would have been impossible at the time to justify realization of Nervi's complex designs if the material reduction didn't lead to cost offsetting (Billington, 1985). Furthermore, many of the ribbed slabs that Nervi is famous for are also a result of his work with ferro-cement, or concrete reinforced with steel mesh that allowed for cheap, non-rectilinear formwork and traveling scaffolding systems (Leslie, 2017). These innovations allowed the geometrically expressive coffering structure as seen in Figure 2-7.



Figure 2-7: Images of Pier Luigi Nervi's famous floor concrete ribbed floor systems, a) Gatti Wool Factory, Rome 1953, b) Tobacco Factory, Bologna 1952, c) The Palace of Labor, Turin 1959

The popularity of the rigid orthogonal system, specifically waffle slabs, continued with the rise of brutalism between the 1950s – 1980s. Striking examples of waffle and ribbed slab construction in North America during this time include The Yale University Art Gallery by Louis Kahn (1953) and the Washington, D.C. metro train stations by Harry Weese (1977) as shown in Figure 2-8. As with many architectural trends, this interest waned due to construction economy tradeoffs, political associations of brutalism, and public critique of exposed concrete (Lack & Korynta, 2020; Mould, 2017).



Figure 2-8: Renown built examples in the United States of waffle slabs, a key spanning system in many brutalist structures. Examples featured include a) The Yale University Art Gallery and b) Washington D.C. Metro Train Stations

Recently, there has been a return of interest in ribbed and shaped concrete floor systems at the research and prototype level that employ structural shaping and material economy principles in the spirit of Nervi. Structural engineering and architectural researchers have achieved shaped beams and developed their design methods in tandem with emerging and novel formwork fabrication methods such as CNC milling, sheet metal and bamboo bending (M. A. Ismail, 2023). Fabric formwork has also been demonstrated to be a viable formwork work for shaped beam elements (Orr et al., 2011) or spanning shell structures (Popescu et al., 2018).

2.3 Lost formwork construction

Generally, cast-in-place concrete slab construction is realized with the use of plywood and steel forms customized for a given project. For waffle slabs, reusable metal and plastic domes are placed on top of the temporary deck and then both are removed post curing. While this results in a more structurally efficient cast-in-place system, there is a significant amount of added labor and cost associated with the installation and removal of these pans. Several systems have emerged that provide similar structural benefits as a waffle slab, but make use of lost-formwork, or formwork that remains integral with the component once it has cured as goes into service. Some of those systems conceal the formwork, while others have the visual appearance of the formwork apart of the aesthetic appeal of the space.

On the industry scale, several examples of lost formwork exist, especially as it relates to spanning systems. Perhaps one of the oldest and most enduring examples of lost formwork construction is the composite steel deck, whose history traces back to 1926 when Loucks and Giller patented a steel deck floor system where the steel was solely responsible for the structural action of the slab and concrete was casted on top to create a flat deck and provide fireproofing for the steel. The modern composite steel deck where the concrete resists structural load and is reinforced by a steel deck with trapezoidal ribs was called Cofar and introduced in the 1950s by the Granco Steel Products Company (Sputo, 2012). As a contrast, the majority of modern cast-in-place two-way systems with lost formwork take advantage of void-forming objects to create cross-sections that most closely resemble a sequence of I-beams. Several manufacturers have emerged in this field including BubbleDeck (Figure 2-9), which uses hollow plastic balls to remove concrete from two-way slabs, Cobiax (hollow cylindrical drums), Nautilus by Geoplast (rectangular boxes), all companies reporting to use recycled plastic for their formwork.



Figure 2-9: Casting of a concrete slab utilizing BubbleDeck technology for Western Michigan University

2.4 Filler slabs

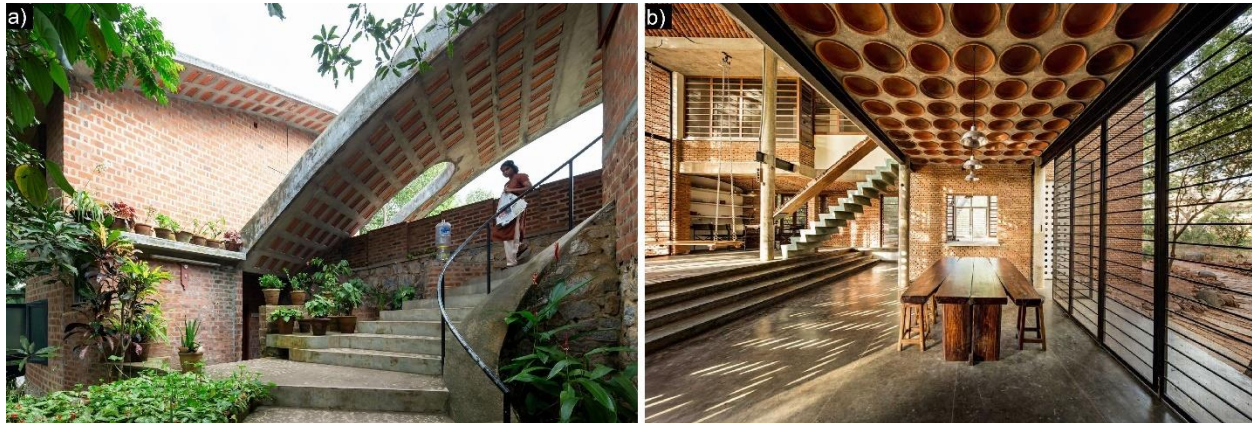


Figure 2-10: Acclaimed examples of Filler Slab construction in India. Structures highlighted include a) SEWA Building by Laurie Baker, Trivandrum, 2004 and b) Wall House by Anupama Kundoo, Auroville, 2000

The filler slab, as shown in Figure 2-10, is a particularly compelling lost formwork technology that could pave the way for materially efficient, context informed design in wider contexts. First popularized in South India by architect Laurie Baker, the filler slab which replaces volume of concrete in the tensile region of the slab with waste, or reclaimed locally available materials such as clay tiles and post was originally proposed as a cost-saving technology by reducing the amount of concrete for flat roof structures. Even though this technology has also been implemented by professional architects and engineers, many self-builders have also been empowered to use this technology in their homes.

Many studies have looked specifically at structural validation with FEA of standard uniform geometries in plan and/or a built-in assumption that the best way to construct the slab is simply to remove material up to the tension zone of the reinforced concrete slab of a set depth (Mahananda et al., 2020). Recently, a case study for the design of filler slab roof in for the Block Resources Center in Bihar, India built a filler slab roof with a cost savings of approximately 23%, compared to a conventional flat slab (Sinha et al., 2020). While these case studies are very important to the acceptance and proliferation of this efficient system, individual boutique examples alone do not provide a framework to understanding nuances in the design and structural performance of filler slab systems, nor are they generalizable to other loading scenarios and conditions.

It should also be noted that as the conversation has shifted to low carbon architecture, the utility of filler slabs as a sustainable architectural technology has also been explicitly demonstrated, as filler slab environmental performance in specific case studies has also been quantified with respect to embodied energy and embodied carbon. In Reddy's work on sustainable materials and design of low carbon buildings, it was found that a filler slab roof with stabilized mud block filler can have between 20% – 25% savings in embodied energy when compared to a reinforced concrete flat slab (Reddy, 2009; Venkatarama Reddy, 2004). Computational design methods have also gained traction in the design of filler slabs for sustainability goals. One example of this, is design optimization research by Fiala & Hájek. which considered optimization of filler slabs for environmental performance (embodied energy, carbon and sulfur content) (Fiala &

Hájek, 2007). With respect to operational energy, Mastrucci and Rao used a parametric building model of single and multifamily homes and found that life cycle energy and upfront investment costs of filler slab roof designs resulted in 7-8% savings of both metrics when compared to a convention reinforced concrete roof (Mastrucci & Rao, 2019).

Thermal performance has also begun to be formally investigated in filler slab systems. Acharya et al. whom used genetic algorithms to select filler material and geometry that would minimizing the U-value of filler slabs. This work also compared the theoretical U-values for these systems to targets for roof U-values in the Energy Conservation Building Code (ECBC) of India and found that filler slabs alone are not sufficient to meet these targets (Acharya et al., 2020). However, filler slabs were still a significant improvement over, solid reinforce concrete roofs that are popular in self-built construction in India. Gavali and Ralegaonkar created a BIM model to compare the thermal performance of a single story residential building with a filler slab roof compared to a conventional reinforced concrete flat slab roof and were able to quantify both embodied and operational energy for their case studies, but only with respect to one type of filler material – hollow clay block (Gavali & Ralegaonkar, 2019). Lastly, Vijayalazmi and Antony performed a field study on a residence in Kerala, India to determine the indoor air temperature difference, and thermal storage metrics such as decrement factor and time lag and saw that the filler slab performed significantly worse for these metrics as compared to a bamboo roof (Vijayalaxmi, 2023). The poor comparative performance of the filler slab, is not surprising, as work on thermal mass by Gascon-Alvarez et al, has shown that it would be more beneficial to increased exposed surface area with ribbing on the interior of the roof element (Gascón Alvarez et al., 2021), whereas the filler material covers up the exposed surface, that would otherwise be provided by the ribbing. This existing research highlights the values of optimization in increasing the performance of filler slabs and/or in quantifying thermal performance metrics, but none of these studies considers structural efficiency or material quantities.

This thesis investigates structural assumptions and best practices in materially and thermally efficient filler slab design using a formalized computational optimization workflow and proposes a method for evaluating emerging and alternatives to traditional filler materials for other global contexts and material availability constraints in Chapter 4.

2.5 Materially and global context-informed fabrication

As illustrated through the development and growth of filler slab use in India, the decision of typology for a structural system is not always driven by material efficiency and sustainability but is the result of a host of factors including: material and labor cost, structural engineering knowledge, fabrication technology availability, and user acceptance of a specific technology. The integration of all these factors leads to a contextually relevant structural system,

The cost of skilled construction labor and materials varies vastly country to country. However, Ismail makes a distinction between More Economically Developed Countries (MEDCs) and Less Economically Developed Countries (LEDCs) to help illuminate trends in residential development cost. For MEDCs such as the United States and United Kingdom, materials and labor costs are closer to parity ranging from between 45-55%, whereas LEDCs, such as India,

where Filler Slabs have grown to prominence, the materials cost dominate, comprising over 75% of the residential construction cost (M. A. Ismail, 2023).

Globally there has been great unveiling of the greater economic and supply chain sensitivities of construction to global events such as the Covid-19 pandemic and the war in Ukraine for both MEDCs and LEDCs. Arcadis, a global sustainable design consulting firm, details many of these consequences in their annual International Construction Cost Index which highlights significant increases in commodity prices in 2021 including up to a doubling of the cost of iron ore, which is significant in steel production. This report also mentions that rising energy costs have led to a price increase of between 10 – 15% for cement, and this has only been exacerbated by the invasion of Ukraine (Beard et al., 2022). Outside of material manufacturing and procurement cost, overall construction costs can have a significant impact, as the cost of staffing the projects for the duration of a build is significant (J. Wight, 2016). Thus, designs that take advantage of standardization and can in theory be built more rapidly may be favored in some contexts.

Of course, this conversation about context-driven construction must include the use of emerging fabrication methods to supplement human labor and realize complex geometric forms at scale. A large area of construction and architectural research has been dominated by digital fabrication, or the use of digital software and computationally controlled machines to supplement the physical design realization process. One exciting candidate that has emerged for concrete construction is that of additive manufacturing or 3D printing. The layered extrusion process contains the potential to realize complex and/or curved geometric forms without formwork or material waste. In large, 3D printing of concrete has referred to in situ printing of walls for single story construction, but has garnered much popular attention in academia and practice (Paolini et al., 2019). While additive manufacturing may seem like an immediate equalizer for the realization of complex form in labor constrained construction contexts, there is still much territory to cover before additive manufacturing is a viable solution, at scale for many reasons including upfront capital cost of machines, print volume and carbon material intensity of printable mortar.

With respect to the carbon intensity of the 3D printing material, researchers have turned to earth and clay-based printing alternatives as a low carbon and locally available material. The other challenge relevant to this dissertation is that currently, 3D printed spanning systems at a scale representative of a column grid (3m-5m) is quite challenging structurally due to the discontinuous behaviors across the print layers and difficulties in integrating traditional steel reinforcement. Compression-only spanning systems such as vaults can be printed without support material and alleviate reinforcement concerns, but cannot yet be printed at these lengths. Recent research has found promising innovation in the journey to realized 3D printed spanning systems with the use of 3D printed shell and vault formwork (Curth et al., 2022) and infill blocks (Digital Structures et al., 2022).

One emerging truth in the research and development of floor systems is that while they all share the same basic structural goals, the material and geometric modes to accomplishing this are incredibly context dependent. This is due to a complex relationship between natural and material resource access, labor availability and compensation practices, as well as knowledge dissemination and user acceptance. For example, a filler slab with Mangalore tiles may be a well-accepted and easy to implement solution in south India, but when considering the transfer

of filler slab technology to a region with no manufacturing infrastructure or waste stream availability for such tiles, the solution may prove more complex from a design standpoint and more expensive and energy intensive than the original context. What is needed are methods for efficient spanning system design that are flexible enough to accommodate these context dependent concerns of material choice and labor intensity, etc., but also help achieve the shared goal of providing a comfortable standard of living to all while minimizing impact on the environment. Furthermore, there also needs to be investigation of commonly held design standards and practices that prevent the proliferation of high performing material systems. This is the only way that structural engineering can fully embrace computation to supplement and support the development of new domain knowledge.

3. Data-driven design of standard two-way concrete systems

This chapter demonstrates how computation, established closed-form expressions, and building code can be used to access materially efficient and cost optimal concrete spanning structures in common, currently deployed typologies – i.e. flat cast-in-place slabs and two-way joist or waffle slabs. Furthermore, by considering concrete slab design as an opportunity for design space exploration rather than as a solved problem with serial, rule of thumb-based methods, feasible solutions that are better for a given building program or economic context may be found. This chapter makes use of the American Concrete Institute (ACI) building code and considers a North American context, but the approach is flexible enough to be applied in any region.

This chapter makes the following contributions:

1. Section 3.3.1: Demonstration of the utility of parametric design and design space exploration techniques to find feasible high performing reinforce concrete flat and waffle slab solutions that outperform ones found with serial sizing methods and rule of thumb benchmarks.
2. Section 3.3.3: Highlights and quantifies the environmental benefits of using waffle slab typologies at shorter spans than generally suggested in concrete design guides.

3. Section 3.3.4: Extends carbon, mass and cost analysis to consider the benefits and tradeoffs of certain commonly proposed carbon intervention policies ranging from low-carbon cement substitutes to decarbonization of steel production.

3.1 Background and state of the art

3.1.1 Two-way flat slabs and waffle slab analysis methods

Two-way flat concrete slabs are a type of horizontal spanning element where both the aspect ratio in plan and supports conditions lead to a distribution of gravity loads in two orthogonal directions. Waffle slabs are a sub-category of a two-way slab, that not only see this bi-directional load distribution, but additional rigidity from its geometric form of evenly spaced ribs running in both directions. Both systems are well-described in concrete structural and design literature dating back to 1910 and textbook design aids (Allen and Iano 2011; Ching et al. 2014; Kamara and Novak 2011).

In 1914, Nichols derived an expression for the total static moment in a concrete bay, which was followed by Westergaard and Slater in 1921, with a method for the distribution of the bending moment throughout a square slab bay (Faulkes 1974). This work led to the establishment of the Direct Design Method (DDM) published in the ACI building code which saw its last major update in 1971 based on experimental testing of $\frac{1}{4}$ scaled prototypes of 3x3 concrete panels at the University of Illinois (Gamble, Sozen and Siess 1961).

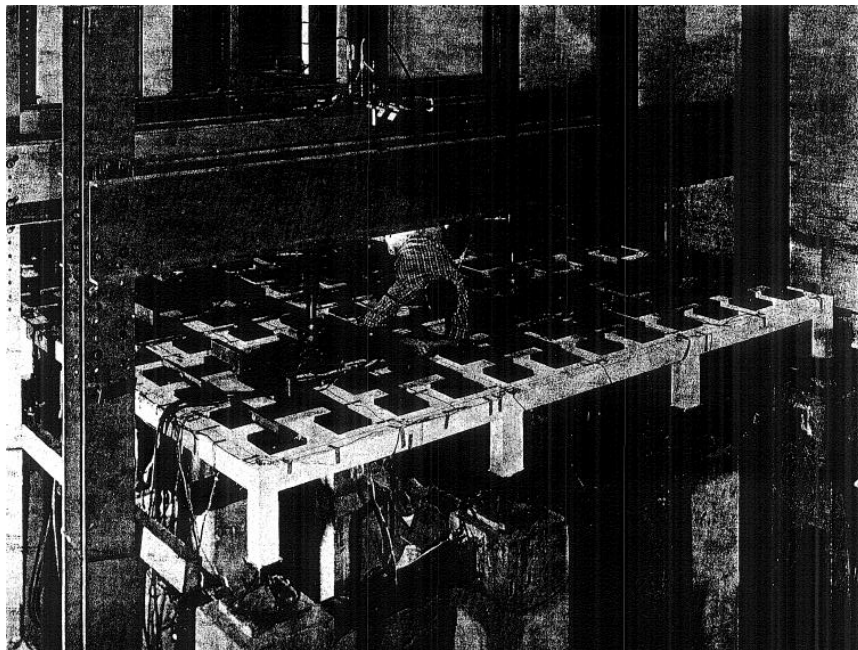


Figure 3-1: View of test structure from Gamble, Sozen and Siess experimental study of a two-way floor slab

Waffle slab design has also been pursued according to the DDM, often with the design of an “equivalent thickness solid slab” or with load, moment, and shear reduction factors. Other approximation methods of analysis for waffle slabs include but are certainly not limited to the Rankine-Grashoff Method (Rankine 1857), orthotropic plate theory (Timoshenko and

Woinowsky-Krieger 1959), effective modulus of elasticity (Abdul-Wahab and Khalil 2000). There is also the use of experimental testing of scaled waffle slabs (Schwetz et al. 2014), and tools such as SAP 2000 and other finite element analysis solvers for the validation of waffle and rib slab design.

This work takes advantage of DDM which is relatively easy to integrate with computational tools and programming languages such as MATLAB or Python to enumerate multiple designs with a fine level of variable resolution of depths and reinforcement ratios without the temporal penalty of FEA. In addition, DDM can be applied broadly to the two main typologies in this work and allows for relative comparison between solutions produced across the typologies, spans, and loading.

3.1.2 Critique of rule of thumb approaches in architectural and structural engineering

Rules of thumb are guidelines that allow designers to quickly approximate a single solution from an accumulation of learned best practice, and perhaps bypass complex analysis methods (such as some described in 3.1.1.) in the early design stage. They are the encapsulation of years of domain knowledge that can be a trusted basis for safe and reliable design practice. However, rules of thumb for structural systems in particular are not often updated, even as new knowledge is gained about performance, tools of analysis have evolved, and new metrics to interrogate what it means for a structural element to perform satisfactorily emerge. This is especially important with respect to the impact of the materialization of structural systems on the built environment, as most of the rules of thumbs consider structural feasibility and safety only, and not metrics related to material efficiency (such as embodied carbon and mass). While the value of rules of thumb are apparent in early stage design approximation, education and engineering practice (Gainsburg, 2003; Rashidi & Sorooshnia, 2020; Ryan et al., 2001), there is always room for reconsideration of this approach with the acquisition of new domain knowledge and desire for more materially efficient design, early in the design process.

For concrete flat slab elements specifically, Radford, Hung and Gero derived new rules of thumb for the design of one-way concrete floor systems to ensure reduced deflection and an economical floor system. This was done with the use of Pareto optimality to inform design rules regarding element sizing (namely structural depth), slab typology, concrete strength, to lead to structurally feasible designs and corresponding expressions to estimate cost (Radford et al., 1984). More recently, Scanlon and Lee proposed an update to the code-based design guideline – which could also be thought of as a rule of thumb – to determine minimum slab depth to not just rely on span, but to also consider applied loads, cracking and time-dependent effects. This updated expression for minimal depth also allowed for differences in prescribed depth based on the one-way or two-way action of the concrete slab and presents deflection as a non-linear function of span (Scanlon & Lee, 2006).

More broadly, several critiques and revisions of rules of thumb with respect to energy use in buildings have also emerged. Slee and Hyde examined current rules of thumb for thermal mass calculations, and proposed the incorporation of holistic building system design and climate specific information to satisfy new building energy savings requirements in Australia (Slee &

Hyde, 2011). Eberhart et al. developed qualitative design guidelines for the design of building components for circularity and used life cycle analysis (LCA) and material flow analysis (MFA) to determine the percentage change on metrics such as global warming potential and material consumption that design interventions for circular building structure can have (Malabi Eberhardt et al., 2021). Petrova et al. suggests using semantic modeling on real building operation data and BIM models to find “motifs” in the performance data and temporal association rule mining techniques to generate energy efficient building design rules with higher fidelity than current building design rules of thumb (Petrova et al., 2019). It is clear that the field has arrived at a nexus point in allowing computation to provide substantive improvement to rule of thumb design practices, for nonintuitive relationships between design form and performance.

3.1.3 Parametric design of flat concrete slabs and waffle slabs

One path forward for high performing design of concrete slabs is data-driven design of concrete slab systems empowered by dense exploration of the design space. As stated in Chapter 2, a parametric model, in this work, is a digital representation of an engineered object, where a set number of critical features and geometric relationships (parameters) are used to define its full form. These models are often couple with sampling schemes and or optimization algorithms to ascertain high performing, optimal structural design solutions.

Cost is a commonly targeted objective for optimal design of concrete spanning systems and features prominently in many parametric design and optimization studies. Sahab et al. performed a study on reinforced concrete flat slab buildings that utilized the equivalent frame method (EFM) for structural analysis and combined both genetic algorithms and exhaustive search methods to find optimal building designs. This work demonstrated that floors were the largest part of the cost and that reinforcement cost savings were the greatest when moving from a conventional to an optimal design (Sahab et al., 2005). Research interest in using parametric workflows to optimize cost has also extended to waffle slab systems and have focused mainly on the feasibility of solving such a highly constrained design problem with a variety of heuristic algorithms (Galeb & Atiyah, 2011; Olawale et al., 2020; Shayegan et al., 2020) versus the generation of general design knowledge of the waffle slab systems.

With respect to embodied carbon efficiency of concrete buildings and structures, several works have recently used parametric design as a means of accessing high performing design systems in complex and constrained design spaces. Hartwell and Mueller coupled parametric modeling and design optimization of filler slab systems which revealed that the optimal embodied energy design of these two-way ribbed systems (which behave structurally as waffle slabs) does not just require carving away material to the neutral axis of an equivalent depth flat slab, but actually leads to an increase in the structural depth of the slab (A. J. Hartwell & Mueller, 2021). Jayasinghe et al. recently used parametric design to evaluated the embodied carbon performance of concrete flat slabs given a variety of depths, column spacing and concrete strengths and found governing criteria such as fire proofing, prescriptive deflection limits and column design that has the greatest impact on embodied carbon performance (Jayasinghe et al., 2022). The Concrete Center also has published an embodied carbon comparison across concrete structural systems, including waffle slabs, which are a focus of this chapter. This report queries several key variables including span and loading and highlights the impacts those factors have in conjunction

with structural system selection on embodied carbon content. However, with respect to waffle slabs, there is no info presented in this study on the sizing of the voids its self, with respect to the spans, which does have a significant impact on savings as shown in the results of this chapter (The Concrete Center, 2022). This is important as general waffle slab design is based on preselection of a catalogue of a few pan sizes for the formwork, and are not “optimized” for the size or loading conditions of a structure.

With respect to multi-objective study of both cost and carbon, Yeo and Potra used constrained optimization to compare the design outcomes of cost and embodied carbon of a reinforced concrete frame under gravity and lateral loading and found that optimizing a design for embodied carbon versus cost lead to solutions with 5% - 15% less carbon. However, these values increase with the addition of compressive forces (such as that of a high-rise building) (Yeo & Potra, 2015). More recently, Gauch et. al performed a comprehensive early-stage design study of multi-story buildings with simple rectangular and complex plan layouts and a variety of framing, grid layout and floor systems including reinforced concrete flat slabs. This work demonstrated that while concrete flat slabs were the most cost-efficient structural solution, the carbon emissions associated with the system scale significantly with increasing span unlike other systems such as steel decking or glulam and CLT. It also highlighted that the choice of using a cost or carbon objective function did not significantly impact the actual embodied cost and carbon of the optimal solutions (Gauch et al., 2022). Gauch et al. acknowledges that the depth specification of the floor slabs in this publication are chosen through span to depth ratios and could be further optimized. Although this chapter here focuses only on two systems in particular, flat slabs and waffle slabs, the analysis makes use of code-accepted, semi-empirical analysis that calculate deflection and consider the non-linear behavior of concrete, in a way that is computationally efficient and suitable for the early design stage.

Building on previous work, this chapter exemplifies how design space exploration techniques such as sampling and data visualization can be used to access optimal design solutions across multiple performance metrics. It presents parametric design as a way to move towards the creation of generalized knowledge for readily deployed reinforced concrete slab typologies – the flat slab and the waffle – in vast design spaces. Finally, this work shows that with closed-form computational analysis and code-based design approaches, there are more optimal design solutions that can be found with typology change and currently available design and fabrication methods vs. material substitution or more speculative strategies for carbon emissions reduction in the built environment.

3.2 Methods for design parameterization, analysis, and data collection

This work provides a comprehensive study and comparison across two reinforced concrete spanning systems capable of exhibiting two-way action: the flat slab and waffle slab, the latter of which is typically only elected for long clear spans. Through enumeration across geometric variables that can be specified by structural engineers and exploring the subsequent design space, it is possible to see advantages and tradeoffs of each slab typology as well as the bounds of feasibility for a variety of different spans and architectural programs. This also illuminates regions of the design space that contain slab designs with greater savings that may not be

accessed with rule-of-thumb designs or structural optimization. The general computational workflow used to achieve these goals are outlined in Fig. 3-2.

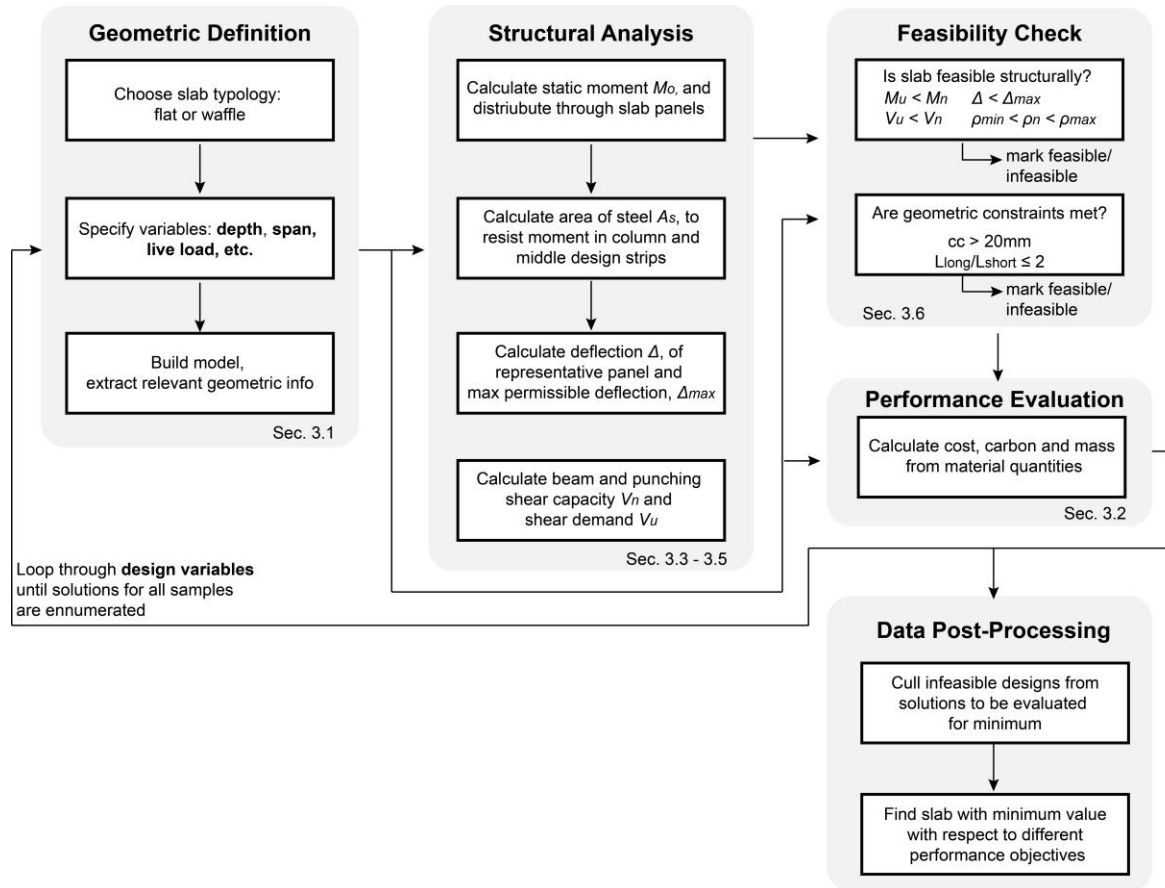


Figure 3-2: Diagram of computational workflow used to design, evaluate and select optimal flat and waffle slabs

3.2.1 Parametric model definition and design space sampling

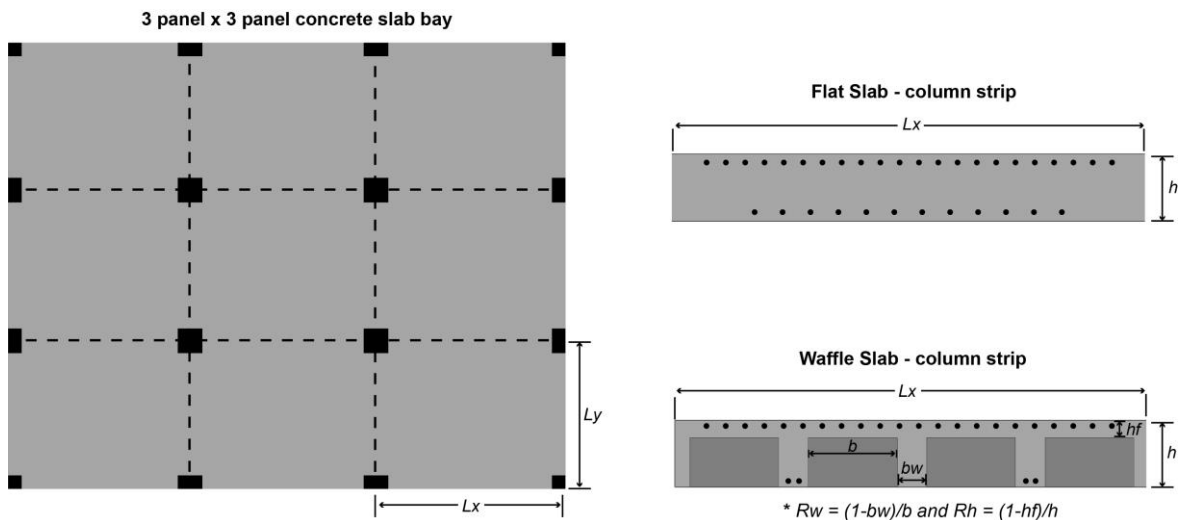


Figure 3-3: Illustration of plan view of 3x3 bay (left) and single concrete slab models for analysis (right).

The basis of this work is a parametric model of both flat and waffle reinforced concrete slabs which are structurally engineered according to processes described in the remainder of this section. This model (Fig. 3-3) comprises a 3 x 3 bay of reinforced concrete slabs supported by columns with no interior or edge beams in the structural system. Drop panels near the columns are also added to resist punching shear failure. It should be noted that this additional material volume is accounted for in the performance metric evaluation. With respect to steel reinforcement, it was assumed that #6 imperial bars were used for cover and deflection calculations. A full list of variables for the concrete portion of the slabs considered in this work is provided in Table 3-1.

Table 3-1: Design variable and bounds for flat and waffle concrete slabs

Variable	Description	Bounds
LL	live load applied to slab	$2 \text{ kN/m}^2 \leq LL \leq 12 \text{ kN/m}^2$
Ly	span length in the y direction	$4 \text{ m} \leq Ly \leq 12 \text{ m}$
Lx	span length in the x direction	$4 \text{ m} \leq Lx \leq 12 \text{ m}$
h	total depth of slab	$40 \text{ mm} \leq h \leq 600 \text{ mm}$
----- Waffle Slab Only -----		
Rh	height ratio, determines the relationship between the void or “pan” height to the depth of the slab	$.6 \leq Rh \leq .8$
Rw	web ratio, determines the relationship between the void or “pan” width to the total width of the waffle section, thus setting the size of the web	$.6 \leq Rw \leq .8$
s	rib spacing, how many meters per rib section	$.125 \text{ m/rib} \leq s \leq 1 \text{ m/rib}$

The span ranges considered for Ly and Lx represent the extremes of what historically has been built with a flat slab horizontal structural system. In addition, these spans allow for structural engineers and designers to consider column density as it relates to their programmatic needs from residential spaces to warehouse spaces. Similarly, the live loading variable bounds also were chosen to assist with early stage design across different program types according to the minimum design load criteria specified by ASCE 7 (ASCE, 2017). The range of structural depths considered in this study was chosen to ensure that feasible solutions could be found for each selected span. With respect to the waffle slab design variables, the height ratio, Rh and web ratios, Rw , were chosen by looking at precedent waffle slab void to solid ratio and “pan sizing” guidelines (Allen & Iano, 2011; Ching et al., 2014). These variables were varied together and specified in the typology selection portion of the workflow in Fig. 3-1, but the model is flexible enough to allow for a decoupled exploration of pan sizing. Although it is possible to search for structural solutions outside these bounds, it is highly unlikely that a structural solution would be selected by designers, and our studies show feasible designs outside these range did not yield savings in these regimes.

With the variables ranges outlined in Table 3-1, a grid sampling scheme was pursued to cover the design space totaling 68,300 samples for both the flat and waffle slab typologies. This is

implemented in MATLAB with a nested loop structure. For a design space with a moderate number of design variables such as the case with the flat and waffle slab model, sampling captures insights and trends from the full design space. It should be noted that formal optimization is not pursued, but rather a search is performed across the solution sets, after the infeasible solutions have been culled. The goal of this search is to find the design that provides a minimal value for a given performance metric (outlined in Section 3.2.12). This is what is being referred to in this work by “optimal.” This approach is practical because of the relatively small number of variables and the analytical nature of the structural engineering calculations, and surpasses challenges found with global optimization methods, which have been found to often struggle with nonconvexity and complex feasibility boundaries in reinforced concrete problems.

3.2.2 Slab design performance metrics and evaluations

Four metrics were considered to compare the solutions generated including structural depth, mass, embodied carbon, cost. Structural depth refers to the total depth, h , of the concrete slabs in the parametric model and is one of the user variables. Structural depth is an important metric as most rules of thumb for concrete slab design specify a target depth for given programs, supports conditions etc. A related variable is d , which refers to the depth from the top of the slab to the center of the rebar. The next metric, mass, is one of the most valuable metrics to consider, as the self-weight of the floor can have significant downstream effects on the amount of material needed for columns and foundations. Mass of the element is calculated using the density of the concrete and steel (2400 kg/m^3 and 8050 kg/m^3 respectively) as well as the volumes extracted from the model.

The volume of steel is calculated based on the moment demand and ductility constraints and that volume is subtracted from the prismatic volume representing solid concrete in the model. Embodied carbon (EC) represents the carbon footprint from the extraction, processing and transportation and construction of the model elements from their raw material. This is found using Eq. 3.1, where the ECC represents the embodied carbon coefficient and m represents the mass of material used in a particular design. These coefficients are set to $0.15 \text{ kgCO}_2/\text{kg}$ for concrete and $1.99 \text{ kgCO}_2/\text{kg}$ for reinforcing steel (Anderson & Moncaster, 2020; Jones & Hammond, 2019). It should be noted that this work initially assumes the use of ready-mix concrete with a compressive strength of 40 MPa.

$$EC_{total} = (ECC_{concrete} * m_{concrete}) + (ECC_{steel} * m_{steel}) \quad Eq. 3.1$$

Finally, cost similarly is calculated via the extraction of material quantities from the parametric model and the unit costs for materials from Building Construction Cost with RS Means 2022. The unit costs used in this study are $\$205/\text{m}^3$ ($\$.09/\text{kg}$) for concrete and $\$2.86/\text{kg}$ for steel (Doheny, 2022). These costs will vary if other grades of steel or concrete compressive strengths are used but generally a total can be found using Eq. 3.2

$$Cost_{total} = (Cost_{concrete} * v_{concrete}) + (Cost_{steel} * m_{steel}) \quad Eq. 3.2$$

Ultimately comparison of these metrics across different programs and structural systems speak to how one can evaluate material quantity and utilization to stakeholders.

3.2.3 Moment analysis with the Direct Design Method (DDM)

The following work focuses on column supported flat and waffle slabs for which ACI 318-14 suggests two methods for analysis – direct design method (DDM) and equivalent frame methods (EFM). DDM was pursued given the standard geometry of the parametric model, the ease of implementation, and reduced computational cost of the semi-analytical method into a computational workflow, when compared to both EFM and Finite Element Method (FEM) analysis. The conclusions drawn in this work speak to broader trends in the design space, and can highlight high-performing solutions for further analysis with other methods if desired. Following the DDM leads to accurate moment analysis given that several limitations are met regarding the number of continuous spans required in each plan direction, panel aspect ratios and loading. Further detail and more scenario-based coefficients can be found in ACI 318-14, Section 8.10.

3.2.4 Reinforcing steel calculations and ductility constraints

Once the moment demand for the respective column and strip sections in a span can be calculated, these values can be used to calculate the area of steel required to resist the moment. This method is similar to the Portland Cement Association’s simplified design method and is adopted from Ismail and Mueller work in the design and analysis of concrete beams with arbitrary section size (M. A. Ismail & Mueller, 2021). The required area of steel can be found given the moment demand M_u , as well as the yield strength of the reinforcing steel f_y , the compressive strength of the concrete f'_c , and a target reinforcement ratio ρ_n , which is estimated as 66% of the maximum allowable reinforcement ratio, ρ_{max} . This is outlined in Eq. 3.3.

$$A_s = \frac{M_u}{.87f_y d \left(1 - 1.005\rho_n \frac{f_y}{f'_c}\right)} \quad \text{Eq. 3.3}$$

Additionally, the maximum reinforcement ratio is found by considering the type of failure desired for an element – in this case a tension-controlled ductile failure. This can be calculated using Eq. 3.4 where $\epsilon_{concrete}$ is the crushing strain of the concrete and $\epsilon_{tensile}$ is the net tensile strain desired for the element. These values were set to .0035 and .0040 respectively.

$$\rho_{max} = \frac{.36f'_c}{.87f_y} \left(\frac{\epsilon_{concrete}}{\epsilon_{concrete} + \epsilon_{tensile}} \right) \quad \text{Eq. 3.4}$$

A lower bound for reinforcement ratio, ρ_{min} , can be found using Eq. 3.5. This is derived by equating the cracking moment to the strength of the cracked section and ensures that the beam will not fail at the formation of the first flexural crack.

$$\rho_{min} = .25 \frac{\sqrt{f'_c}}{f_y} \quad \text{Eq. 3.5}$$

The actual reinforcement ratio, ρ , is calculated given A_s and the section dimensions. If the actual required ρ is higher than ρ_{max} this means that the moment capacity of the element M_n within the ductility limits is not sufficient to resist the bending moment in the section. (Generally speaking, the insufficient steel will also result in a violation of the deflection constraint as well). However, if ρ is below the minimum, more steel can be added to the section to meet the ductility limits. This logic is incorporated into the analysis code and applied automatically, including a flag for “infeasible” designs that cannot be reinforced to meet moment demand while failing in a ductile manner.

3.2.5 Shear design of two-way concrete slabs and preliminary column sizing

Shear design is of particular importance for concrete slab and flat plate design. This is especially true for the case study presented in this work as the slabs are designed such that the concrete section alone is responsible for the total shear resistance (typical in slab design). To ensure a greater number of feasible designs in the design space, drop panels are added around the columns to resist punching shear. In order to complete the shear demand and resistance calculations, estimates on expected column and drop panel sizing had to be made using code and practice guidelines. This study is chiefly concerned with the optimization and design of the spanning elements, and not the framing system and thus, there is no guarantee proposed columns themselves are optimal.

Textbook references proposes a square column with a side length L_{column} , that is at least twice the depth of the slab for preliminary design for two-way flat slabs (Allen & Iano, 2011). This sizing estimate generally holds for waffle slabs, yet the guide makes provisions for a column size reduction or increase depending on the loading scenarios. For drop panels, minimum width is dictated by ACI 318-14 Section 8.2 which states that a drop panel’s total width, L_{drop} , should be at least a third of the span of a slab and the additional depth below the slab, d_{drop} , should be at least one quarter the depth of the main slab element. With these dimensions L_{column} , L_{drop} and d_{drop} , it is possible to calculate a slab’s shear demand and resistance.

Two forms of shear strength must be accounted for in the design of flat slabs. The first is a beam shear behavior which models the entire slab as a beam spanning between the column supports. The second is punching shear which considers a shear failure occurring along the face of the supporting column(s) (Darwin et al., 2010). For a flat slab with no additional shear reinforcement, Eq. 3.6 and Eq 3.7 describe beam shear and punching shear, respectively in metric units.

$$V_{n,beam} = .17\lambda\sqrt{f'_c}b_wd \quad \text{Eq. 3.6}$$

$$V_{n,punching} = .33\lambda\sqrt{f'_c}b_o d \quad \text{Eq. 3.7}$$

$$b_o = 4(L_{column} + d) \quad \text{Eq. 3.8}$$

In Eq. 3.6 and Eq. 3.7, λ is a modification factor based on the concrete mix used. In this study we assume normal weight concrete and therefore this factor is equal to one. Factors such as b_w refers to the width of the slab element for a flat slab and the width of the web (or rib width) for a waffle slab, and d refers to the effective depth of a slab. Eq. 3-8 can be used to find b_o , which is defined as a critical perimeter surrounding the column.

Shear demand can be found by considering the appropriate tributary area for both beam shear behavior and punching shear behavior. The shear demand can be found using Eqs. 3.9 – 3.11. where the tributary area will vary depending on which shear action is being accounted for, and whether or not drop panels are present.

$$V_u = q_u * A_{tributary} \quad \text{Eq. 3.9}$$

$$A_{tributary,beam,y} = L_y \frac{L_x - L_{drop,x}}{2} \quad \text{Eq. 3.10}$$

$$A_{tributary,punching} = (L_y * L_x) - (L_{drop,x} * L_{drop,y}) \quad \text{Eq. 3.11}$$

3.2.6 Serviceability and prescribed minimum depth

Generally, one benefit to using the rules of thumb in the early design stage of slabs is they prescribe slab depths conservatively, with the assurance that the deflection serviceability requirement will be met. While this is an advantage, it could in many cases lead to an overestimate of material needed for a feasible slab design solution. In this work, slab depths are a variable and not necessarily linked to span length. For a slab with drop panels/solid heads near the columns, and no edge beams, the suggested minimum slab depth is given by Eq. 12. where L is the long span in the element being designed (ACI Committee 318 et al., 2016).

$$h_{min} = \frac{L}{33} \quad \text{Eq. 3.12}$$

In this work, deflection is found with an equivalent frame approximation method established by Nilson and Walters which maintains the same definitions of column and middle strips from the direct design method and applies a formulation for deflection of a slab as a result of combined bending from x and y directions (Nilson & Walters, 1975). The subsequent section summarizes key expressions to determine long-term deflection of a characteristic panel in the 3x3 panel array as well as highlights differences that must be headed when considering a waffle slab versus a rib slab for analysis.

3.2.7 Moment of inertia and section properties

Under the service loading of a reinforced concrete member, it is not unusual for flexural cracks to form. This means that traditional beam equations for elastic deformation of isotropic materials are no longer applicable in their most basic forms. It is still important to find the gross moment of inertia for the section under analysis which varies for a flat slab and to a waffle slab strip under analysis. In Eq. 3.13, the b is equal to the span length (L_x or L_y) as it is easy to consider the full rectangular span at once for the equivalent frame analysis. For a waffle section, the gross moment of inertia is found for an individual T-section of a waffle strip and then multiplied by the number of ribs in the strip (Eq.15). Here b_f refers to the effective flange width of the T-section as defined by ACI 318-14 Section 6.3, b_w refers to the width of the web, h_f refers to the height of the top flange portion and y_t is the distance between the neutral axis of the T-section and the tension face. Another layer of complexity is added when one considers that if a frame strip is being analyzed, there are solid rectangular sections near the columns from the drop panels that must be accounted for in addition to the T-rib sections. This is described in greater detail for a waffle slab in the materials published by the Portland Cement Association (Portland Cement Association, 2018).

$$I_{g,flat} = \frac{bh^3}{12} \quad \text{Eq. 3.13}$$

$$y_{t,flat} = h/2 \quad \text{Eq. 3.14}$$

$$I_{g,waffle} = n_{ribs} \left\{ \left[\frac{(b_f - b_w)h_f^3}{12} \right] + \left[\frac{b_w h^3}{12} \right] + \left[(b_f - b_w)h_f \left(h - \frac{h_f}{2} - y_t \right)^2 \right] + \left[b_w h \left(y_t - \frac{h}{2} \right)^2 \right] \right\} \quad \text{Eq. 3.15}$$

$$y_{t,waffle} = h - \frac{b_w h^2 + (b - b_w)h_f^2}{2[b_w h + (b - b_w)h_f]} \quad \text{Eq. 3.16}$$

The gross moment of inertia for a section considers an uncracked section with no reinforcing steel, but the opposite extreme, which would be a completely cracked section, must be analyzed as well. I_{cr} , the moment of inertia of the cracked-transformed section, describes a beam where all

the concrete in the tension zone of the beam has been cracked and accounts for a steel-equivalent amount of concrete (transformed). Eq. 3.17 details a general expression for I_{cr} , where A_s is sum of the reinforcement (positive and negative considered separately) spanning the analysis strip, and kd is the depth of the compressive region.

$$I_{cr} = \frac{b(kd)^3}{3} + nA_s(d - kd)^2 \quad \text{Eq. 3.17}$$

$$kd = \frac{\sqrt{2dB + 1} - 1}{B} \quad \text{Eq. 3.18}$$

$$B = \frac{b}{nA_s} \quad \text{Eq. 3.19}$$

$$n = \frac{E_{steel}}{E_{concrete}} \quad \text{Eq. 3.20}$$

I_g and I_{cr} can be combined with material strength and load-based parameters such as M_{cr} , the cracking moment and M_a , the maximum applied moment, to calculate the effective moment of inertia, I_e for the strip under analysis. This method was developed by Branson and is summarized by Eq. 3.21 (Branson, 1977).

$$I_e = \left(\frac{M_{cr}}{M_a}\right)^3 I_g + \left[1 - \left(\frac{M_{cr}}{M_a}\right)^3\right] I_{cr} \quad \text{Eq. 3.21}$$

M_a can be found taking the frame strip under analysis and finding the maximum moment value along its span. M_{cr} , however, is a function of the modulus of rupture of the concrete, f_r , y_t , and I_g and can be found using Eq. 3.22 and 3.23.

$$M_{cr} = \frac{f_r I_g}{y_t} \quad \text{Eq. 3.22}$$

$$f_r = .62\sqrt{f'_c} \quad \text{Eq. 3.23}$$

In the case of a section with drop panels, a variation in effective moment of inertia across the frame strip, I_e , can be calculated for both the midspan and the end moment sections of the analysis strip and then combined via a weighted average to get $I_{e,avg}$, the average effective moment of inertia for the analysis strip. This must be repeated for both spanning directions.

3.2.8 Deflection of a rectangular panel and maximum possible deflection

The $I_{e,avg}$ values for the frame strips in the representative panel can now be used to find the deflection, Δ . This is done using an equivalent frame method and is detailed fully in *Design of Concrete Structures* (Darwin et al., 2010). The deflection can be found using Eq. 3.24, where Δ_{cx} and Δ_{cy} are the deflections at the midspan of the column strips in the x and y direction, Δ_{mx} and Δ_{my} are the deflection at the midspan of the middle strips in the x and y directions, and λ_{Δ} is a long-term deflection multiplier. The deflection contributions of the column strip and middle strips can be found using Eq. 3.25 and 3.26. It should be noted that if the representative panel chosen is a center panel, as is the case here, then it is fully continuous over the supports, meaning support rotations would be negligible.

$$\Delta = \frac{(\Delta_{cx} + \Delta_{my}) + (\Delta_{cy} + \Delta_{mx})}{2} * \lambda_{\Delta} \quad \text{Eq. 3.24}$$

$$\Delta_c = \Delta_{f,ref} * DF_{2,col} * \frac{I_{e,avg}}{I_{g,column\ strip}} \quad \text{Eq. 3.25}$$

$$\Delta_{f,ref} = \frac{wl^4}{384 * E_{concrete} * I_{e,avg}} \quad \text{Eq. 3.26}$$

The long-term deflection multiplier, λ_{Δ} , which is calculated using Eq. 3.19 where $\xi = 2$, and represents a time-dependent coefficient for a duration of 5 years or more and ρ' is the compressive reinforcement ratio, which in this work is zero.

$$\lambda_{\Delta} = \frac{\xi}{1 + 50\rho'} \quad \text{Eq. 3.27}$$

The deflection can now be compared to the maximum permissible deflection dictated by ACI code, for a given type of horizontal member and support condition. In this work, the deflection limit under dead and live load is equal to span/240.

3.2.9 Post-processing of data for feasibility: direct and indirect constrain application

Table 3-2: General structural and geometric constraints for concrete slab design

Constraint	General Form	Reference Section
Moment	$M_u < M_n$	3.2.3
Shear (Beam)	$V_{u,beam} < V_{n,beam}$	3.2.5
Shear (Punching)	$V_{u,beam} < V_{n,punching}$	3.2.5
Deflection	$\Delta < \max(L_y, L_x)/240$	3.2.8

Ductility	$\rho_{\min} < \rho < \rho_{\max}$	3.2.4
Clear cover	$cc > 20 \text{ mm}$	-
Plan Aspect Ratio	$L_{\text{long}}/L_{\text{short}} \leq 2$	-
Loading	$LL \leq 2 * \text{Self Weight}$	-

The above sections have outlined constraints for moment, shear, and deflection, that would apply in any equilibrium structural loading model as well as some of the geometric and loading constraints dictated by DDM. Table 3-2 details the constraints used to mark designs as infeasible and cull from consideration as optimal designs in the sampled space.

3.3 Results

This parametric design study shows that reductions can be achieved across a variety of metrics of importance for both flat and waffle slabs including embodied carbon, mass, and cost. This is achieved by integrating structural analysis in a computational workflow for sampling and exploration of the design space, as opposed to traditional rule of thumb design methods, which yield a single, not necessarily optimal solution. Looking at the 3x3 bay comprised of flat square concrete panels under residential live load, the computational method in this work yielded savings of 29% in slab depth, 19% of embodied carbon, 28% of mass, and 14% of material cost at the shortest span of 4m (found using benchmarking plots seen in Fig. 4). These saving diminish as span length increases and at 12m optimal solutions found showed negligible differences across those performance metrics.

Additional savings can be achieved with a different concrete slab system, the waffle slab. By changing to the most materially efficient typology in the study, the waffle slab with an 80% void volume, feasible designs for the 3x3 bay were found across the wide range of spans and live loading scenarios that are responsible for between 62% - 67% of the embodied carbon (reduction of 33% – 38%) of a bay with the optimal flat slab panels. The waffle slab system also only comprises 46% - 51% (reduction of 49% – 54%) of the mass of the optimal flat slab panel and lastly 73% – 78% of the material cost (reduction of 22% – 27%). These results, as well as those of waffle slabs with other void volume percentages are further detailed in the subsequent sections. Furthermore, studies on the embodied carbon impact of coupling efficient geometry selection with commonly proposed carbon reduction strategies for the building environment such as cement alternatives and steel decarbonization are detailed in the subsequent section.

3.3.1 Flat square concrete slab studies

The first set of parametric studies look exclusively at flat, square reinforced concrete slabs with drop panels surrounding the columns for punching shear resistance. Fig. 3-4 shows the minimal embodied carbon and cost values that can be theoretically achieved at a given depth for a square flat slab under residential live loading 2 kN/m². The values for embodied carbon and cost have been normalized for the floor area in the 3-panel x 3-panel bay in order to make comparisons across spans. We see that the minimal feasible depth does increase with span, which is supported by literature. Another interesting feature shown in the 4m and 8m span in both the embodied carbon and cost plot is that there is a point in which the performance curves across spans meet

when considering depth (~ 325mm). This indicates a point where the embodied carbon and cost contributions from the concrete start to dominate at a given structural depth.

In the studies performed in this work, it was found that when adhering to code serviceability constraints, the minimal design solution for one metric, such as embodied carbon, serves as the minimal solution across the other metrics considered (structural depth, mass, and cost).

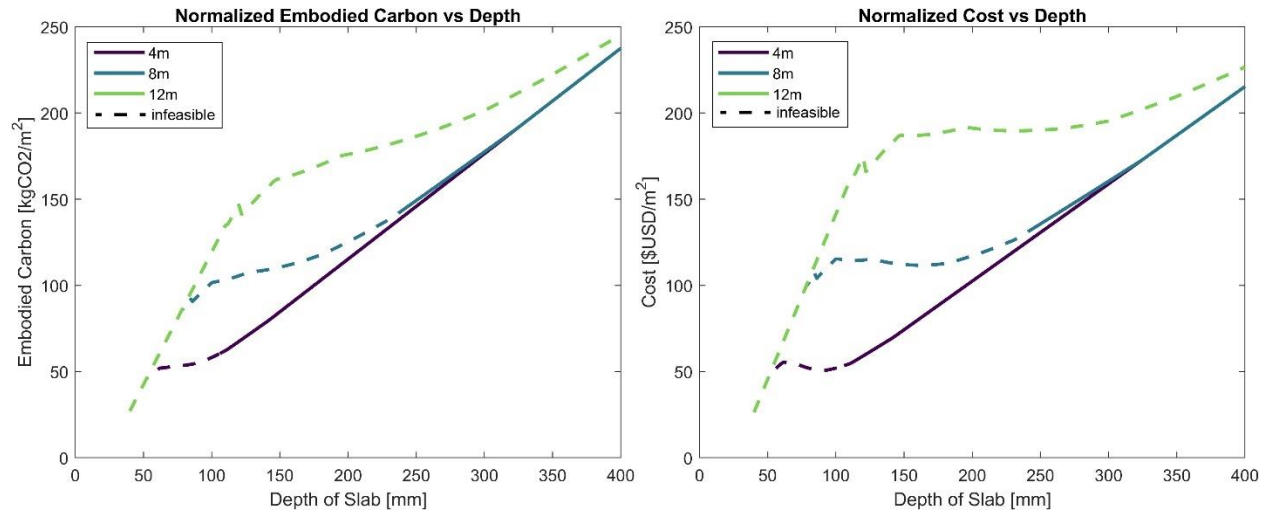


Figure 3-4: Variation with structural depth in embodied carbon (left) and material cost (right) of a square flat slab under residential loading conditions. Infeasible designs do not meet constraints given in Table 3-2.

While Fig. 3-4 provides important benchmarks to understand what is the best (minimal) outcome that can be achieved, it is also useful to know how deviations from the optimal solution impact performance. Fig. 3-5 shows the optimal slab depth for a given span and compares that to the prescribed depth based on the ACI minimum slab thickness rule of thumb, $L/33$. This figure also highlights the region surrounding the optimal solution that shows a 10% performance decrease from the optimal solution with respect to embodied carbon, mass and cost. This helps evaluate how consequential the addition of material can be. These regions are nearly identical for each metric shown (embodied carbon, cost and mass), meaning that under this geometric specification and loading conditions, these metrics carry similar weight.

For a residential live load of 2 kN/m^2 , a design solution can be found at a depth below the ACI minimum up until 5.8m. In fact, the results show that square slabs with spans up to this length that are designed by the rule of thumb minimum will be outside the 10% performance bounds for the three performance metrics. At 8m, the rule of thumb for minimum depth no longer yields design solutions that are feasible. When looking at the optimal flat slab designs for an assembly live-load of 7 kN/m^2 , the analysis method saw an increase in optimal depth and no regions of feasibility across the spans surveyed. As live load increases, this trend persists and there are no spans for which the ACI minimum depth solution is feasible, and a greater slab depth is needed to support the total factored load.

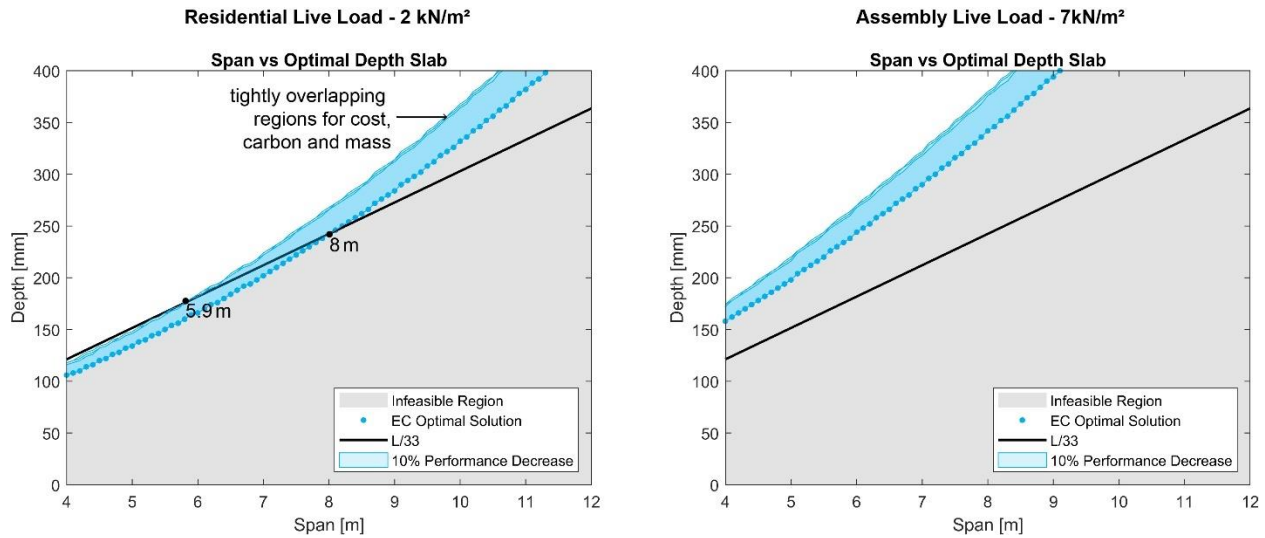


Figure 3-5: Optimal depth for a given span of a flat concrete slab with 1:1 aspect ratio. Application of a typical residential live load of 2 kN/m² (left) and assembly live load of 7 kN/m² (right) are presented.

3.3.2 Design solution space for flat and waffle slab typologies

Whereas the previous section focuses exclusively on square flat concrete slabs (ratio of L_y to L_x is 1:1), it is not always realistic to have a square plan. This subsequent work in this section examines design trends for optimality along aspect ratio for flat slabs and also introduces a comparison between a flat slab and a 70% voided waffle slab. Fig. 3-6 is a section of slices taken of the design spaces of these two typologies, where the optimal embodied carbon depth is shown based on the plan dimensions. The contour lines representing depth are spaced every 50mm. Just as above, minimal solution found via this method for one performance metric also served as the minimum design solution for all. This was even true for waffle slab typologies, where there in theory is more room to negotiate tradeoffs of mass and carbon from concrete and the structural capacity that can be achieved through shaping and steel specification. Several overall conclusions can be drawn from the results shown in Fig. 3-6. The first is that for both typologies, there are a smaller amount of feasible design solutions available with the increase of live load.

This is largely due to violation of the structural constraints. However, for the highest live load and the longest spans in the study, 11m - 12m, there are no structurally feasible solutions for the flat concrete slab typology. This is supported by design guides that recommend joist systems or waffle slabs (two-way joists) under these conditions.

The shape of the contours also provides insight on how moving towards a one-way system would impact the required slab depth. Even spaced concentric contours across the area of the plot show that the optimal embodied carbon depth solution yields the same depth for both one- and two-way systems. This appears to be the case for majority of the feasibly design space for both the flat and 70% void waffle slab. However, under warehouse loading conditions, for the waffle slab, we see a deviation from the concentric contours and it appears that lower structural depths can be found for waffle slabs under high loading conditions as one-way structural action starts to dominate.

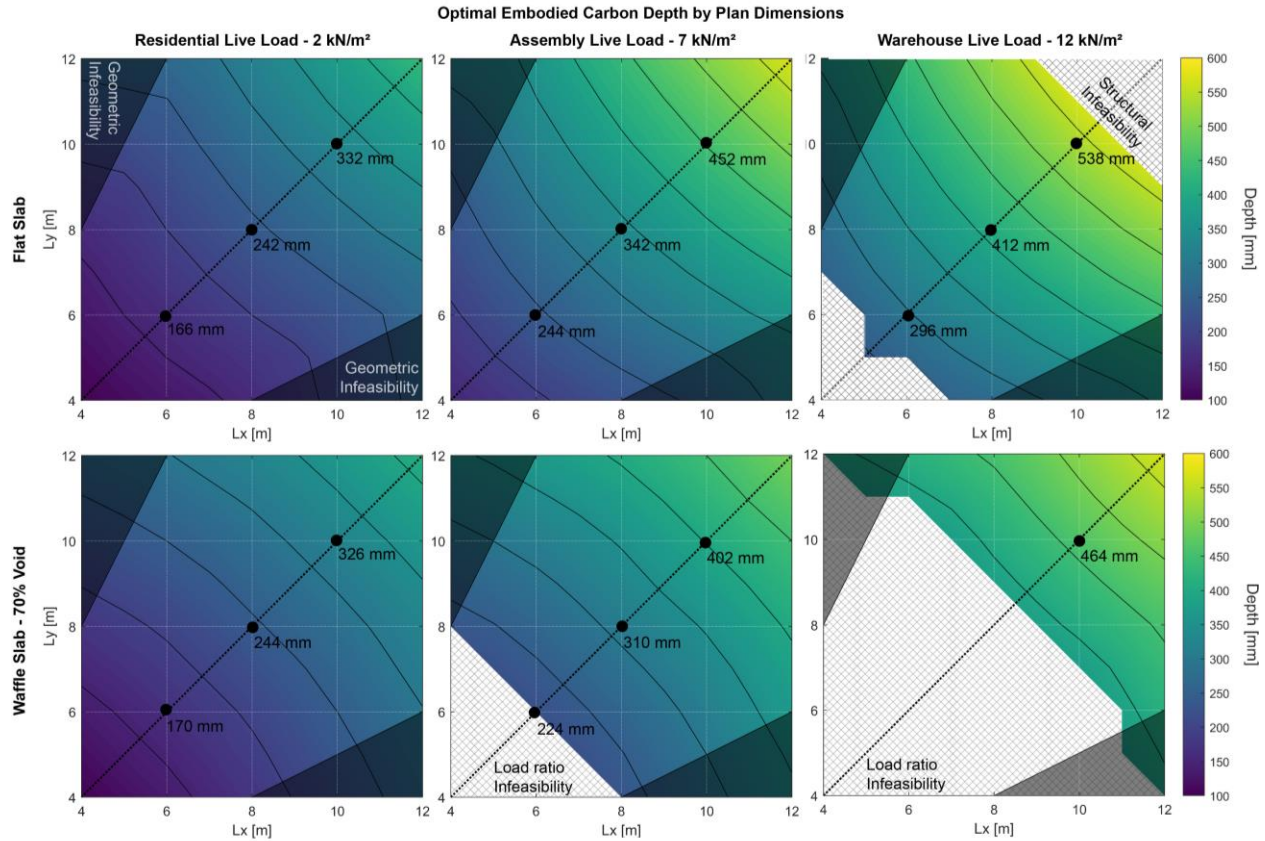


Figure 3-6: Optimal depth across given L_x and L_y dimensions for both flat slabs (top) and a 70% voided waffle slab (bottom). Geometric infeasibility are aspect ratios not permitted for analysis by DDM and load ratio infeasibility regions are those where the live load to self-weight ratio exceeds the boundaries set for DDM.

3.3.3 Performance evaluation based on a programmatic need and slab typology

In order to understand the tradeoffs that appear across typology, span and loading, it is useful to view the results from the various studies together. This is done comprehensively in Fig. 3-7, which plots the performance metrics of depth, embodied carbon, mass and cost against live load respectively. The data is then separated by span and slab geometry. One trend that can be observed with a composite visualization is between geometry and feasibility.

For both the 4m spans and 8m spans, feasible solutions can be found for higher live loads with a flat slab typology than the waffle slab typology, and furthermore as the void volume percentage increases, the maximum live load, for feasible solutions decreases. This trend did not continue for 12m spans and instead, decreasing the void volume percentage of a slab (one can think of the solid flat slab as a waffle slab with 0% void), meant that the maximum live load for a feasible solution also decreased. This demonstrates the flexibility of the waffle slab typology and highlights why it is a go-to suggestion for longer spans; however, it is clearly feasible and beneficial from the perspective of carbon, cost, and mass, to consider waffle slabs at shorter spans and low (residential level) live loads as demonstrated by the 4m and 8m results.

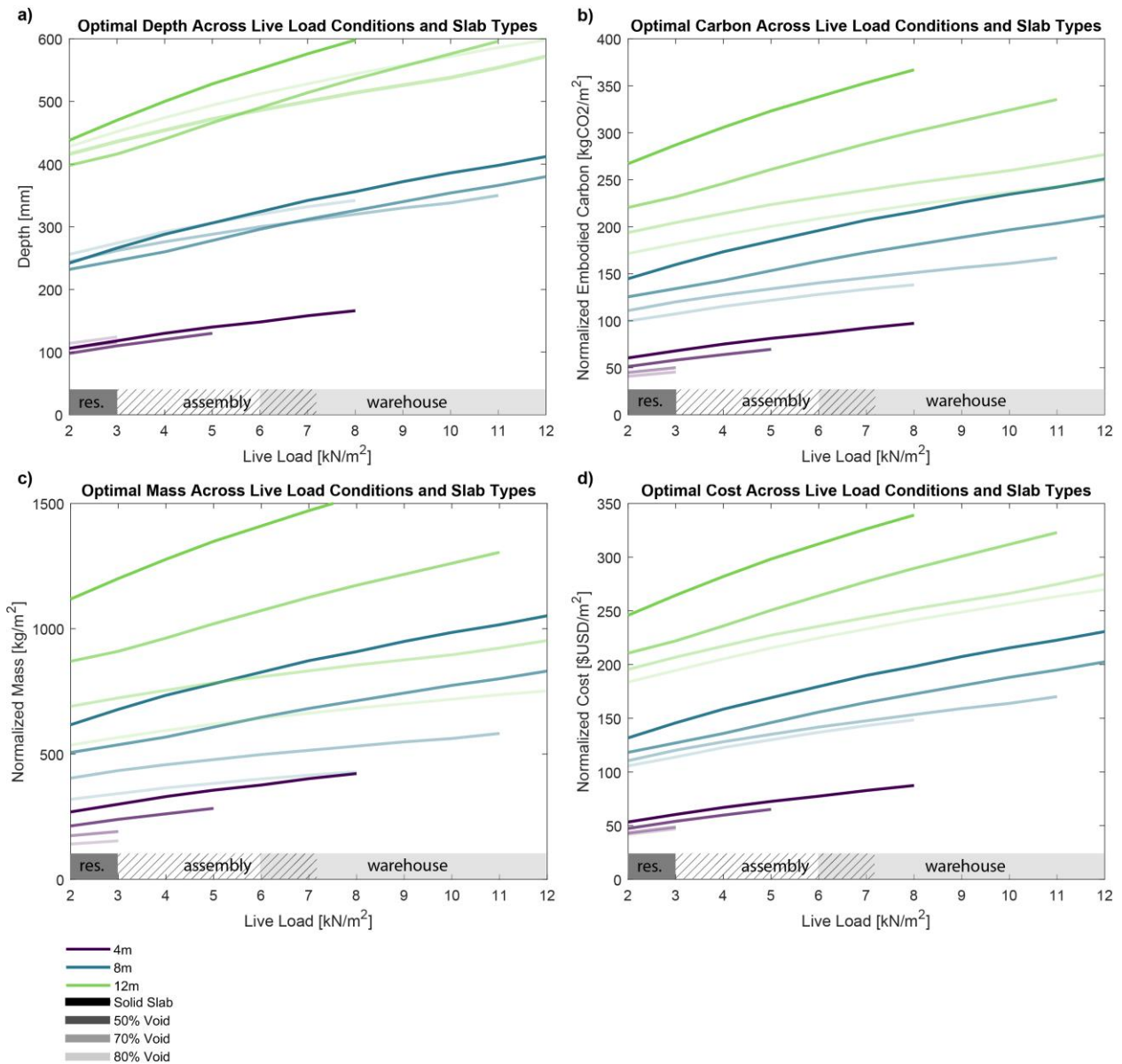


Figure 3-7: Optimal solution sets for depth, mass, carbon and cost across square flat waffle slab typologies, and three selected spans.

Looking at 3-7b – 3-7d, there is a decrease in embodied carbon, mass and cost moving from a solid slab to towards the waffle slab with the largest void volume. This is true for all the spans in the study but does not map in any discernable way to slab depth as seen in 3-7a. Let’s compare the solid slab to the waffle slab with the largest voids (80%). For a 4m span, the waffle slab with the largest void ratio of 80% is deeper for the limited range of live loads a feasible solution can be found for it. Increasing to the 8m span shows that for residential and the lower end of assembly live loads, the optimal 80% waffle slab is deeper than the optimal flat slab, but as load increases, the relationship flips. Lastly for the 12m span, the optimal solid flat slab is always deeper than the 80% waffle slab, but the waffle slab is feasible across a larger range of solutions.

While this is just the comparison of two of the typologies, other intersection points and changes in the ranking of optimal depth are visible in the 70% and 50% waffle slab as well. What is key from this plot is that design by rule of thumb alone would not allow a designer to access these same nuances of optimal depth since the only governing factor is the span. Subsequently, the savings highlighted in these results, would not be accessible through traditional approaches for element sizing.

It's also interesting to quantify the level of reduction across embodied carbon, mass and cost seen in Fig. 3-7. Fig. 3-8 shows the ratio of the performance metric for a selected slab typology to the optimal flat slab. These performance ratios are averages across all live loads where a feasible solution existed. This is highlighted for the middle span range of 8m, but the same trends and similar ratios are found for 4m and 12m and can be extracted from Fig 3-7. For a slab spanning 8m, a reduction in embodied carbon of 34% is possible, 51% for structural mass, and 23% for material cost if the waffle slab with the largest void volume is used.

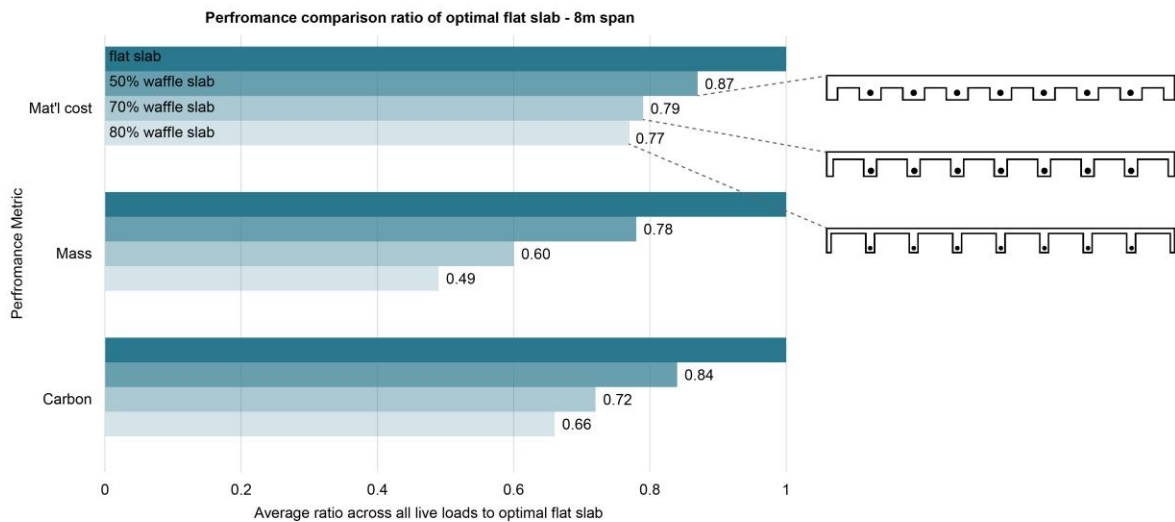


Figure 3-8: Average ratio of optimal slab typology to optimal flat slab for embodied carbon, mass and cost for 8m spans.

3.3.4 Potential impact of policy and carbon intervention strategies

The previous results highlight the performance benefits and savings that can be found through design space search and closed-form analysis, where the resulting optimal design solutions are materially efficient structural horizontal systems. The implementation of one of the optimal designs over the baseline contributes to reducing the demand for carbon intensive structural materials. This does not take place in isolation and is just one approach to achieve net zero climate goals as outlined by the Paris Agreement. The Organization for Economic Co-operation and Development (OECD) and New Buildings Institute have proposed several interventions, including but not limited to proposals to use cement substitutes and alternative binders, incorporation of embodied carbon regulation in building code through carbon content limits and decarbonization of structural material production (Bataille, 2020; Bowles et al., 2022).

This purpose of this final study is to understand the potential that commonly proposed energy policy recommendations and carbon reduction interventions could have in conjunction with the optimal geometry solutions on embodied carbon, mass and material cost. The four strategies assessed through the tuning of embodied carbon coefficients and material properties were 1) use of a low-carbon cement substitute, 2) use of a low-strength concrete, 3) use of a high-strength concrete, 4) decarbonization of steel rebar manufacturing.

Strategies 1-3 at first glance are propositions of tuning concrete mix design to positively impact environmental performance; Strategy 1, the use of a low carbon substitute, assumes the same strength and mechanical properties can be achieved with its implementation. Perhaps the most commonly proposed and abundant cement substitute is fly ash from steel production which could replace anywhere between 55% to 80% by weight of traditional ordinary portland cement (OPC); however, the availability of this material stream may decline as renewable energy plays a larger role in steel production (Millward-Hopkins et al., 2018).

Strategy 2, use of a low-strength concrete, and Strategy 3, use of a high-strength concrete, may not yield directly intuitive results due to the dependence of the material quantities on concrete strength and in turn the relationship between strength and other material properties such as modulus. With Strategies 2 and 3, one might expect a concrete with a lower embodied carbon coefficient to result in a lower embodied carbon of the slab, but more concrete volume and mass will be necessary to resist the loading on the lower strength matrix (and vice-versa with a high-strength mix). The exact tradeoff between these two opposing forces can result in unexpected outcomes. This points to a larger opportunity that has been explored by in literature uniting concrete use and structural element function with concrete mix design optimization for embodied carbon reduction (Gan et al., 2019; Purnell, 2013).

Strategy 4, the decarbonization of steel, speaks to a long term opportunity in manufacturing and energy resource management. Despite the large portion of structural steel (60%) and reinforcing rebar steel that is already recycled (90-100%), significant emissions are still associated with the process of recovering and reusing the steel as compared to virgin material (Purnell, 2013). While recent study has focused on the over specification of steel, or increasing the circularity of steel components themselves, key options proposed for significant carbon reduction include decarbonization of the manufacturing sector via electricity-powered plants and biomass substitution of coke-based fuel (Karlsson et al., 2020). This decarbonization of steel rebar manufacturing is thus represented in this work with an embodied carbon coefficient of zero .

The institution of Strategy 1 and 4 led solely to reduction of embodied carbon coefficients while Strategy 2 and 3 required the adjustment of the embodied carbon coefficient, compressive strength and modulus values supported by literature (Anderson & Moncaster, 2020; Iffat, 2015; Jones & Hammond, 2019) and structural code. The new values used for this study are outlined in Table 3-3.

Table 3-3: Updated material property values for structural analysis with carbon intervention strategies

Strategy	Embodied Carbon	Cost	Embodied Carbon	Cost	Compressive Strength	Modulus
	<i>Steel</i> kgCO ₂ /kg	<i>Steel</i> \$USD/kg	<i>Concrete</i> kgCO ₂ /kg	<i>Concrete</i> \$USD/kg	<i>Concrete</i> MPa	<i>Concrete</i> GPa
Benchmark	1.99	2.86	.15	.086	40	27.5
1	1.99	2.86	.12	-	40	27.5
2	1.99	2.86	.09	.100	25	23.5
3	1.99	2.86	.20	.084	55	34.9
4	0.00	-	.15	.086	40	27.5

Fig. 3-9 reports the results of these carbon reduction intervention for 8m square slabs of flat and waffle slab typologies (.5 m/rib spacing) under a residential live load of 2 kN/m². A reinforced concrete flat slab designed for the minimum depth specified by the ACI rule of thumb is used as a benchmark and the ratios reported in the figure are of the selected geometry and intervention with respect to this baseline. A number less than one means that the strategy and the methodology in this paper were successful in designing a bay of concrete slabs with performance improvements compared to the baseline. Alternatively, a number greater than one shows that the strategy was unsuccessful compared to the flat solid slab designed for the ACI rule of thumb depth.

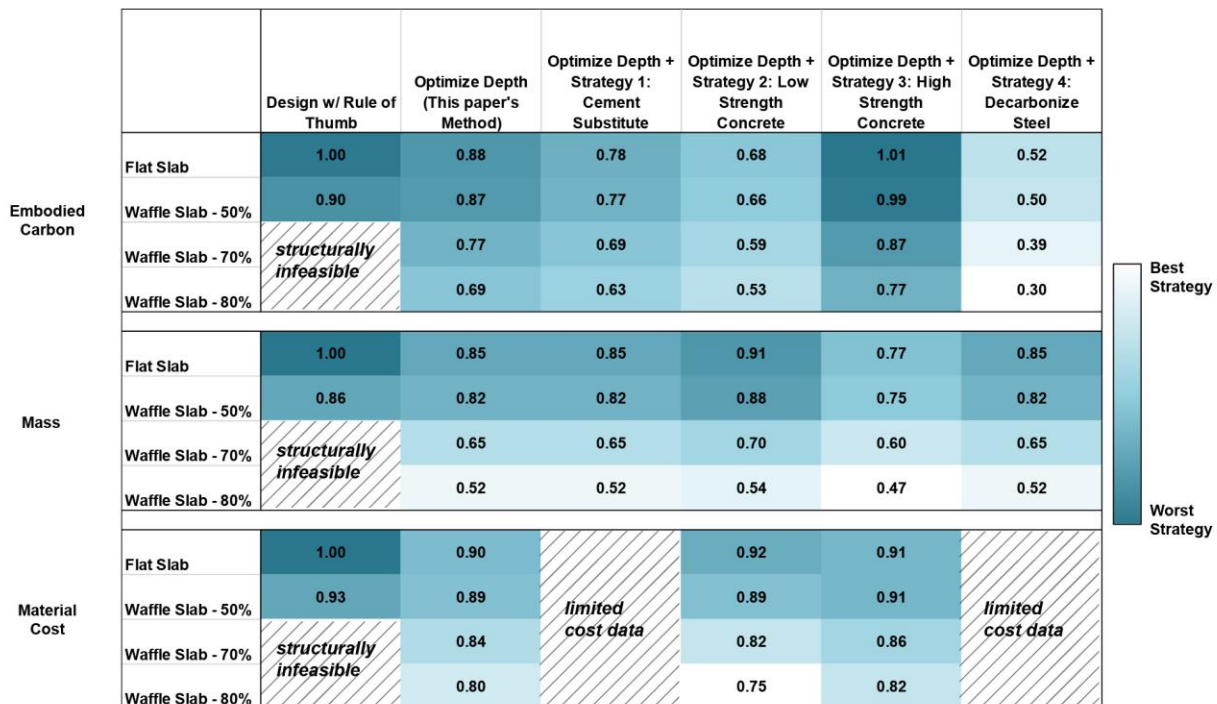


Figure 3-9: Carbon reduction strategy matrix for 8m square slabs, subject to residential live loading (2 kN/m²)

When considering the embodied carbon metric only, Fig. 3-9 shows improved performance across all typologies studied and strategies with the exception of Strategy 3, which is that of a high-strength concrete substitute. Here there is no reduction in embodied carbon for an optimal depth flat slab when compared to the benchmark design solution and the smallest benefits in the embodied carbon study for waffle slab typologies when compared to the other carbon reduction strategies. This means that the tradeoffs of additional concrete matrix strength cannot always overcome the embodied carbon penalty from the material content.

The greatest reductions found were through the implementation of Strategy 4, the decarbonization of steel manufacturing. Coupled with an optimal depth and efficient design typology of the 80% waffle slab, this methodology produced a design for a concrete bay that was responsible for only 30% of the carbon the traditionally designed benchmark case. However when putting the strategies in this paper in context with their time to implementation, a key insight can be found. For example, let's compare the embodied carbon results of Strategy 2: Use of low-strength concrete, an intervention that implemented now, with Strategy 4, the decarbonization of steel which is a longer term and more speculative solution. Nearly equivalent savings are achieved with an 80% voided waffle slab designed in conjunction with Strategy 2 as an optimal depth flat slab designed with decarbonized steel rebar. In other words, coupling this paper's method of optimal depth and the selection of a more efficient typology (waffle slab) with material substitution can currently yield the savings now that the building industry hopes to achieve in the long term.

The performance metric of mass tells a different, but perhaps more intuitive story. Here it seems that the greatest determination in mass savings is typology selection, with little to no additional savings garnered from combining an optimal depth solution with Strategy 1, use of a cement substitute and Strategy 4, decarbonization of steel manufacturing, since the concrete and steel material properties are unchanged in these scenarios. Here, Strategy 3 yielded the greatest savings across all typologies, with the potential to design a waffle slab solution that comprised 47% of the mass of the flat slab benchmark design.

Lastly, there is a metric of material cost, which was only assessed for the Strategies 2 and 3 where information on cost as a function of mix strength was available from RSMMeans (Doheny, 2022). Once again, typology selection seems to dominate the impact on performance, but one interesting note is that despite a higher unit cost of low-strength concrete mix, Strategy 2 yields the solutions with the best overall outcomes for an 80% voided waffle slab; however there is greater similarity in the solutions for all other typologies studied.

As a final conclusion of this carbon intervention strategy study, it is noteworthy that combining a typology change (from flat slab to 80% waffle) combined with optimal depth selection can often achieve savings across all performance metrics that are substantial, even without the implementation of these more forward-thinking but potentially costly strategies. While the results support pursuing them, especially Strategy 4 (decarbonizing steel production), they also suggest that there is underexploited opportunity to reduce carbon emissions substantially using readily available and cost-neutral or low-cost engineering and construction techniques.

3.4 Conclusions

3.4.1 Future work and remarks

There are several future paths for development of the methodology presented in this chapter for the design of flat and waffle concrete slabs. The first is with the parametric model itself, which is limited to a rectangular or square bay of varying aspect ratios. While there are plenty of buildings for which this is a fair starting parametric model, there are just as many with a plan area that may take on a variety of irregular shapes or asymmetric arrangement of floor panels. Similarly, this model doesn't consider floor systems that make use of interior beams, which will increase the efficiency of gravity load distribution. Finally, the cost calculations in this work only include concrete and steel material cost and not the cost of formwork or labor which could have varying levels of significance depending on the construction context, building story number, formwork material etc.

Despite the presence of these current limitations, it is clear from the results in this chapter that the integration of structural performance evaluation that allows for rapid feedback and wide search of the design space is key to accessing efficient concrete systems for the future. Despite the conventional nature of both flat and waffle slabs, this work shows computation can still provide access to materially informed solutions specifically through parameterization and exhaustive design space search. This method can be extended to more complex structural conditions and reveal further opportunity for savings and other nuances about the appropriateness of rule of thumb-based design practice in an increasingly performance driven world.

3.4.2 Summary of intellectual contributions

The computational approach in this work found flat concrete and waffle slab design solutions that out-performed code-prescribed minimum design depth flat concrete slab baselines for a variety of spans, load conditions, and geometric variations. Furthermore, it highlights the validity of using computation to rapidly traverse the design space for common structural solutions, versus pursuing traditional and/or serial design methods, and provides a methodology that doesn't feature the same temporal constraints of other structural analysis methods, which is especially important in the early design stage. This work also makes a quantitative case for the reconsideration of the waffle slab typologies, especially at shorter spans than typically proposed in design guides. Broadly this work demonstrates waffle slab typologies and similarly joisted systems as highly materially efficient typologies which are valuable structural interventions given both the urgency of meeting climate goals and the demand for construction.

4. Multi-objective optimization of thermally and materially efficient filler slabs

This chapter considers one promising alternative to traditional flat slab concrete systems, filler slabs, which replace underutilized concrete in the tension region of a concrete slab with a low-carbon filler material that stays in place post casting. Previous work has suggested that if this filler material is insulating, it can positively improve the thermal utility of the flat slab, which could be especially important as we think of roof systems and slabs-on-grade. The computational approach presented in this work quantifies the impact that insulating solid formwork can have thermally and structurally in concrete slab construction when used appropriately, and further demonstrates how structural optimization and heat transfer principles can produce high-performing building components that are applicable in a variety of global contexts.

It should be noted that parts of this chapter have previously been published by the author as a conference paper (A. J. Hartwell & Mueller, 2021). In addition to what has been presented previously, this chapter makes the following contributions:

1. Section 4.2.4: A methodology that uses structural shape optimization to design two-way filler slabs that incorporate two key design objectives: first, minimization of total embodied energy and second, minimization of thermal conductance (U-Value) of the slab when compared to a solid concrete two-way slab under the same load.

2. Section 4.2.2, 4.2.3: Validation of closed formed structural and thermal models for filler slabs with Finite Element Analysis (FEA)
3. Section 4.2.1: Ashby-based framework for incorporating discrete filler material selection into optimization workflow to reduce computational complexity

4.1 Background

4.1.1 Filler slabs in context

As previously discussed in Section 2.4 of this dissertation, filler slabs were first popularized by Laurie Baker to support low-cost housing in South India (Tewari et al., 2017) and have since been utilized throughout the region, to the extent that there are allowances in the national building code for their construction. The original purpose was to use low cost, locally available (often waste) materials as lost formwork to reduce the overall volume of concrete needed for residential roofs. In addition to reduced cost, the filler materials, such as Mangalore tiles, stabilized mud blocks, and coconut shells, tend to be less dense than concrete and therefore the resulting filler slab reduces the overall dead load of the horizontal spanning component. This can lead to significant reduction of material requirements for the foundations, lateral, and gravity systems of a building as number of stories are increased and in total embodied energy of a built project. Lastly, filler materials generally are less thermally conductive than concrete and the replacement of concrete with insulating material has been proposed as a method to help improve thermal comfort and reduce operational energy when deployed in roof structures (Chougule et al., 2015). Despite many reported benefits of insulation provided by the filler materials, especially in conjunction with an air gap, their use hasn't grown outside of India mainly due to construction economy trade-offs.

Structurally, filler slabs can be modelled with the same methodologies as waffle slabs or two-way joists systems with the assumption that the filler material is only serving to replace volumes of concrete and not behaving structurally (Chougule et al., 2015). The common approach to analysing filler slabs is to treat them as waffle slabs or connected T-beams spanning in two directions. The T shape is generally more structurally efficient due to the increased moment of inertia provided from the shape when compared to a rectangular block. It is composed of the compressive flange at the top of the T and the tension web at the bottom where the reinforcing steel is placed.

4.1.2 Agricultural waste as formwork

While there has been an emergence of commercially available structural systems with void forming lost formwork in the form of hollow plastic spheres and boxes. The energy expenditure required to process petroleum-based products is not insignificant. In parallel to this challenge, in many developing contexts, agricultural by-products and waste are a pressing issue, leading to landfilling and burning of carbon-sequestering material. Previous research has identified the possibility of incorporating agricultural waste streams as building material alternatives, with the potential to reduce concrete consumption. In addition to addressing environmental challenges, upcycling waste also presents an economic solution, as the use of agricultural waste in

construction can provide farmers with additional income streams. Current solutions that include agricultural waste streams in structural engineering and design propose the incorporation of crop residues and hulls into concrete mixes to replace a more carbon intensive component (Asim et al., 2020), or using agricultural waste as insulation instead of petrochemical based standards such as extruded polystyrene (XPS) without sacrificing thermal aspects of performance (Panyakaew & Fotios, 2008, 2011). However, until now, there has been relatively little research on the use of agricultural waste to directly reduce concrete in horizontal systems, which are typically the most carbon-intensive parts of building construction.

4.1.3 Building performance metrics for filler slabs

This section also aims to assess the performance of individual filler slab designs from the perspective of material efficiency and thermal efficiency. In this way there are multiple objectives being held in prominence to determine what constitutes a good design, however the framing allows results to speak to both the embodied (material efficiency) and operational (thermal efficiency) performance of a building. In this work, two closely related metrics are reported to assess the material efficiency: the mass of the element and the embodied energy of the slab that can be found with the material amount. In this work, thermal efficiency is assessed by finding the thermal conductance or U-value of the filler slab and working under the assumption that for a thermal barrier such as a roof or slab-on-grade, minimizing the U-value of the integrated filler component is desirable. While operational energy would require a much more complex study, to minimize computational overhead, U-value and building energy intuition is a reasonable stand in for an early design stage problem.

Previous research has shown that embodied energy and operational energy are often considered in isolation, but greater savings are possible when they are addressed in an integrated manner (Brown & Mueller, 2016). In particular, the thermal conductivity of the exterior building envelope (walls and roof) can have a large impact on thermal comfort and operational energy by controlling heat flow and regulating indoor temperatures.

4.2 Methodology

A filler slab is designed, modelled, and analysed with its performance with respect to embodied energy, mass, and thermal conductance compared to a solid two-way concrete slab of the same span, loading and support conditions. This procedure begins with filler material selection in order to best serve objectives of interest for this work including the reduction of embodied energy, U-value, and total mass of element (Section 4.2.1). Next, we integrate analytical solutions for thermal and structural behavior of a two-way slab into a computational parametric model to find the best performing designs across a variety of spans (Sections 4.2.2 – 4.2.4). Lastly, computational optimization is pursued to discover high performing designs (Section 4.2.5).

For the scope of this chapter, the filler slab and flat slab used as a benchmark are considered under self-weight as well as a uniform live load of 4000 N/m^2 . The slabs are considered simply supported along their edges, but this method could be modified to produce solutions for other boundary conditions and loading scenarios. More complex geometric scenarios are considered in

Chapter 5. Furthermore, the building code used for analysis was Indian National Building Code IS-456 (Bureau of Indian Standards, 2000), as this region has the widest adaption of filler slabs.

4.2.1 Material analysis

For the design of filler slabs presented in this chapter, the goal is to find designs that demonstrate improved performance from both an embodied energy and operational energy perspective. Embodied energy by volume is a metric of importance because the filler replaces a volume of concrete set by the size of the void. Filler material candidates are evaluated with respect to several qualitative and quantitative criteria. Quantitative factors include density, thermal conductivity and embodied energy while, the qualitative considerations include a candidate materials historical precedent either as a filler material or as insulation and whether its manufacturing processes amenable to residential building industry scales. All relevant material properties are presented in Table 4-1

Table 4-1 Material properties used for analysis and optimization in Chapter 4

Material	Value	Source
	<i>Density - kg/m³</i>	
Concrete	2400	(M. Ismail, 2019)
Steel	7850	(M. Ismail, 2019)
Straw	130	(Cascone et al., 2019)
Bagasse and ash composite	1230	(Madurwar et al., 2015)
Rock wool	100	(Al-Homoud, 2005)
	<i>Embodied Energy by Volume - MJ/m³</i>	
Concrete	2400	(Deshmukh & More, 2014; M. Ismail, 2018)
Steel	330000	(M. Ismail, 2019)
Straw	120	(Deshmukh & More, 2014)
Bagasse and ash composite	990	(Madurwar et al., 2015)
Rock wool	1680	(Deshmukh & More, 2014)
	<i>Thermal Conductivity - W/m²K</i>	
Concrete	1.4	(Al-Homoud, 2005)
Straw	.06	(Cascone et al., 2019)
Bagasse and ash composite	.47	(Madurwar et al., 2015)
Rock wool	.04	(Al-Homoud, 2005)

	<i>Modulus - GPa</i>	
Concrete	29	(Dolan & Nilson, 2016)
Steel	200	(Dolan & Nilson, 2016)
	<i>Failure Strengths - MPa</i>	
Uniaxial Strength – Concrete	40	(Dolan & Nilson, 2016)
Yield Strength – Steel	415	(Dolan & Nilson, 2016)

The materials are plotted in Fig. 4-1 according to key factors: embodied energy by volume, thermal conductivity, and density, which impacts the total mass of the slab and overall dead load of a structure. The method of plotting materials with different properties on the two-axis chart is in the spirit of Ashby charts (Ashby et al., 1993), but displays average values for specific materials vs bubbles corresponding to the composition-based range of property values in broader material families.

In the first plot, the diagonal dashed line represents the concrete equivalence line; or the line of increasingly air-entrained concrete. Any materials that fall on this line can be thought as physically analogous to a “low density” concrete substitution when considering embodied energy by volume and density. The shaded gray region in each of the plots represents a region where materials perform worse than concrete for both of the particular metrics shown. The charts can be interpreted as follows: If a material falls in the gray region in all three plots, then it is not a suitable candidate for a filler material. If the material is in the gray region of one or two of the three plots, then the material can be used, but multi-objective optimization should be followed for the computational design process. Lastly, if a material is in the white region in all plots, then a single objective approach is sufficient to find a solution that will minimize both metrics of interest – embodied energy and U-value. This approach can be applied when evaluating filler materials candidates for selection with other objectives such as acoustic performance, another objective often highlighted as one that could be improved with the implementation of filler slab technology.

4.2.2 Structural design and validation

As stated above, the slab assumes a distributed live area load of 4000 N/m² while the dead load is found by the extracting the volume of concrete, steel, and filler from the CAD model. Using the density values in Table 4-1, the factored load, q_u was found using Eq. 4.1 in accordance with the Indian Standard IS-875 Part II Code of Practice for Design Loads. Since we've assumed a simply supported concrete slab with uniformly-distributed load, the coefficient method, outlined in both ACI-318 and IS-456, can be used to evaluate moment and shear demand.

$$q_u = 1.6 \times q_{live} + 1.2 \times q_{dead} \quad Eq.4.1$$

Flexural demand M_u is calculated in both the x and y span direction by first dividing the slab into T shaped strips along the selected span. These t-shaped strips make up the rib or web region at the bottom that holds the reinforcing steel as well as half of the compressive flange on either side of the web at the top of the slab (see Fig. 4-7). The goal is to now find the moment per unit width along these T shaped strips using Eq 4.2. Here $\alpha = 0.0625$ is the moment coefficient, which is a function of the aspect ratio and support conditions, w_d is the factored load and l_x is the shorter span of the slab panel. This moment is then multiplied by the unit width to find the total moment at a prescribed location along the T strip, where n is the number of filler modules in Eq. 4.3

$$M_{xf} = M_{yf} = \alpha \cdot w_d \cdot l_x^2 \quad Eq.4.2$$

$$M_u = M_{xf} = \alpha \frac{l_y}{n} \quad Eq.4.3$$

Moment capacity, M_N is found by adapting equations from IS 456 and using a methodology outlined fully by Ismail and Mueller (M. Ismail, 2019) for identifying the moment arm for an arbitrary unit cross section. This is summarized in Eq. 4.4 below where A_c is the compressive area of concrete, f'_c is the uniaxial strength of concrete in compression, and z is the moment arm. The value of f'_c as well as other material parameters for concrete and steel used in these optimizations are found in Table 4-1 above.

$$M_N = 0.36A_c f'_c z \quad Eq.4.4$$

Shear demand is found using the coefficient method under the same boundary conditions as the flexural moment demand and Eq. 4.5 where $\beta = 0.33$ is the shear coefficient. Shear capacity is found based on an approximation in the ACI 318 and is summarized in Eq. 4.6 where b_w is the rib width of the T section trips unit cross-section and d is the effective depth for slab.

$$V_x = V_y = \beta \cdot w_d \cdot l_x \quad \text{Eq.4.5}$$

$$V_N = 2b_w d \sqrt{f'_c} \quad \text{Eq.4.6}$$

The deflection, Δ , of a filler slab design is found by considering the structural part of the filler slab an interconnected section of T-beams and finding the deflection at the center T-beams in both directions. According to Euler-Bernoulli beam theory, this is calculated with a double numerical integration over the curvature at the center of these T-beams and summarized in Eq. 4.7 where M_a is the applied moment (unfactored), E is the modulus of the concrete, and I_e is the effective moment of inertia at location x along the beam's span

$$\Delta = \iint \frac{M_a(x)}{EI_e(x)} dx + C_1 x + C_2 \quad \text{Eq.4.7}$$

Let's consider one of these beams. In this work, sections are taken along the T-beam, with the number of sections taken at even intervals equal to the number of voids, n , along the spanning direction. For each of these T-sections, its geometry, the amount of steel, and loading are used to find a cracked I_{cr} and uncracked moment of inertia I_g . The values can be used to find an effective moment of inertia for each individual section in a beam with non-uniform stiffness i.e. non-uniform cross-section along its length. This is presented and described fully by Bischoff and Gross (Bischoff & Gross, 2011) but is summarized in this chapter by Eq. 4.8-4.11. More information on moment of inertia for T-shaped sections and cracking moment M_{cr} , can be found in Chapter 3.

$$I_e = \frac{I_{cr}}{1 - \gamma \eta \left(\frac{M_{cr}}{M_a}\right)^2} \leq I_g \quad \text{Eq.4.8}$$

$$\gamma = \frac{1.6\xi^3 - 0.6\xi^4}{(M_{cr}/M_a)^2} + 2.4 \ln(2 - \xi) \quad \text{Eq.4.9}$$

$$\xi = 1 - \sqrt{1 - \frac{M_{cr}}{M_a}} \quad \text{Eq.4.10}$$

$$\eta = 1 - \frac{I_{cr}}{I_g} \quad \text{Eq.4.11}$$

The structural checks comparing the slabs demand from loading to its capacity from its geometry, as well as the deflection, are key parts of the structural feasibility analysis and optimization workflow, described in greater detail in section 4.2.5.

While the structural modelling for the filler slab solutions was all completed with closed-form analytical solutions accepted by structural code, it is not uncommon for structural engineers and designers to incorporate FEA analysis into their design workflow. It is not pursued here because of the computational expense such analysis methods add in the early design stage. However, to ensure that the closed-form analysis produced reasonable results, a finite element model was deployed under the same loading scenario and support conditions for several of the spans highlighted in the study. Then the moment and shear demand were then compared for both analysis methods by individual T- beam and then by T - section along the span.

The results are shown in Fig. 4-2, which highlights in blue the analytical solution for the T-beams in one of the spanning directions. The slab modelled was square, meaning the moment demand would be equal in both spanning directions and exhibit symmetry across the middle beam. With respect to moment demand and shear demand, the same values are observed for each T-beam (labeled from outer edge beam to inward middle beam – edge,3,4, middle), but vary along the length by section. When reviewing the moment demand specifically, there is significant variance not just by beam location in plan, but also by section along the spanning length of the beam. It is reassuring to note that the average across those respective sections (indicated by the dashed lines) do correspond well to the constant values found using the analytical structural model. For shear demand (right) the same trends are observed again: the average by section aligns well with the analytical model. More on the implications of this closed-form analysis will be discussed in Section 4.3.3.

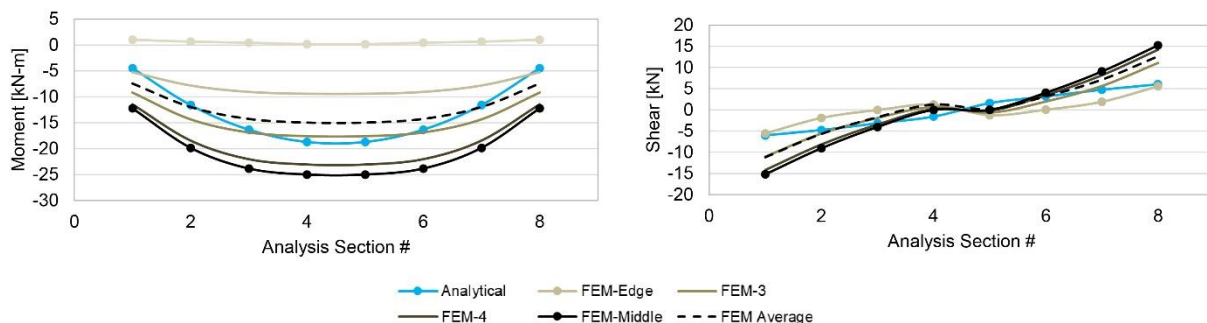


Figure 4-2: Comparison of the moment (left) and shear (right) demand found from the closed-form code-based approach and a FEA model.

4.2.3 Thermal design, validation, and structure-property relationships

The U-value of a filler slab design is calculated using geometric information from a representative cross section in Rhino as shown in Figure 4-3 and applying a 1D conduction model using the thermal circuit analogy. This allows the quantification of the impact of replacing a volume of concrete with an insulating material would have on composite resistance of the slab element. It should be noted that although the results in this chapter only compare the structural elements themselves, validation of the closed form analytical model with the two-dimensional FEA model did include the boundary air films on both the inside and outside of the slab. In

addition, the contribution of the steel rebar to U-value was not considered as the area of the rebar would only account for at most 2% of the T-cross section.

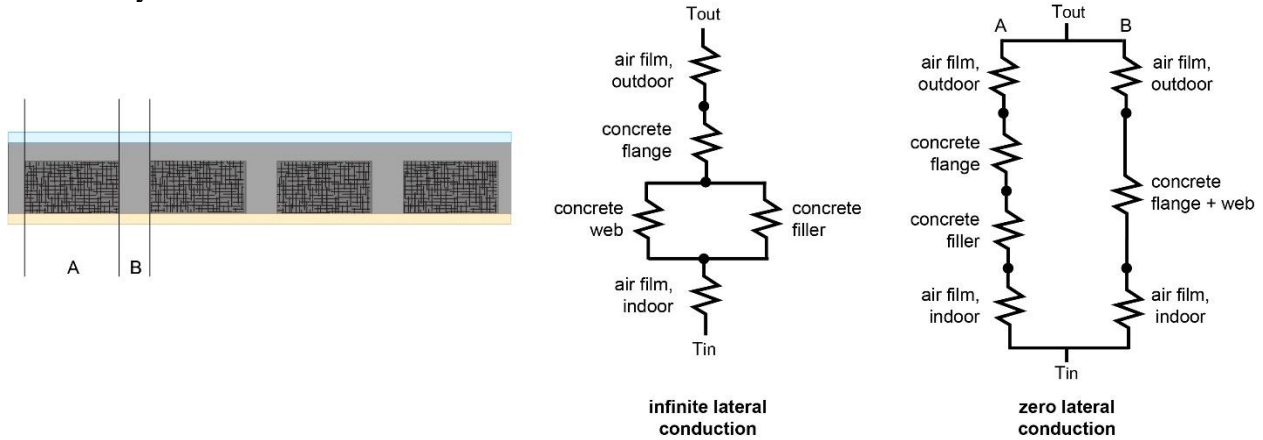


Figure 4-3: Drawing of thermal circuits for both the infinite lateral conduction and zero lateral conduction heat transfer model of the filler slabs.

Two models, as shown in Fig. 4-3, could be considered as appropriate for the a thermal one-dimension convective analysis - one that assumes infinite lateral conduction horizontally through the concrete flange, and a second that assume zero lateral connection along the top horizontal concrete flange. The latter is a model pursued by in earlier work on thermal optimization of filler slabs by Acharya et.al [11]. We can think of these two models as bounding extremes of the physical reality of the filler slab's thermal behavior, with a model representing infinite lateral conduction providing a conservative estimate of the system or an upper bound on U-values, and a model representing zero lateral conduction providing a lower bound of the U-values of a filler slab design. The resistance of each of the different resistors in the model can be found using Eq. 4.12 and 4.13 and then combined using the conventional rules for series and parallel circuits. In Eq 4.12, L refers to the length of conduction (along the same axis as the slab's depth is measured), k , the thermal conductivity of the material, and A the cross-sectional area for conduction (plan area of segment being analyzed). Eq. 4.13 specifically applies to the convective resistance from the air films surrounding the slab on both sides, where h is the heat transfer coefficient of $26 \text{ W/m}^2\text{K}$ for the outside air film and $5 \text{ W/m}^2\text{K}$ for the inside air film. Finally, Eq 4.14 can be used to convert the composite resistance to a U-value.

$$R = \frac{L}{kA} \quad \text{Eq.4.12}$$

$$R_{airfilm} = \frac{1}{hA} \quad \text{Eq.4.13}$$

$$U = \frac{1}{RA} \quad \text{Eq.4.14}$$

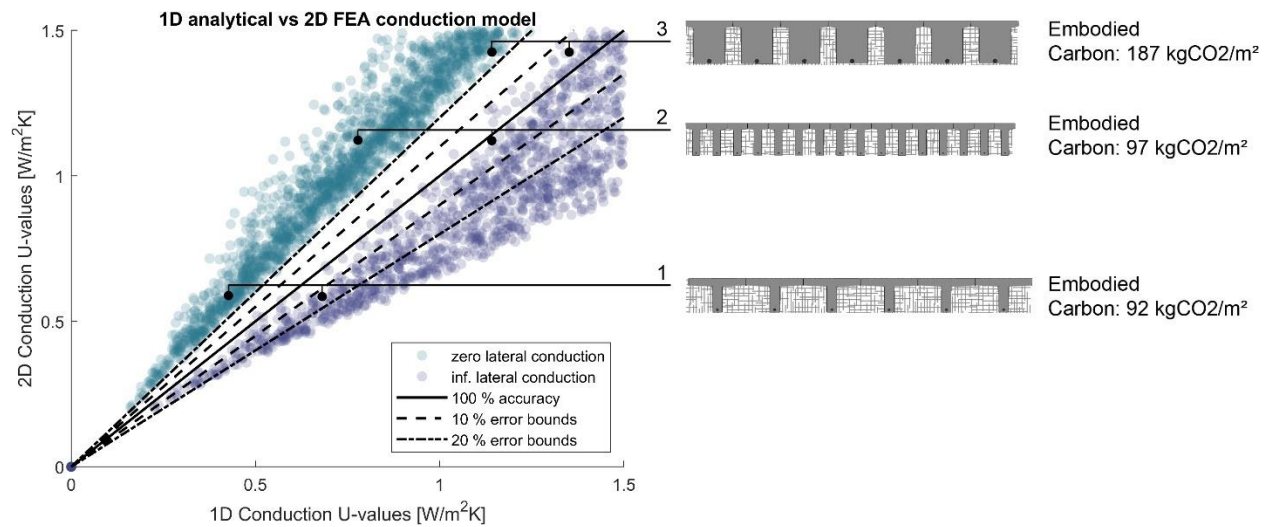


Figure 4-4: Comparison of 1D (closed form analytical) and 2D (THERM) conduction models for filler slabs

Sampling was used to model 5000 filler slab cross sections with a filler material of EPS ($k = .035$ W/mK). Geometric properties and material properties were used to calculate the U-Value of the component using the above described 1D conduction models, as well as served as inputs into THERM, a 2D conduction finite element model developed by Lawrence Berkeley National Laboratory (Finlayson et al., 1998) and integrated with Grasshopper via the Ladybug Tools plugin suite. The results from the THERM model were then considered as the point of comparison to determine if the upper and lower bound behavior as expected was observed, and to assess model accuracy.

Figure 4-4 highlights the results of this assessment, with the results of the THERM model plotted against the results of the 1D models. Points along the solid black line represent 100% accuracy of the 1D model, points above the solid line indicate the U-value from the 1D model proves an underestimate of the U-value given from the THERM analysis and points below the solid line indicate an overestimate to the 2D analysis. With this in mind, it makes sense that the model that assumes zero lateral conduction in the concrete flange and between the filler material and the concrete returns a lower thermal transmittance than the THERM model and lays above the solid line (blue points). Conversely, if one presumes that heat can conduct infinitely in this top concrete flange, the transmittance value will be higher than the value a 2D model returns and this behavior is also captured by the points below the solid line (purple).

Additionally, we also see that for the 1D infinite lateral conduction model, some of the points lie above the solid line, which is not expected to happen. These points represent geometries that are extreme representations of a waffle slab, i.e. incredibly thick concrete web and flanges and or very narrow voids and high number of ribs for a set span, that are unlikely to be selected in practice and likely pose issues of feasibility. One such example is highlighted as slab 3 in Figure 4-4, and comprises twice as much carbon as better performing solution. Furthermore, for the filler slab sections modeled, there is a minimum of 20% error between the 1D zero lateral conduction model and the THERM model, while the infinite lateral conduction model performs much better,

especially as the U-value decreases (which is desirable for the design objectives in this chapter). Analysis of the infinite lateral conduction U-values shows that 66% of the values are within 20% of the THERM model, and 32% of the data falls within the 10% error bounds. It should be noted that the better accuracy of the infinite lateral conduction model is likely because the conductivity of concrete is about two orders of magnitude higher than that of the EPS used in the simulations, and this more accurately represents the physical circumstances. Future work to assess this would have to consider a wider range of filler material thermal conductivities in addition to the geometric diversity of the sections.

The infinite lateral conduction 1D model serves as a better proxy for the 2D FEA analysis performed by THERM as its values are not just more accurate overall, but that accuracy improves in the high performing regions of the design space as illustrated in Figure 4-4. But what about the model's ability to order solutions appropriately? As Mueller highlights, in the early conceptual design stage, it may not be as important to predict a performance value as accurately as possible (within reason) as it is to correctly compare performance of different designs to one another (Mueller 2014). They propose novel error measures for surrogate models that can be applied in this work here, specifically Mean Rank Error (MRE), which captures the average magnitude of difference in predicted and actual rank in a set of data regardless of direction and normalizes by the average rank on the data set. This can be found using Eq. 4.15 where N is the number of samples, r is the actual rank (THERM) and \hat{r} is the predicted rank (1D models).

$$MRE = \frac{1}{N} \sum_{i=1}^N \frac{|\hat{r}_i - r_i|}{N/2} \quad Eq.4.15$$

Of course, we can also evaluate the two proposed 1D models with traditional error measures as well such as mean squared error (MSE), where U is the actual U-value and \hat{U} is the predicted U value.

$$MSE = \frac{1}{N} \sum_{i=1}^N (\hat{U}_i - U_i)^2 \quad Eq.4.16$$

Results for these accuracy metrics with the 1D thermal models are shown in Table 4-2. The results show a lower MSE for the infinite lateral conduction model which supports the previous assertion that this model provides more accurate U-Values compared to the zero lateral conduction model. However, the zero lateral conduction model has a significantly lower MRE, meaning that it may be an overall choice depending on the goals of the early design stage investigation being performed. This is shown graphically in Figure 4-5, where the ranks for the 1D conduction models are plotted against the THERM results. When looking at the full set of 5000 samples, a much tighter bounding to the solid 100% accuracy line can be observed for the zero lateral conduction results here vs. the large bulging spread present in the middling ranked designs values resulting from the infinite lateral conduction model. However, when zoomed in on the top 50 designs as shown in the bottom row of plots in Figure 4-5, the rank performance is not very dissimilar qualitatively.

Despite, the rank accuracy superiority of the zero lateral conduction model, this work proceeds with the infinite lateral conduction model in the interest in being conservative of the reported U-Values, which is especially important given the 2-way ribbing in waffle slabs that will impact heat transfer but cannot be adequately captured by any of the models in this scope of work. The infinite lateral conduction model is sufficient for a first order rapid estimate, that will enable design space exploration of filler slabs, and serve as a theoretical comparison for other roof and insulative systems.

Table 4-2 Qualitative error measures for thermal modeling

Error Measure	Zero Lateral Conduction	Infinite Lateral Conduction
MSE (all)	.3728	.1546
MRE (all)	.0517	.1594

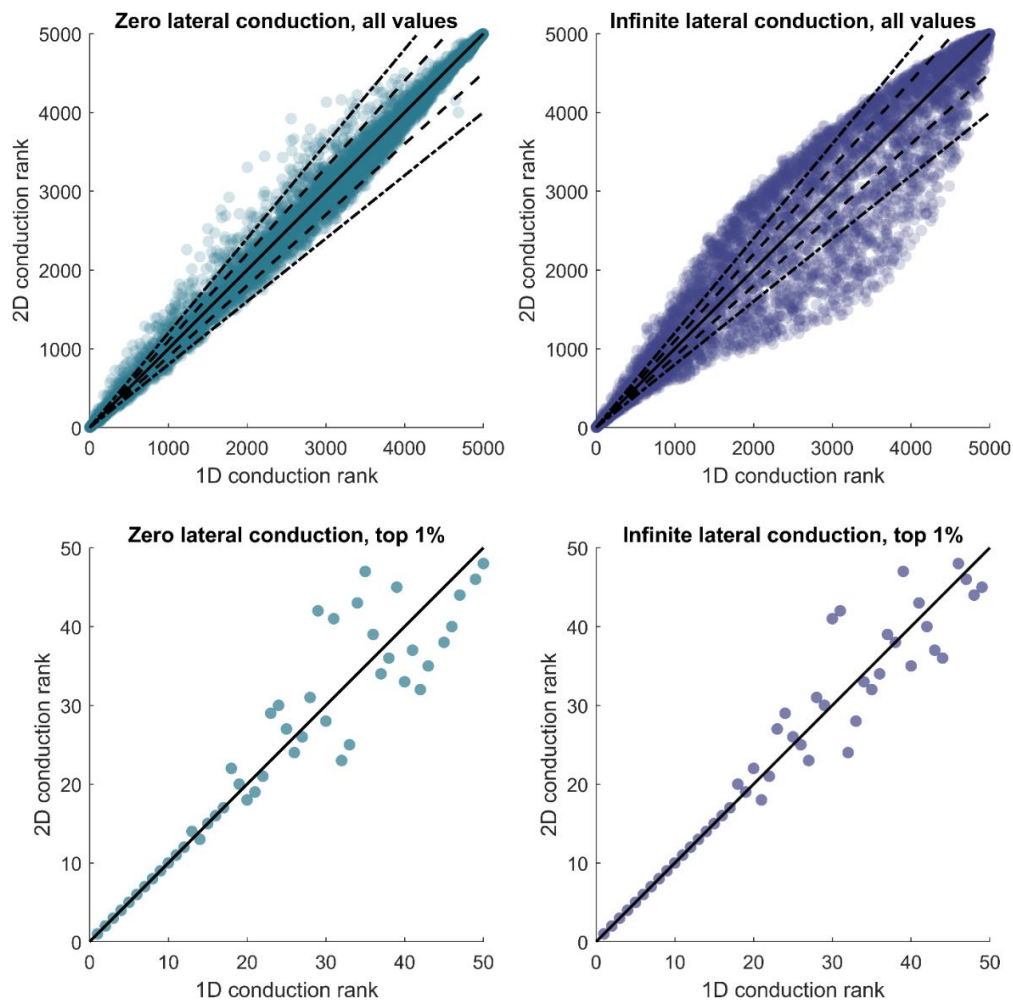


Figure 4-5: Comparison of 1D and 2D models with respect to the ranking of the solutions by U-Value

4.2.4 Computational integration and filler module parameterization

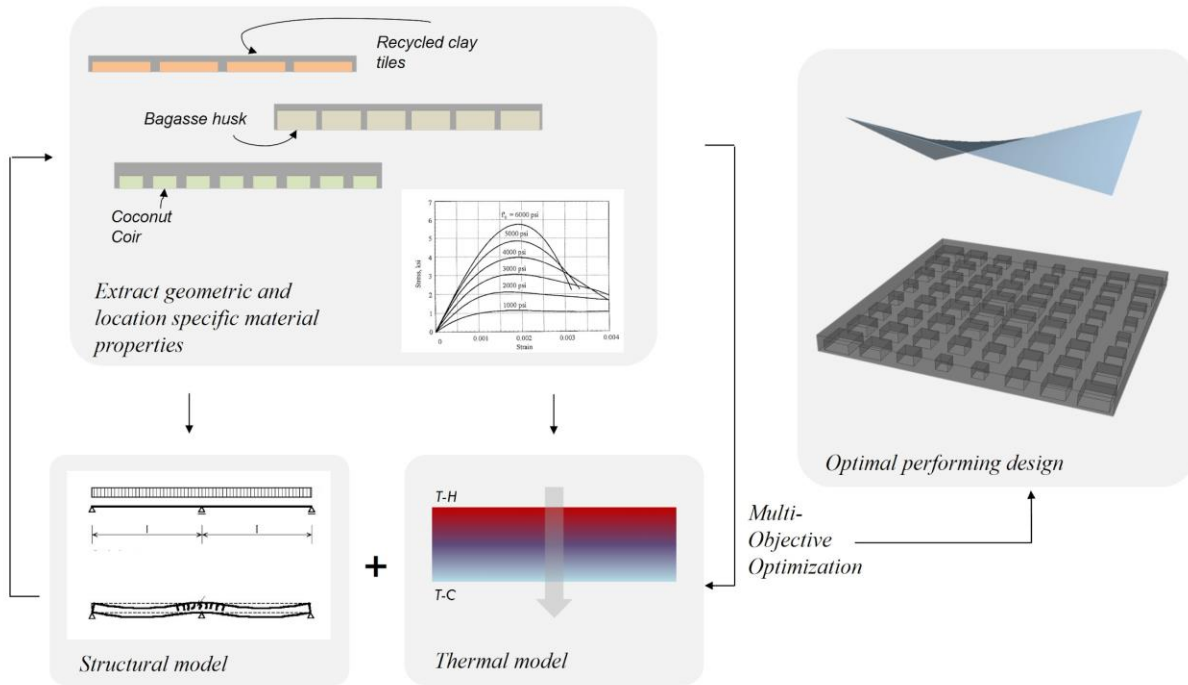


Figure 4-6: Overview of computational work flow for multi-objective optimization of filler slab

The computational method, summarized by Fig. 4-6, in this chapter extends one proposed by Ismail and Mueller in their work on shape optimization of beams for ribbed one-way floor systems (M. A. Ismail & Mueller, 2021). Here, a parametric model of a two-way filler concrete slab is created for a given span and filler material where the total slab depth, as well as the width and height of the square voids or filler modules in the slab which control the rib and flange dimensions respectively. A more comprehensive description of the design variables can be found in Table 4-3 below. This model is implemented in Rhino, the CAD modeling software and grasshopper, its companion parametric workplace with allows for the extraction of the geometric properties from a filler slab design and the input of material properties necessary to perform the structural (Section 4.2.2) and thermal analysis (Section 4.2.3). Once the analysis of the performance objectives is performed, the parameters, constraints, and objective function are input into Radical, a constrained optimization tool available in the Design Space Exploration toolkit for Grasshopper, which makes use of the COBYLA non-linear constrained optimization algorithm (Powell, 1994) .

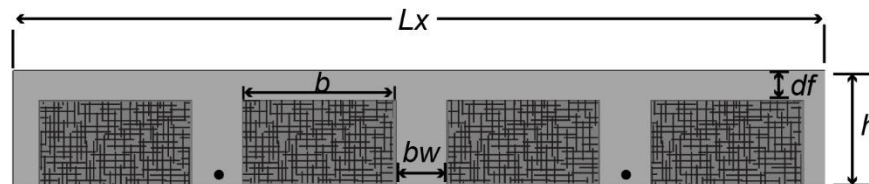


Figure 4-7: Section drawing of parameterized filler slab, with $n = 4$ modules and straw filler material

Table 4-3: Design variable vector for filler slab with associated bounds and values

Design Vector	Variable Description	Value
x_1	type of filler material	straw, rock wool, bagasse + ash
x_2	number of modules	$0 < n < 1$
x_3	span length	$0 < l_x = l_y < 1$
x_4	depth of slab	$1 \text{ cm} < h < 50 \text{ cm}$
x_5	flange depth ratio	$0 < \frac{d_f}{h} < 1$
x_6	area of steel	$250\text{mm}^2 < A_s < 2500 \text{ mm}^2$
x_{7-10}	scaling surface control point(s) heights	maps to b

With respect to the concrete portion of the filler slab geometry that carries the structural loads of the slab, the size of the filler modules is controlled through the use of a flat surface with a grid distribution of square apertures and a “scaling surface” which allows one the manipulation of control points on the surface to globally scale the aperture sizes as illustrated in Fig. 4-8. Recently, Rivera et al. (Rivera et al., 2020) used a scaling surface to control the sizes of perforations in shell structures, and then optimized the pattern topology directly using strain energy with Radical. Radical allows the user to input the entire surface as a variable, or to specify specific control points the user would like to modify. In this work, four control points on the scaling surface are used to size all the modules on a flat surface, and then a solid difference is used to create the filler slab geometry. What this scaling surface method essentially does is decouple the number of variables in the workspace, from the number of items to be sized, simplifying the design space for optimization.

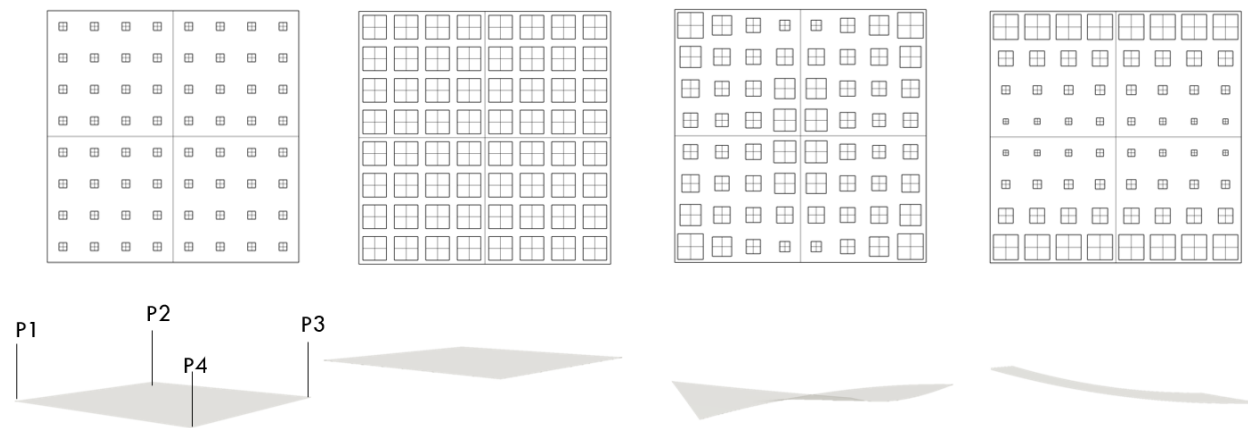


Figure 4-8: Examples of module size distribution in plan (top), based on a representative width scaling surface (bottom).

The optimization is formulated in the following manner:

$$\min J(x) = \frac{EE_{filler}}{EE_{flat\ slab}} \quad Eq.4.17$$

subject to the following $g(x) =$

$$M_n - M_u > 0 \quad Eq.4.18$$

$$V_n - V_u > 0 \quad Eq.4.19$$

$$\frac{l}{250} - \delta > 0 \quad Eq.4.20$$

$$\rho - .004 > 0 \quad Eq.4.21$$

$$.019 - \rho > 0 \quad Eq.4.22$$

$$4 - \frac{d}{b_w} > 0 \quad Eq.4.23$$

$$b_w - .07 > 0 \quad Eq.4.24$$

$$1.5 - \frac{l}{n} > 0 \quad Eq.4.25$$

$$d_f - .037 > 0 \quad Eq.4.26$$

Because of the material property analysis pursued in Section 4.2.1. this multi-objective problem can be formulated into a single objective function. Here the objective embodied energy (EE) is normalized by selecting the minimum depth flat concrete slab with equivalent span and structural performance under the same load as a performance benchmark. This is summarized in Eq. 4.15.

Eqs. 4.16 and 4.17 show constraints for moment and shear respectively, while 4.18 refers to the maximum allowable deflection of a slab. Eqs. 4.19 and 4.20 are constraints on the reinforcement ratio ρ that are calculated to result in ductile failure mode of the slab. Eqs. 4.21 – 4.24 represent geometric constraints for ribbed slabs and T-beams outlined in the Indian building code IS 456-2000. Eq. 4.21 is a relaxed formulation of the constraint on flange depth, which assumes a less energy intensive solution for fire resistance could be achievable compared to added concrete thickness.

4.3 Results

4.3.1 Span and filler material variation

The first study investigates the impact that filler material selection has on the optimal filler slab geometry and to understand design performance variation as span increases. Three filler materials were selected: straw, bagasse and ash composite and rock wool, representing three material categories of early investigation materials, region-specific structural materials, and traditional insulation, respectively. The spans highlighted were 6m, 9m, and 12m, which gives a total of 9 optimal filler slab designs found. For this study, there was an assumed 8 filler modules in both the x and y direction in plan. The optimal solutions were found from the termination of the Radical optimizer and then were compared to a solid reinforced concrete slab benchmark using Eq. 4.25. This provides an assessment of the savings that can be achieved with the method presented in this work.

$$Savings\ Percentage = \left(1 - \frac{Metric_{optimum}}{Metric_{benchmark}} \right) * 100 \quad Eq.4.27$$

As highlighted in Fig. 4-9, resulting optimal filler slabs for all materials are generally deeper than equivalent solid concrete slab benchmark. This demonstrates that removing material up to neutral axis of a solid slab is not alone the most structurally efficient approach for design of filler slabs. Optimization results in this study show that this removal of material volume should be accompanied with the addition of structural depth to the slab to yield better performance across multiple objectives.

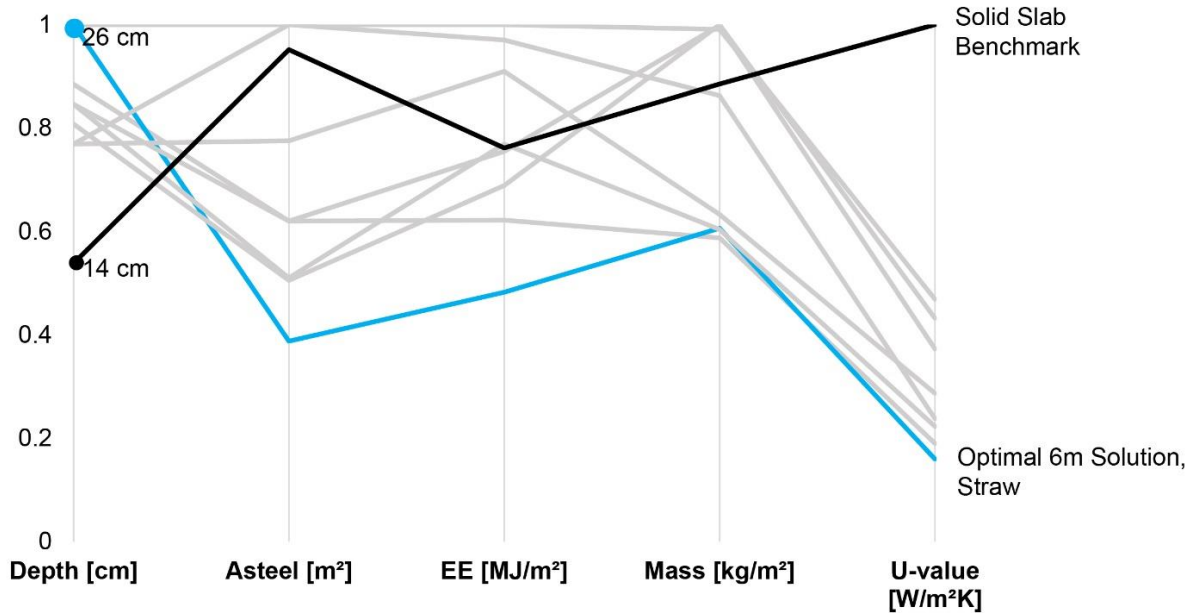


Figure 4-9: Parallel coordinate plot of 6m span designs generated with the three filler materials and the benchmark

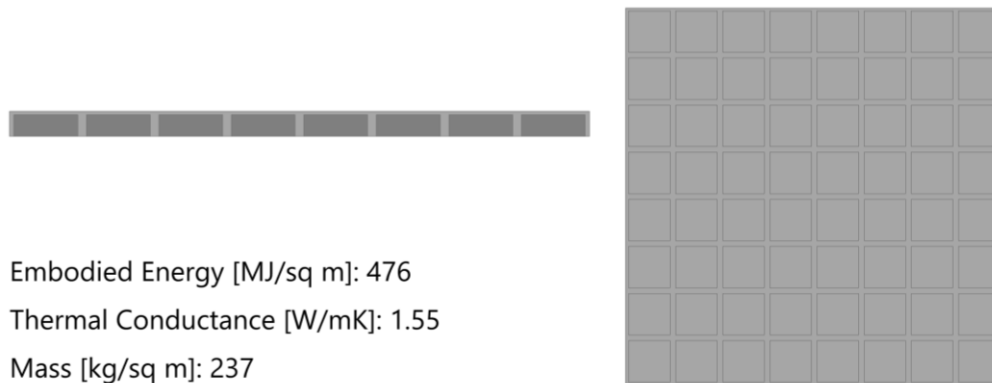


Figure 4-10: Drawing of the best performing solution for 6m – straw filler slab. Scaling surface has 1 control point.

Adding structural depth does have implications on the embodied energy savings for some materials chosen as shown in Table 4-4. For example, design of a slab with bagasse and ash composite material, which has a lower density and embodied energy by volume than concrete, generates solutions that approach a break-even point for embodied energy when compared to the benchmark. Similarly, the selection of rock wool filler material, which has a density two orders of magnitude lower than concrete, but a fairly high embodied energy, yields optimal designs with reduced U-values when compared to the benchmark, but embodied energy values are nearly equivalent to the benchmark. This is because the extra concrete material volume that is being replaced by filler (due to the increased structural depth), increases the total embodied energy of the generated filler slab design. Similar trends are found across each span and material, as the ultimate goal is to replace as much concrete as possible without violating structural and geometric constraints.

Table 4-4: Performance savings of optimal designs compared to minimum depth flat slab benchmarks

Metric	6m	9m	12m
<i>Straw</i>			
Embodied energy	-36%	-24%	-25%
Mass	-32%	-35%	-19%
U value	-85%	-85%	-85%
<i>Bagasse + Ash Composite</i>			
Embodied energy	1%	2%	5%
Mass	13%	46%	56%
U value	-63%	-71%	-76%
<i>Rock Wool</i>			
Embodied energy	3%	1%	0%
Mass	-32%	-37%	-20%
U value	-78%	-89%	-82%

With respect to mass savings, all the optimal filler slab designs generated with straw and rock wool as the filler material saw mass savings when compared to their respective benchmark. There is a decrease in percentage saved with span when compared to the equivalent solid concrete slab. This makes sense as the larger the span, the more difficult it is to satisfy moment and deflection constraints and the more structural material is needed to resist the additional load. The optimal solutions for the bagasse and ash composite filler material had higher mass than their benchmarks, and that mass percentage only increased with span. This suggests that given the optimal depth of a waffle slab, there is a density threshold the filler material must be below in order to guarantee mass savings.

Calculated U-values are similar across the three spans analysed with respect to each filler material. This represents a theoretical upper bound that is achieved not only through material choice, but by relaxing a flange minimum thickness requirement that exists for concrete-based fireproofing. Previous work (Acharya et al., 2020) saw u value reductions in thermally optimized slabs between 24% and 52%; results in this paper show reductions between 71% and 89% when compared to a solid concrete slab most likely due to this constraint relaxation. Further thermal simulation should be included in future work to validate these analytical values and explore other heat transfer metrics of interest. This is expanded upon in Section 4.4.

4.3.2 Filler module number variation

Table 4-5: Comparison of reductions achieved with different number of filler modules

	8 filler modules	10 filler modules
Embodied Energy	-36%	-37%
Mass	-32%	-25%
U Value	-85%	-86%

For a 6m span filler slab with straw as the filler material, number of modules is varied between 8 modules and 10 modules. More than $n = 10$ proves to be computationally intensive and begins to cause issues with meeting cover and web dimension constraints for the 6m span, and lower than $n = 8$ produces large modules that in practice would be difficult to manufacture. Module number does not appear to have a significant effect on any of the key metrics of embodied energy, mass or U-value. This suggests that when designing a slab, module number can be selected based the ease of manufacturing the filler insert, or overall constructability of the slab.

4.3.3 Uniform versus non-uniform module sizes

A 6m span with 10 straw filler modules in both the x and the y direction was modelled to investigate the potential of custom module depths throughout the filler slab. The scaling surface, which controls the width of the modules was modified from using a single point to control the height of the surface to four points at the corners of the surface which models a distribution that can be mapped to the void widths in the slab.

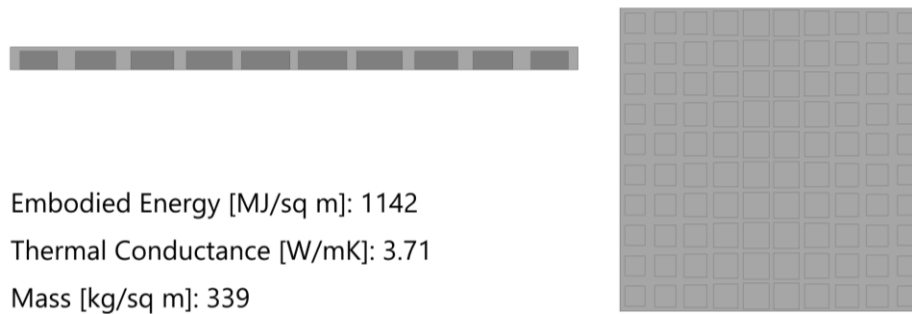


Figure 4-11: Feasible but non-optimal performing solution designed with 4 point-controlled scaling surface for a 6m span with $n = 10$ straw filler with a 53% increase in embodied energy, 65% reduction in thermal conductance and 3% reduction in mass.

Feasible solutions like the one shown in Fig. 4-11 are common within the sampled set. Here the most material is removed from the middle of the slab as shown by wider voids in the center (presumably to reduce the dead load in a region where the bending moment is expected to be highest), and extra material is provided at the corners presumably to resist shear as shown by smaller voids at the edges. This is in contrast with the intuition that more material should be placed at the center of the slab in order to provide additional capacity where the moment is the highest. Further investigation into the relationship between geometry, capacity and demand is

thus explored in Chapter 5, to understand this solution, and similar geometries that while feasible, do not outperform a waffle slab with standard void sizes.

Ultimately while the method proposed in this chapter is flexible enough to allow for voids of different sizes, optimal solutions that show improvements with respect to embodied energy, mass and thermal conductivity move towards a uniform module size solution when a scaling surface is used to control the widths of the modules. This is most likely due to the assumptions about uniform gravity load distribution (and thus equal moment demand) in each rib section as well as support conditions and the 1:1 aspect ratio of the filler slab. This will be investigated further in Chapter 5.

4.4 Scaled prototype of filler slab with agricultural formwork

This chapter suggests the use of repurposed agricultural waste streams as lost formwork for the construction of a more insulating, and sustainable filler slab. Several agricultural materials such as straw, cork, and bagasse and ash composite materials were evaluated as candidate materials based on their quantitatively suitability (density, embodied energy and thermal conductivity) and manufacturability. Here manufacturability is looked at more holistically; materials suitable for formwork for these filler slab systems were chosen because of the quantity of waste material available for reuse in the design region and the existence of manufacturing processes to create blocks from the waste material that could serve as formwork. Straw bales were standout candidate with respect to structural and thermal performance from the optimization results in Section 4.3 and with consideration of the current manufacturing reality. Furthermore, it is reassuring that active research exists in order to use these elements as insulation at scale and provided methodologies to address concerns outside of the scope of this work such as fire resistance and moisture infiltration (Gaspar et al., 2020).

A scale prototype of a filler slab (30 cm x 30 cm x 7 cm) was made using miniature straw bales (3 cm x 6 cm x 2.5 cm) as filler blocks as well as steel wire rebar and plywood molding. The straw bales were arranged in an orthogonal grid between the rebar cage (Figure 4-12, left) and then ready-mix concrete was casted atop the molds. As illustrated in the right of Figure 4-12, upon demolded, the straw bales remain integral with the structure, and provide the waffle shape for the concrete. This lab-scale prototype takes inspiration from traditional filler slab construction methods and as such can be scaled up with this suggested filler materials. Small straw bales at industry scale generally measure 35 cm x 45 cm x 91cm and can be as large as 91 cm x 122 cm x 228.6 cm, which is more than a sufficient size range to produce straw bales for formwork purposes (Fears, 2016).

Manufacturing errors at the prototyping scale mainly were the result of movement of the straw bales during the concrete pouring. Using straw bales for optimally-sized formwork for a full-scale component would result in heavier bales and hopefully minimal movement from target location. In this construction of this prototype this could have been addressed by decreasing the pour speed, or using some sort of fixturing for the bales.

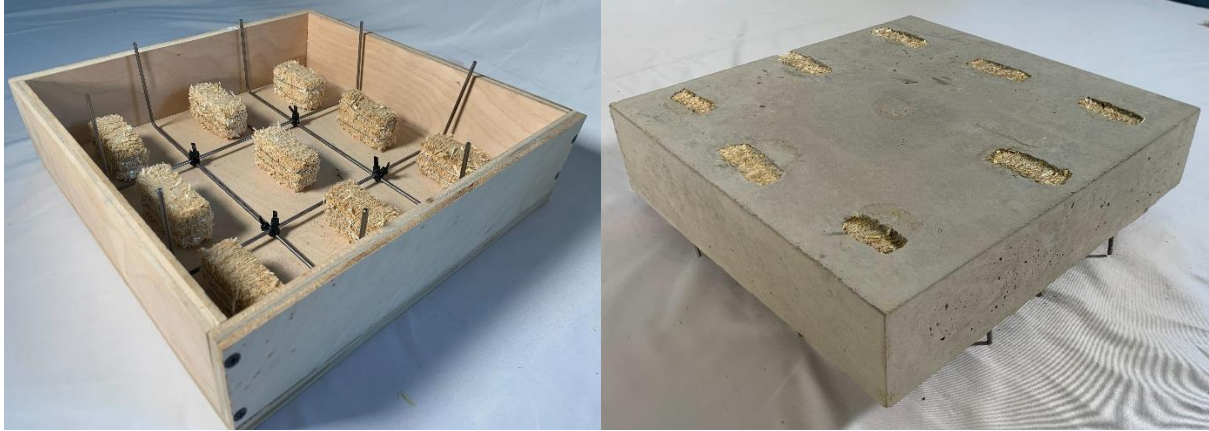


Figure 4-12: Left - Image of the straw bale formwork and scaled conventional construction materials for a concrete filler slab (left), Right- image of the bottom of the filler slab with straw bales integral to slab and concrete waffle.

4.5 Discussion

While the results of this study show that filler slab construction with insulating lost formwork can significantly reduce the U-Value of the structural element, one final comparison point for the utility of construction of these structural elements is whether they can alone meet ambitious targets for U-values of roof components. One such standard relevant to the context of this work is the Energy Conservation Building Code (ECBC), authored to set regulations for building emissions in India. For roof assemblies to be compliant with these standards U-value targets range from 0.2 W/m²K for hospitality buildings to 0.47 W/m²K for schools (*Energy Conservation Building Code*, 2017). The range of U-values found for 6 m span, 8 x 8 void filler slab design solutions are shown Table 4-6 below and do not meet these targets. However, when compared to a flat concrete roof element which can have a U-value between 5 – 10 W/m²K, the solutions with the alternative filler material do show noted improvement. While a filler slab alone cannot meet these requirements, the construction of these elements can decrease the amount of additional continuous insulation needed atop the structural element, with no added labor when compared to construction of filler slab with traditional materials such as clay pots. The reduction of that continuous insulation needed to meet the ECBC standard could still mean lower embodied energy and carbon for the roof assembly as a whole.

Table 4-6: Thermal transmittance ranges for optimal 6m slabs design with this chapter's method

Filler Material	U - value Range [W/m ² K]
Straw	1.6 – 2.4
Bagasse + Ash	3.7 – 4.7
Rock Wool	2.2 – 2.9

The findings in this chapter can support designers by providing them with quantitative support for the utility of filler slabs systems in regions that have not seen wide adaption of this technology. In particular they highlight a solution that takes advantage of efficient structural typology selection, that can be built without proprietary formwork, and can integrate secondary objectives. Although not the focus of this particular chapter, in addition to thermal transmittance,

other objectives sound transmittance reduction do correlate well with the findings here (Broyles et al., 2022).

4.6 Conclusions

4.6.1 Future work and remarks

Future work from this chapter can take many avenues with tuning of and validation of the thermal performance, a more comprehensive assessment of the validity of adding complexity to the filler slab geometry, integration of these elements into a building scale model, and even the consideration of the principles of filler slab construction as integrated insulative façade components. While the latter two suggestions are outside of the scope of this thesis, the first can be discussed in this section and in future chapters with some level of specificity.

With respect to thermal performance, this work pursues an infinite lateral conduction model, due to its conservative estimates of thermal performance and better alignment with the finite element model in regions of the design space of interest (low-embodied energy solutions), it could be worth pursuing a more nuanced model where the closed form model applied is a function of the thermal conductivity of the materials and geometry of the slab. Another option could be a fin resistance model for the concrete slab, which may prove more accurate in scenarios with a significant order of magnitude difference between thermal properties of the concrete and the filler material selected.

Future work will expand the method in this chapter to allow for different support conditions and asymmetric loading. This will allow for a more accurate embodied emissions assessment of the potential of filler slabs with customized filler slab as well as the integration of manufacturing constraints directly into the workflow to realize these systems.

4.6.2 Summary of intellectual contributions

This chapter presents a computational method to design two-way filler slabs that provide an integrated solution to addressing both embodied and operational energy. A graphical method is presented for filler slab material selection that reduces the complexity of optimization. In addition, this chapter presents design solutions for filler slabs that quantify performance savings for embodied energy, mass, and U-values for a variety of representative test cases with different filler options and spans. This chapter accomplishes its analysis with finite element validated, closed-form analytical models that allow the optimization to remain contained within Rhino/Grasshopper environment, a common tool for architecture and structural engineering practitioners. The computational design method presented in this chapter is flexible enough to design non-uniform voids lengths and widths due to moment and shear checks at intersection points throughout the span instead of just at the center, and the incorporation of deflection calculations for variable stiffness through a section. With respect to system specific design knowledge, the results of this chapter reveal a key nuance in the structural design of these filler slabs not yet reported in design literature of these systems: the optimized solutions for the filler slabs don't simply remove material from the volume from a slab the same depth of the flat slab,

but increase the structural depth of the filler slab when compared to the benchmark for its respective depth.

5. Parametric customization of waffle and filler slab systems

Recent advances in computation and digital fabrication have coalesced to bring about the potential of mass customization at the building scale. This chapter focuses on assessing opportunities for carbon savings when customizing the shape of waffle and filler slab voids based on their structural demand. It repurposes the computational workflow from Chapter 4 and uses a case study of a utility shed roof for a more realistic loading scenario, hypothesized to be a better candidate for shape customization than slabs with more symmetric distribution of supports and loads. The intuition here would be that additional customization and only placing material where it needs to be would always be better from a carbon perspective, but from a structural mechanics perspective, there is more nuance to be discovered.

This chapter adapts part of a case study published by the author that focused on the design of custom fabrication of shell formwork (Curth et al., 2022). This chapter will highlight this work, but ultimately focuses on the necessary mechanical understand to determine the value of shape customization against carbon and manufacturing objectives.

5.1 Background and state of the art

5.1.1 The intention of structural logic in architecture

The search for material economy by architects and structural engineers has led to many innovative structural systems and fabrication methods to achieve visual interest while meeting other constraints such as mass, cost etc. One method is the adoption of *structural logic*, which is defined here as, the use “exposed structure” or geometric forms that evoke the structural relationships sustaining the loads of a building as a visual feature of the design, not as elements to be hidden away from occupants. This has been met with various forms of both praise, critique, and renewed interest, as structural efficiency has been proven to be a key pathway to a carbon neutral future.

Acclaimed built examples of concrete systems that feature structural logic that reflect actual behavior include the geometrically complex and patterned slabs of Pier Luigi Nervi (Section 2.2.2). Nervi slabs were designed using experimental and theoretical analysis to find isostatic lines of the principal bending moments by which to place the concrete ribs in his slabs (Halpern et al., 2013). In addition, there is Tagore Hall by Mahendra Raj (Figure 5-1), a visual delight of structural system efficiency from its folded plate, rigid frame exterior to the Nervi inspired interior sculpted columns that twist upwards, and are shaped to accommodate the resultant moment of the cantilevering beams it supports (M. A. Ismail & Mueller, 2019).

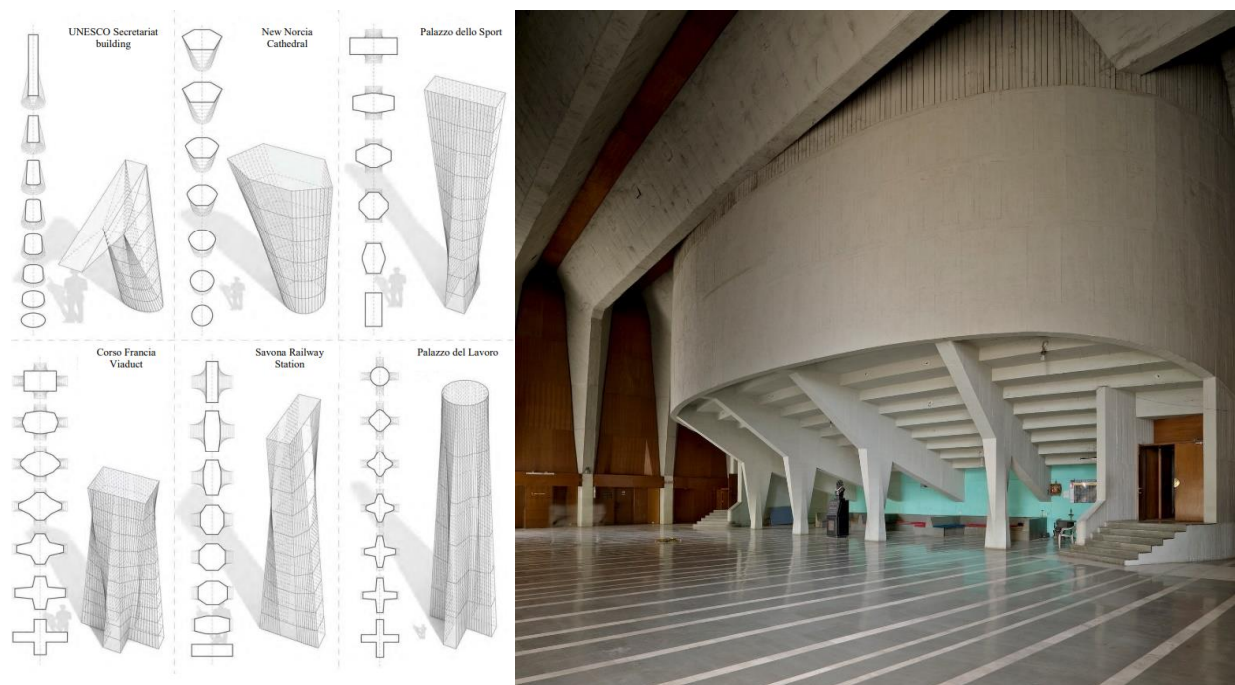


Figure 5-1: Images of shaped and twisted columns that respond to loading demands by Pier Luigi Nervi (left) and shaped column and folded plate structural system of Tagore Hall by Mahendra Raj (right)

Recent research-scale work has leveraged digital fabrication and computational design to aid the expression of structural logic. This includes the Stereoform slab designed by SOM in 2019 spanning over 45 feet and using around 20% less material than a conventional concrete system.

This slab was made with formwork fabricated using a robotic hot wire cutting technique. Prior to this installation, Ismail and Mueller demonstrated a shaped beam at scale of 1 m in length that was fabricated with custom formwork created from CNC milled foam (M. Ismail, 2019). This work led to the construction of a full-scale pavilion in Mexico called *Sueños con tierra y concreto*, that not only provided proof of concept of their computational method at scale, but integrated custom 3D printed clay blocks as infill, highlighting the role that low-carbon indigenous materials can play in a digital fabrication future (Digital Structures et al., 2022).

While the previous works were empowered by formal and informal principles of shape optimization, topology optimization, or the optimization material distribution with a 2D and 3D space, has also been touted as a design method to realize structurally efficient floor and beam systems. Topology optimized structures generally feature a characteristic skeletal aesthetic most commonly realized with digital fabrication techniques, specifically additive manufacturing (Stoiber & Kromoser, 2021). This field can be traced back to the work of Bendsoe and Kikuchi (1988) and has evolved rapidly in the aerospace and automotive industry, but has resulted in fewer examples past the research prototype scale in structural engineering and architecture. Jipa et al. built two structural examples of a topology optimized floor slab made at scale fabricated with 3D printed formwork (Figure 5-2). However these slabs are fabricated solely with feature fiber reinforcement in the concrete mix and no longitudinal reinforcing, (Jipa et al., 2016) which is not yet accepted or structurally viable in many regions of the world.

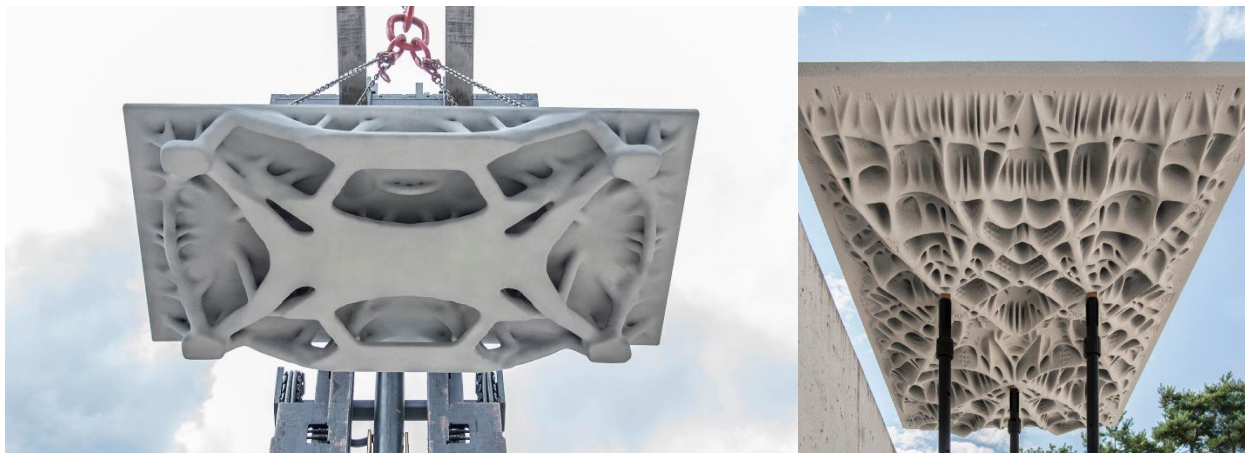


Figure 5-2: Topology optimized floor slabs from ETH Zurich with cast-in-place additively manufactured formwork

Key issues standing in the way of concrete spanning elements designed with shape and topology optimization methods include incorporation of steel reinforcement, and of course access and cost of digital fabrication technologies need to realize these methods at the column-grid scale for the individual elements, and to meet structural needs for countless multi-story buildings vs individualized endeavors.

Outside of concrete architecture, structural logic via material placement, material removal and shaping has also seen huge interest. With respect to mass timber, Mayencourt and Mueller have introduced a methodology for the shape optimization of cross laminated timber (CLT) beams that includes consideration for efficient cut layout (Mayencourt & Mueller, 2020) for example. Moving away from beams, structural patterning of shells and surface structures has been

highlighted as a way to push the boundaries of efficiency of spanning technologies and has been displayed in built examples such as Footbridge Trumpf by schlaich bergermann partner (Figure 5-3a), as well as with new frameworks that reduce computational time in the conceptual design phase of these structures as shown in Figure (5-3b) (Rivera et al., 2020).



Figure 5-3: Examples of work expanding the fields of structural patterning of shell structures a) Footbridge TRUMPF in Ditzingen, Germany (2018), b) adaptive framework to reduce computational time in the design process of perforated shell structures (Rivera et al., 2020)

While it is clear that structural logic can be executed in conjunction with material efficiency, counterexamples do exist which have borrowed the visual aesthetic of the examples shown previously in this section, but resolve the structural forces separate to the action being displayed. This includes the Chhatrapati Shivaji International Airport in Mumbai (SOM, 2010), which displays fluid multidirectional ribbing in its ceiling and large columns spanning the exterior and interior spaces of the airport terminal, but at its structural core, is a steel roof truss supported by mega columns, covered in glass fiber gypsum coffering panels (Besjak et al., 2013). Similarly, there is the Qatar National Convention Center (Yamasaki Architects, 2011) whose facade was designed with a topology optimization algorithm and evoked images of a large, organic tree-like

structure, when in reality, it is made from straight steel elements and then wrapped in non-structural cladding (Jewett, 2018). Both of these examples are shown in Figure 5-4.



Figure 5-4: Images of systems evoking structural logic and expression but realized via conventional systems and cladding. Left: Chhatrapati Shivaji International Airport, Right: Qatar National Convention Center

Unmistakably, there is a desire for visible structural expression and acceptance of its forms in modern architectural aesthetic. However, that cannot be achieved without scalable methods for manufacturing as well as demonstrated benefit for stakeholders whether that is carbon and/or cost. The challenge explored in this chapter is two-fold: to understand and evaluate a scenario in which the deployment of customization and structurally expressive logic in a filler and waffle slabs can outperform an optimized standard waffle slab, and to highlight fabrication methods that can enable the fabrication of these systems, at the scale of the building column grid. This is especially relevant, because the results of optimized waffle and filler slabs presented in this chapter and the preceding ones presents sizes of waffle voids that are sized relative to the spans of the systems and a discrete, user specified number. This is a slightly different paradigm from the reality of practice, where the formwork for waffle slabs is expensive, proprietary, and limited to a few select pan dimensions, regardless of span.

5.1.2 Mechanics of reinforced concrete section

The mechanics of reinforced concrete spanning elements are based on a complex relationship between the steel rebar that resists tensile loads in the element and the concrete matrix surrounding it that not only holds it in place but resists compressive forces as well. An understanding of isotropic material behavior and elastic bending is often not sufficient to predict service behavior of these elements. Structural engineers have often resorted to semi-empirical mathematical expressions, finite element analysis, and over prescription of material to ensure safe and desirably behavior of concrete elements in service. However, embedded in these methods to design concrete elements are several assumptions about mechanical behavior of equilibrium structures that are reflected in the design.

When we produce concrete slab designs for concrete elements that are uniform and symmetric, whose cross-sectional dimensions and steel content are the same throughout, the result is a slab

with the same structural capacity at every location, generally designed for the highest value of moment and shear in the slab. This does not correlate to efficiently meeting the reality of a spatially varied demand across the spanning directions. What we may think of as intuitively optimal, at least for a filler and waffle slab, might voids sized differently as a function of location and demands, carving away at the web's width and compressive flange until the minimal amount of material required remains. It is also important to remember that the levers that are available to structural engineers and architects to improve structural performance from modifying a slab's section geometry may not be the ones that make the most visual impact. For example, changing the amount of steel specified to each spanning section could be very impactful, but the steel is covered by concrete. Similarly, depth of the compressive flange in a waffle and filler slab may have impact on moment resistance of the section, but may not always be visually discernable. For visual impact of these two-way ribbed systems, the main variables to tune will be void width (which controls the thickness of the ribs) and overall depth.

Design Variables	$x =$	$\begin{bmatrix} L = \text{span} \\ * h = \text{total depth} \\ * R_w = \text{web ratio} \\ * R_h = \text{flange ratio} \\ A_{\text{steel}} = \text{area of steel} \\ * s = \text{rib spacing} \end{bmatrix}$	$x =$	$\begin{bmatrix} L = \text{span} \\ * h = \text{total depth} \\ R_w = \text{web ratio} \\ R_h = \text{flange ratio} \\ * A_{\text{steel}} = \text{area of steel} \\ * s = \text{rib spacing} \end{bmatrix}$
		visual impact		increased fabrication complexity

Figure 5-5: Design variable highlighted in blue and with * correlated to visual impact and fabrication complexity for waffle and filler slabs

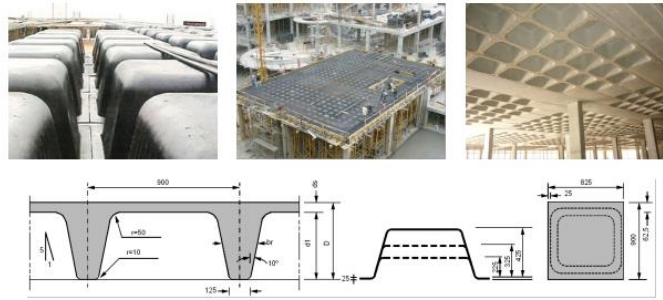
This chapter is first concerned with producing structurally feasible waffle/filler slab designs that maintain constant structural depth and constant area of steel for ease of manufacturing, but it's possible, that these compromises may limit the carbon benefits of customization of the shape of waffle and filler slab voids. Generally plastic and metal waffle slab formwork is available for purchase or rent in a set of standard sizes (Figure 5-6). These formwork size options have to work for a variety of spans, depths, desired rib spacing and density, but are not plentiful enough that it would prohibit stocking on the end of the manufacturer. Optimizing the waffle slab formwork for a given span and loading conditions introduces one level of construction complexity and additional cost, which would only increase without an appropriately developed method to also customize the depth of the ribs to optimally meet a particular demand scenario as well as the void sizes.

2.1 FG 900 MOULDS

“FG 900” moulds are used on the construction of waffle slabs with bidirectional orthogonal ribs, also called fungiform slabs, producing modules with 900 mm distance between the ribs axis.

There are three different types of “FG 900” moulds, with heights of 225 mm, 325 mm and 425 mm. They were designed with two narrower edges so that they can be removed three days after the concrete casting, keeping the vertical support structure.

They are internally reinforced, guaranteeing very small deformations. Its low weight allows an easy handling on site.



Mould Height	Top Layer Thickness	Total Height	Average Rib Width	Cross Section Area	Distance to G.C.		Inertia (per rib)	Flexion Module (per rib)		Void Volume		Self-Weight	Concrete Volume
					Upper Face	Bottom Face		cm ² /rib	cm ² /rib	m ³ /mould	m ³ /m ²		
mm	mm	mm	mm	cm ²	mm	mm	cm ⁴ /rib	cm ² /rib	cm ² /rib	m ³ /mould	m ³ /m ²	KN/m ²	m ³ /m ²
225	50	275	172	816	83	192	49561	5971	2581	0,113	0,139	3,45	0,136
	75	300	176	1040	87	213	65670	7548	3083			4,05	0,161
	100	325	180	1266	95	230	84158	8858	3659			4,65	0,186
325	50	375	192	1043	122	253	125718	10304	4969	0,156	0,192	4,60	0,183
	75	400	197	1268	123	277	159245	12947	5749			5,20	0,208
	100	425	203	1493	128	297	194449	15191	6547			5,85	0,233
425	50	475	207	1310	165	310	255029	15456	8226	0,197	0,242	5,85	0,233
	75	500	212	1536	163	337	314390	19347	9315			6,45	0,258
	100	525	217	1761	165	360	374573	22701	10450			7,10	0,283
d1	ds	D	br	A	rs	ri	I	Ws	Wi	Vv	25 KN/m ² Concrete		

Figure 5-6: Sample of standard sized waffle slab formwork available for purchase or rent for slab construction (Fercanorte - Structures, Slabs and Formworks Ltd.)

5.1.3 Shape optimization and customization in waffle spanning structures

Perhaps closest to the point of investigation in this chapter us the shaped waffle slab ribs is the Shri Ram Center for Arts and Culture in New Delhi, designed by Shiv Nath Prasad and Mahendra Raj (Figure 5-7). This cast-in-place work features a shaped-waffle slab top floor cantilevering 6m in each direction from its four cross shaped column supports. This structure was completed in the late 1960s without the aid of modern computational design tools.



Figure 5-7: Left - ShriRam Centre for Arts and Culture, New Delhi, India, middle – close up shop of shaped waffle slab ribs for cantilevered roof element and right – roof framing drawing.

Danhaive presented a method in their dissertation work to design a waffle shell structure, with shell thickness distribution and material density realized via topology optimization and strain energy as a performance metric. In this work, regions of “thickness depressions” were created giving a waffle structure visual effect for the shell (Danhaive, 2020). Although the results of this study are a key demonstration of the use of latent variable models at exploring geometric complex design spaces, this work is not technically rooted in concrete mechanics and structural behaviors, despite that being the presumed materialization of the resulting designs.

The computational analysis of this work foundationally is rooted in modern structural shape optimization, which can be thought of as the refinement of a parameterized boundary region, subject to structural constraints (Haftka & Grandhi, 1986) is key to the ability to design a customized waffle slab. This chapter adapts shape optimization workflows from Ismail and Mueller for shaped concrete beams for two-way ribbed slab system (M. A. Ismail & Mueller, 2021). It makes use of closed-form beam analysis for capacity to avoid temporally expensive numerical methods. This chapter also presents the first work to look at the shape optimization of waffle slab system, guided by concrete mechanics and with optimal carbon performance as a goal.

5.2 Methodology

The computational methodology to design custom waffle and filler slab systems is similar to the one outlined in Chapter 4, with key differences highlighted in the rest of this section. The first is that the structural analysis now utilizes finite element analysis to determine the demand at each section under analysis, and second this method utilized sampling and local optimization to overcome challenges associated with increasingly complex structural and geometric constraints. Lastly this chapter focuses exclusively on the structural behavior of the slabs and as such will feature the use of waffle slab to refer to the reinforced concrete structural element whose design is being optimized, recalling that filler slabs can be designed as waffle slab structures.

5.2.1 Parameterization of waffle slab typology

This waffles slab evaluated for customization is parameterized the same way as Chapter 4 (See Figure 4-7 and 4-8). Two scaling surfaces in total are used to control the geometry of the waffle voids, with a four-point surface controlling the width of the boxes, and another controlling the heights. The values of the control points range from 0 to 1, representing the ratio of void to the total depth or flange width. This technique allows the sizing of 60 voids (the number in the case study detailed in this chapter) in three dimensions with 8 total variables (z-coordinates of control points) vs 120 individual variables.

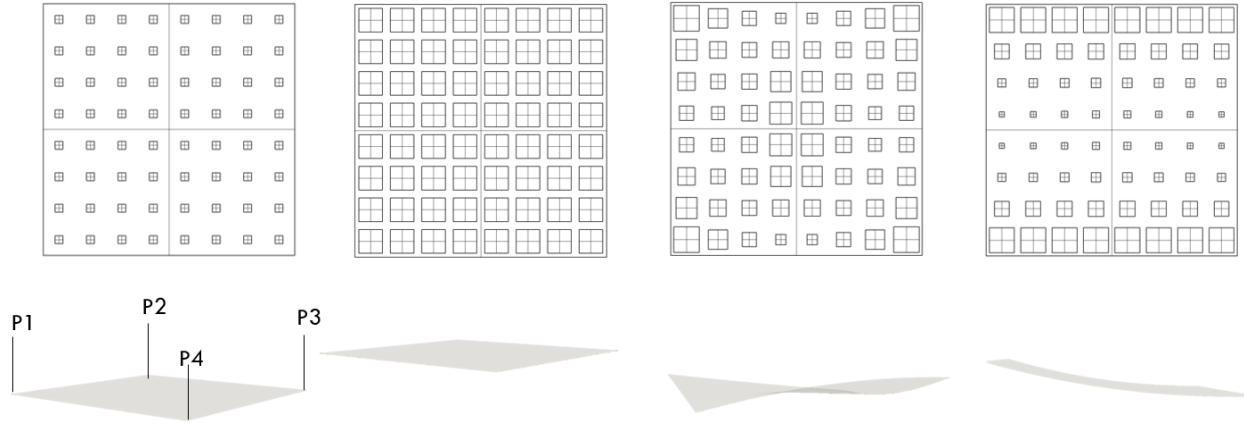


Figure 5-8: Demonstration of the variation in void widths that can be achieved with the manipulation of control point heights on a scaling surface

Table 5-1: Design vector variables for parametric waffle slabs, with multiple scaling surfaces

Design Vector	Variable Description	Value
x_1	number of modules, x	$0 < n_x < 1$
x_2	number of modules, y	$0 < n_y < 1$
x_3	depth of slab	$1 \text{ cm} < h < 50 \text{ cm}$
x_4	area of steel	$250\text{mm}^2 < A_s < 2500 \text{ mm}^2$
x_{5-8}	scaling surface control point height, void width	distribution maps to $.5 < bw < 1$
x_{9-12}	scaling surface control point height, void depth	distribution maps to $.5 < \frac{d_f}{h} < 1$

5.2.2 Hybrid structural modeling and analysis

In designing a structurally feasibly reinforced concrete element, the general idea is that the distributed demand from the loading and support conditions cannot exceed the structural capacity governed by the geometry of the element, the location and volume of steel, as well as the material properties of both. As long as these constraints are satisfied, there is no strict governance that the same type of methods i.e. fully analytical, semi-empirical, and computational must be pursued to estimate both the demands and capacity. The case studies presented in this chapter are for reinforced concrete waffle and filler slabs that are designed to support their self-weight, determined from a volume analysis conducted using Rhino3D/Grasshopper as well as a live load of 4000 N/m^2 with corresponding load factors (ASCE, 2017). From there a hybrid approach is pursued where the structural demand is then determined using FEA, while the structural capacity is found with closed-form analytical solutions and the geometric information defining the waffle slabs ribs.

To build the finite element model for the moment and shear demand, the concrete waffle slab was modelled as a grillage of beams spanning in the x and y direction with the number of beams

equal to the number of T-shaped ribs in the main design and equivalent depth. Next a uniformly distributed mesh load was applied to represent the factored load of self-weight and a concrete waffle slab with a void volume of 50%. The resulting moment and shear demands are extracted from distances on the beams in the FEA model corresponding to T-sections found evenly along the length of a rib, at the midpoint of a waffle/filler void (Figure 5-9). At each of these T-cross sections, the moment and shear capacity were calculated using the methods highlighted in 4.2.2 to ensure they were not exceeded by the FEA demands. The deflection of the center of the slab was also calculated, accounting for variable cross-sections and cracked sections. The serviceability check for deflection, as well as the moment and shear checks at the various sections along the length of the T ribs spanning in both directions, and the geometric constraints for cover, rib spacing, etc. at each section mean that for a given design there can likely be upwards of 100+ constraints that must be satisfied for a design to be feasible.

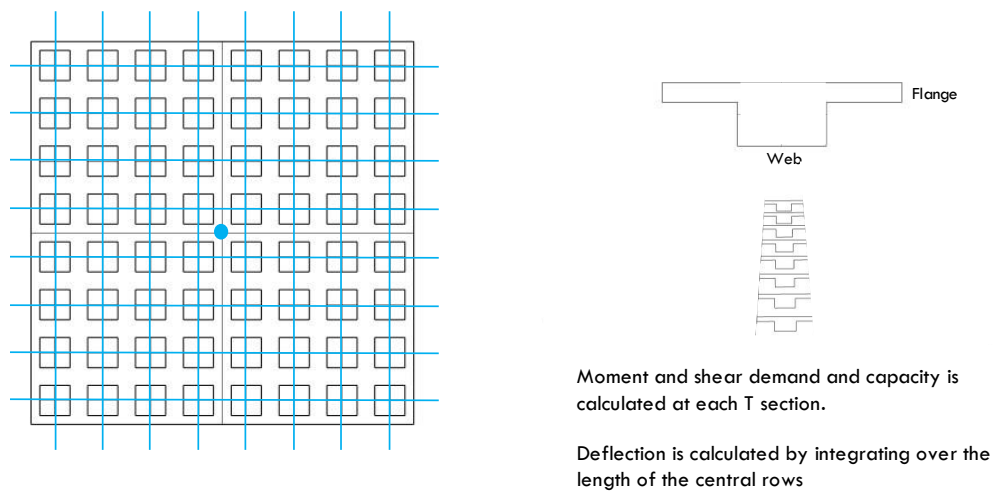


Figure 5-9: Sample waffle slab with standard void sizing and blue lines to illustrate the locations of the T sections used for analysis

5.2.3 Grid sampling and local optimization

While the first instinct may be to solve this problem with constrained optimization since that method was effective for the non-hybrid approach, the reality is the increased number of constraints, as well as the spatially varied demand and capacity, means that this problem can be difficult for the optimizer to tackle, especially as the number of variables and their respective bounds grow. There are several ways in the traditional computational field that optimization problems can be formulated to achieve the same goal in a less computationally difficult way. This can include the use of penalty functions instead of direct constraint application, a change to a heuristic method vs. a gradient-based one, or even by using numerical scaling of constraints and the objective function.

In this chapter a two-part approach is found in which the design space sampling is employed using the Sampler and Capture components from the Design Space Exploration toolbox to record the variables and the objective function values and the Writer component to record the values of all the constraints (Brown et al., 2020). The dataset is then post-processed where structurally infeasible designs are culled from the dataset and regions of the design space where high

performing designs are located, and the bounds of the parametric model are adjusted to just these high-performing regions. Finally, optimization is performed locally using Radical to refine the high performing design solutions and locate the solution with minimum embodied carbon.

5.2.4 Case study: Roof for a 3D printed utility shed

This method is demonstrated with a case study structure: the roof of a small utility building near Twente Additive Manufacturing's (TAM) facility in British Columbia, Canada. A parametric model of a 6m x 3m waffle slab is generated in Rhino/Grasshopper with a distribution of 12 x 6 voids, 4 column supports, and overhanging spans of .5m in both short directions and in one of the long directions (Figure 5-10). The number of voids were determined based on print volume size constraints, as well as computational intensity of design generation. There was a desire by the partners at Twente, to highlight geometric variation to showcase the potential of their concrete and cement-based 3D printers, upon fabrication of the final design of the roof.

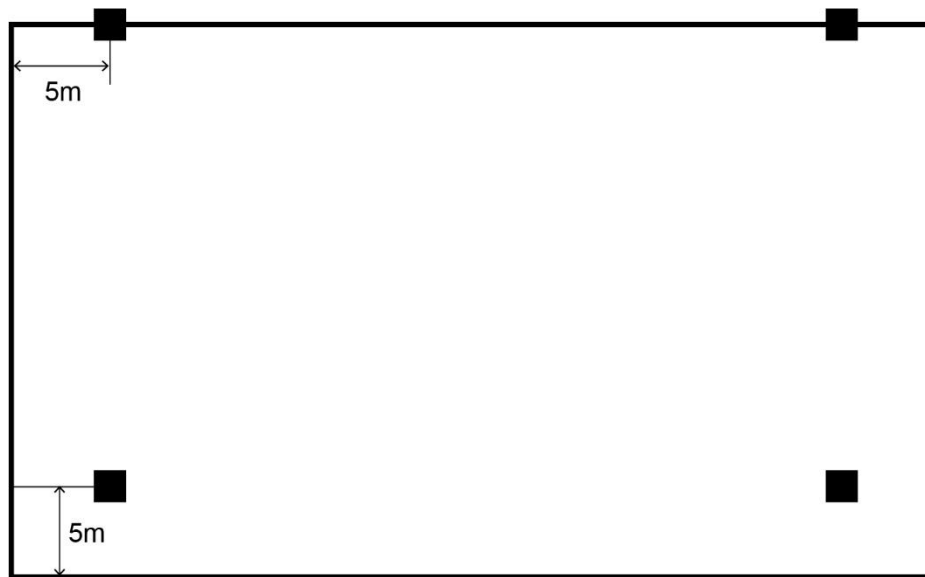


Figure 5-10: Plan image utility shed roof with 3 overhanging spans. Squares indicate column locations

5.2.5 Additively manufactured formwork for filler slab customization

Although 3D printing of concrete most commonly refers to extrusion-based printing of walls for 1-story construction, there has been some recent work in the realization of beams, connections and columns (Block et al., 2017). At the moment, 3D printed of spanning structures, floors and roofs at the scale of the 3m - 5m column grid remains challenging due to machine limitations and cost. This work in this chapter is designed for additively manufactured shell formwork, referencing the clay pot formwork common of traditional filler slabs in India, as well as masonry logic. This allows for the achievement of waffle slab geometry without proprietary formwork and with voids, tuned to the particular span and loading conditions. More details on the methods for designing the formwork are available in previously published work (Curth et al. 2022).

5.3 Results

5.3.1 Structural demand forecasting highlights problems suited for customization

Geometric customization realized with 3D printing is not necessarily a new phenomenon, but what is less established, are analysis methods that help evaluate the appropriateness of pursuing shaping and customization that are informed by the structural mechanics of a system and not just the cost. Figure 5-9 shows the distribution of moment and shear demand for 3 different waffle slabs, a square waffle slab (1:1), rectangular waffle slab (2:1) with spans similar in length to the long span of the case study for a fair comparison. The square waffle slab as expected has a lot of repeated values and the smallest spatial spread, whereas the roof in the case study in this chapter with overhanging sections, has the widest distribution of points as well as the least number of overlapping points. Performing a demand distribution analysis like this can serve many purposes, in this case, it can help evaluate a particular slab's loading scenario, and determine if it would be a good candidate for a structurally customized design. The intuition here was that the roof with overhangs would be a good candidate for customization because of the wide range of moment and shear demand, but this also means that the structural constraints may be harder to meet.

Figures such as 5-11 help quickly understand what the worst-case scenario design sections are, but this figure also abstracts away the spatial relationship to these points. This is a key drawback because the slab system is by nature continuous. Even how the waffle slab is parameterized, via the extrusion of rectangular prismatic forms and geometric cuts and solid division operations, and how demand is calculated, is reliant upon a shared basis of where in space the analysis is taking place. For this reason, a plot like this is limited in explicit design of slabs but could be values in systems more amenable to the catalog of parts approach such as truss or grid shell node connections (Lee & Mueller, 2023)

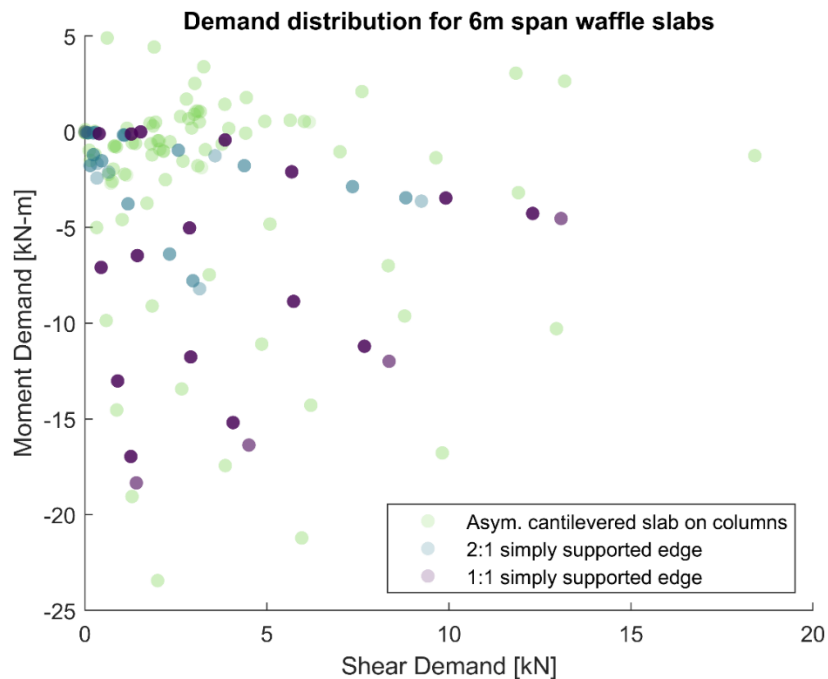


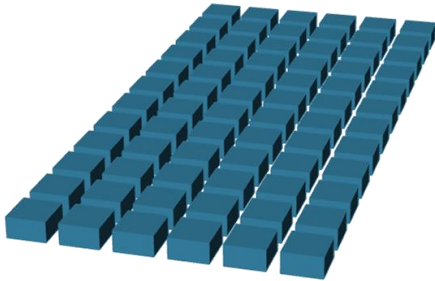
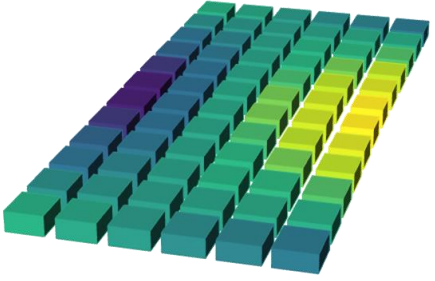
Figure 5-11: Moment and shear demand for every point of analysis in the waffle slab for 3 different aspect ratios and support condition. The darker the point, the more times that combination of demands appears in a slab.

5.3.2 Design of size customized waffle slab roof improves utilization.

After sampling both scaling surfaces, two feasible, high performing designs were identified, including one in which the waffle slab voids are the same volume throughout the slab (standard solution), as well as an optimal design in which a void size distribution is generated. This design displays this structural logic discussed in previous sections where there is less volume removal in sections with the highest moment demand; in other words, where there is a greater need for structural material, and there is more volume removal in parts of the slab with lower moment demands. The exception to this is the small boxes in the upper corners of the slab, most likely thickening to account for higher shear demands near the column supports.

In Table 5-2, the value for the performance metrics of embodied carbon and mass are displayed. Although there is some improvement when moving from a design with voids of the same size to an optimal size distribution, that change is within 5% percent for these two metrics. As both of these designs specify the same rebar size, this savings for embodied carbon and mass is strictly a result of concrete material reduction. It's possible that design refinement could return increased savings, but perhaps more importantly, this result supports previous work in Chapter 3, which showed that a waffle slab that is sized optimally for voids of the same size and voids sized relative to its spans is already incredibly efficient. Added benefits from a size distribution of the voids tailored to spatially-distributed demand is modest at best.

Table 5-2: Performance metrics for parametric slab with standard void sizes, vs with a size distribution.

Metric	Standard Void Sizes	Size Distribution
		
Mass [kg/m ²]	346	331
Embodied Carbon [kgCO ₂ /m ²]	58	55
Moment Utilization Range	0 - .69	0 - .82
Shear Utilization Range	0 - .62	0 - .69

This can be interrogated further by looking at the utilization values for the slab. Utilization is the ratio of demand to capacity. A small utilization would mean a section under analysis is oversized and could be improved via optimization. Despite the solutions found being optimal with respect to embodied carbon and mass, the range of utilizations reported in Table 5-2 are a bit lower than expected from a shape-optimized design. It is promising that the slab with size distribution has a higher moment and shear utilization ranges, but this summary as well as analysis of the design indicate that there are multiple analysis sections with little to no utilization. To interrogate this further, Figure 5-12 displays histograms of the utilization ratios found for the T sections analyzed in the case study. We can see a right skew in these plots indicating that majority of the utilization ratios fall at the beginning of the range. In other words, most of the sections are underutilized with respect to the amount of moment and shear resistance provided with the shape optimized design.

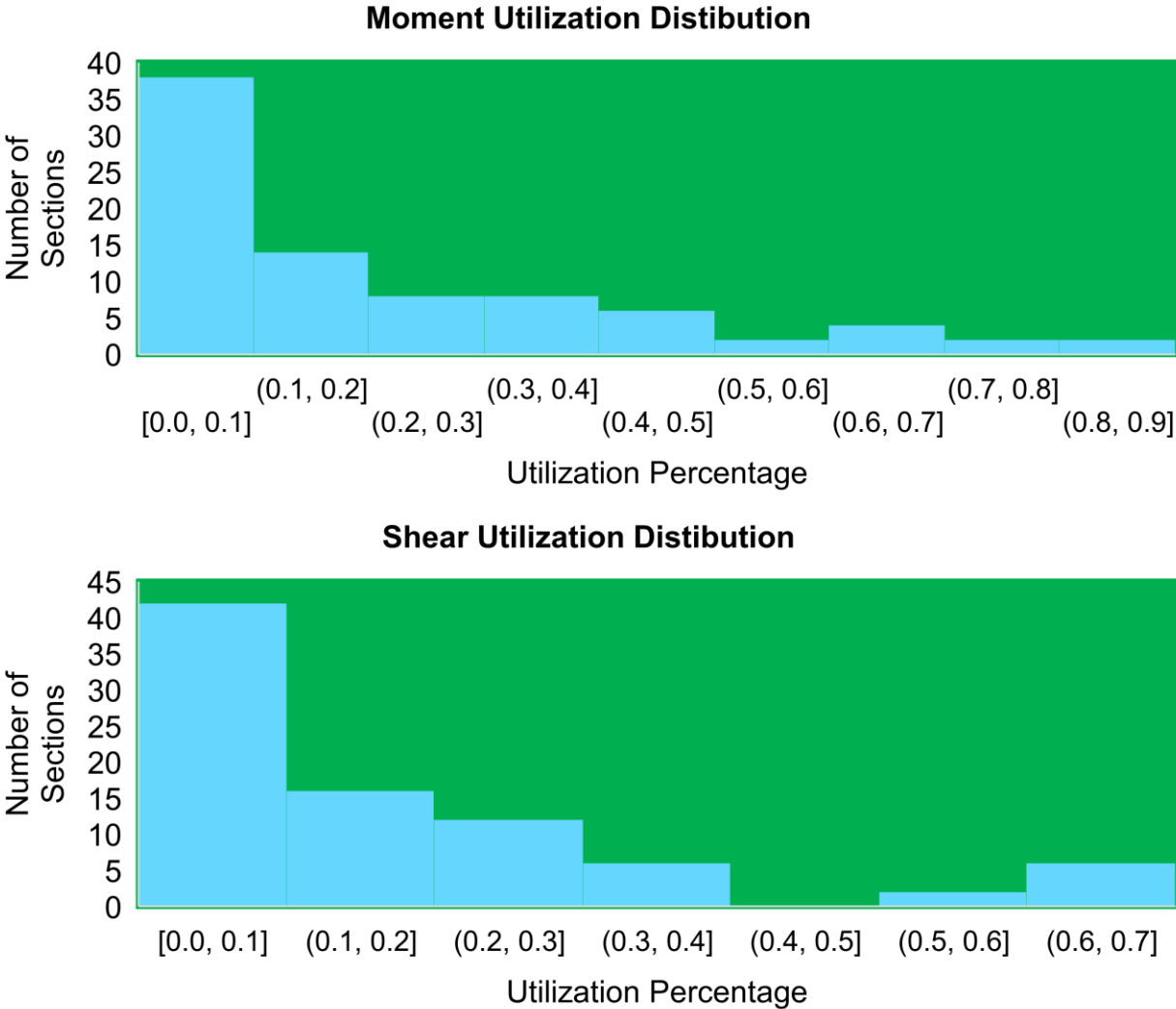


Figure 5-12: Moment and shear utilization histograms for the shape optimized waffle slab example.

5.3.3 Structural efficiency is limited by geometric and manufacturing constraints.

Just as there is distribution of structural demands whose distance is determined by its support conditions and loading, there are a variety of sections that can be designed to suit the capacity needs of a concrete slab. This structural capacity is governed by the section geometry and the amount of steel. Recall that for visual impact of customization, the two key variables the occupants can see are the section's structural depth and web ratio. To further understand the impact at the T-section level, 5000 sample sections were sampled, returning 419 feasible section designs. The designs were plotted in Figure 5-13, highlighting their moment capacity vs. embodied carbon and their shear capacity vs embodied carbon. The optimal sections would be ones that maximize their possible capacity while minimizing embodied carbon. The Pareto front of these designs is displayed with filled in circles. All designs are then colored via these two variables of visual impact.

When tracing along the Pareto front for maximum moment capacity and minimum embodied carbon, there is a range of depths that can accommodate this need. In other words, structural depth of the section is a significant factor when looking to change the moment capacity of the section. This isn't so surprising, with the revisiting of first-principle knowledge of moments of inertia, where generally speaking, the depth is a dominating factor. Conversely, when looking at the points along the Pareto for web ratio, all the optimal solutions have the same web ratio. This, plus the coloring of the plot, shows that the full range of web ratios can be used to generate a section for any given moment capacity, but, if the goal is to minimize embodied carbon, it's better to make the web as thin as possible, minimizing the volume of concrete. Moving to the lower row of plots in Figure 5-13 tells a slightly different story as the Pareto front for minimal embodied carbon and maximum shear capacity highlights both a variety of structural depths and web ratios. This makes sense as intuitively the web thickness plays a key role in resisting shear forces.

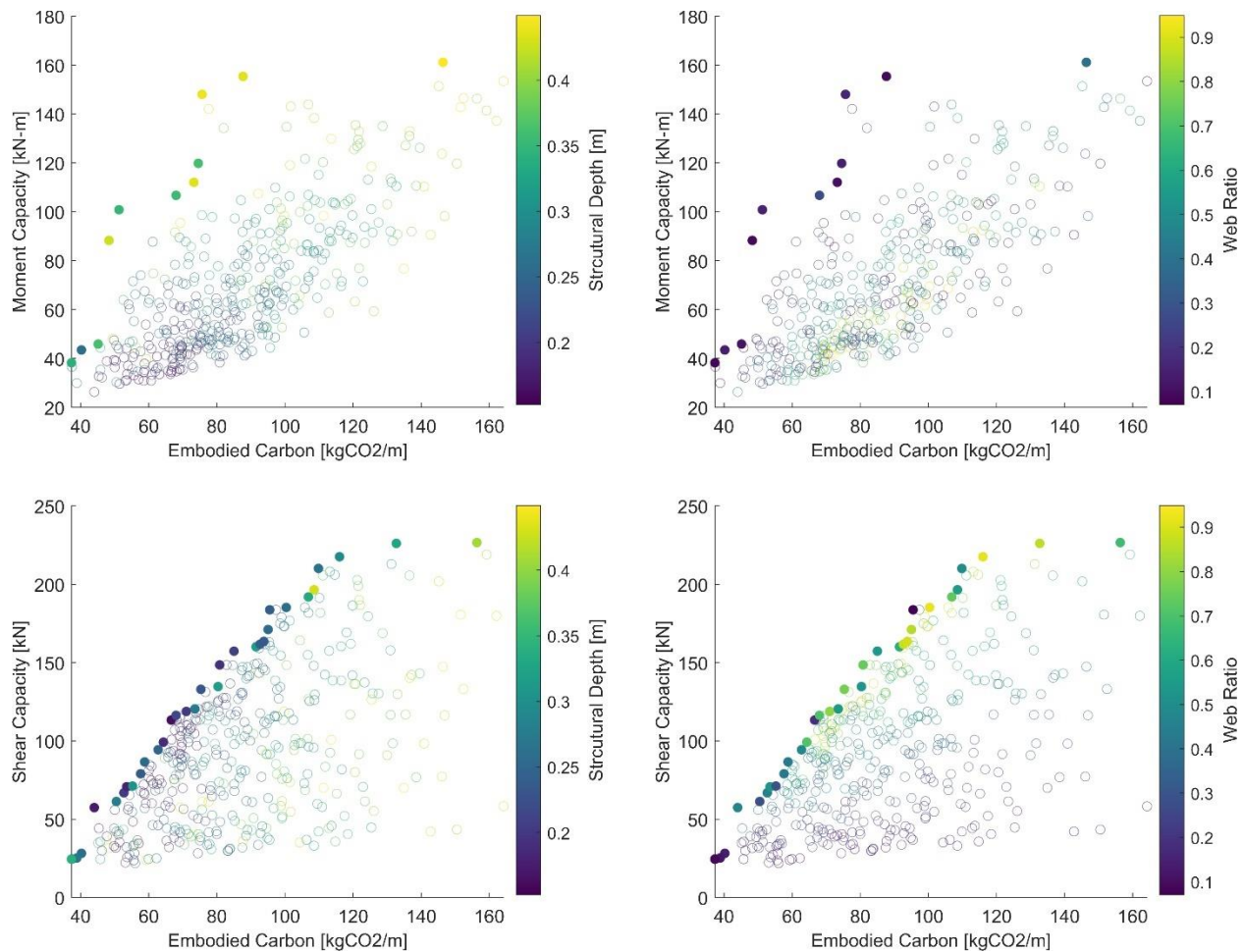


Figure 5-13: (Top row) Moment capacity of sampled *t*-section vs. embodied carbon (Bottom row) Shear Capacity of sampled *T*-sections vs. embodied carbon. Figures are colored by structural depth in the left column and web ratio in the right column.

The results of this sampling exercise lead to conclusions about customization for as it pertains to waffle slab systems and generally ribbed systems with *T*-shaped geometries. Structural depth is the most significant parameter within a designer's control for improved embodied carbon and structural performance overall, and secondly, customization of these systems may also be more beneficial or and visually perceptible in shear dominated loading scenarios.

This also has implications with respect to the manufacturability of waffle and filler slabs systems. This work indicates that shaping along the depth could be beneficial, but that drastically increases the labor required to design these systems and may require technologies not widely available. The constraint on structural depth as well as constant steel area means the design techniques in this work can be applied broadly and more rapidly. While voids of the same size are highly efficient, this sizing may not correlate to what's available by expensive proprietary formwork. Even filler slabs constructed with locally available materials, are restricted in how much material can be removed from the void bases on the height of the found object. In addition, there is still the open challenge of customization if the optimal design solution in this case study were to be selected. The next section, 5.3.4, highlights a manufacturing method that can address these concerns.

5.3.4 A prototype of a filler slab with additively manufactured shell formwork



Figure 5-14: Proof of concept for fabrication of flat concrete element with conventional rebar and fabrication methods, and additively manufactured formwork that can be sized according to optimal dimensions for slab

To demonstrate proof of concept of the additive manufactured formwork for customization, a 1m x 1m prototype was designed and fabricated using the methodology outlined in previously published work (Curth et al., 2021, 2022) which extracts the box shapes from the optimal design, and then creates custom toolpaths for shell formwork mapping to each individual box. As seen on the left in Figure 5-14, conventional rebar cage layout and cast-in-place techniques can be deployed in conjunction with optimized shell formwork. The right image in Figure 5-13 reveals the underside of the element slab element, with the printed squinch vault formwork remaining integral with the element. Although this method allows for a support-free print, about 47% of the optimized filler void volume was lost. Designs with other vault shapes such as those inspired by traditional cloister vaults have recovered some of this lost volume, to a new loss of 40%, but this is still quite large. Future iterations of this process will require additional study on self-supporting formwork shapes that could more closely align with the box geometry modeled for the filler slab as well directly optimizing for a scaled version of the formwork shape, versus extracting the boxes and then generating a toolpath.

5.4 Discussion

One key previous challenge in the design of the optimized waffle slab with custom size distribution voids was the computational expense added from increasing the number of voids. As the number of voids in the design grew, there was increased difficulty in ensuring that all constraints were met and inhibited the utilization of direct constrained optimization or optimization methods with penalty functions. While this is addressed in this chapter with a sampling of a full design space and then culling of infeasible solutions, a more streamlined method to handle constraints would be desired.

This work also suggests the utility of spatial distribution analyses to forecast the benefit of customization – the wider the distribution of the demand, the more likely the utility of deviating from a one-size-fits-all solution. However, customization can only be realized with integrated

design and manufacturing methods that more precisely align with the opportunity for material reduction. In other words, we need to develop manufacturing methods that can target the strongest design and geometric levers for structural performance. In the case of the work presented in this chapter, void size only was target for custom sizing because of manufacturing ease concerns, but custom sizing of the voids did not make up for efficiency lost with the depth restriction enforced.

5.5 Conclusions

5.5.1 Future work and remarks

Future work in the parametric customization of waffle slabs can take two main paths: improvement of the design methods and parameterization, and well as improvement on the fabrication process. With respect to the former, this method could be adapted to allow for shaping along the bottom exterior of the slab, thereby adjusting the structural depth of the section in addition to the interior dimensions of the waffle void. Of course, this would necessitate serious thought on a non-carbon intensive way to accomplish these topographically varied slabs. Additional studies could also allow for differences in steel rebar in a spanning t-beam to take greater advantage of the capacity from the concrete matrix. In the sections with little to no utilization this is almost always a result of a lower sectional demand, and more steel needed than is necessary. As steel's embodied carbon coefficient is an order of magnitude larger than concrete, these volume reductions, while seemingly small could help push the limits of the embodied carbon reductions we can achieve with these systems.

With respect to the design of the shell formwork in particular, more exploration is needed to design self-supporting printable formwork that can more closely match the shape of the designed voids. The other path way could be parameterizing the waffle directly with the vault shape, instead of the box, and seeing if that has a larger impact on embodied carbon and mass savings. In addition, these test studies were printed with a cement-based mortar, but in the future, it would be desirable to use earth/mud-based material as it is locally available in many contexts and has a significantly lower carbon impact.

More broadly, this work highlights the importance of rigorous assessment of embodied carbon and performance impacts at multiple stages of the design and construction process of structural elements. This is especially true with the emergences of novel fabrication methods and construction strategies. It may be counterproductive for something to have a display of structural logic without realizing true efficiency. The quantification of performance will continue to ensure that solutions proposed by structural engineers and designers are not needlessly complex without improving carbon outcomes.

5.5.2 Summary of intellectual contributions

This chapter presents a hybrid method for the parametric customization of waffle and filler slab systems. This approach allows a structural designer to introduce complexity into a difficult optimization task with more control and eliminates some of the assumptions of evenly

distributed demand and similar structural behavior along the length of a T-section that end up expressed geometrically in the final design. Furthermore, this chapter utilizes a real-world case study to contrast the benefits of a waffle slab with voids customized in size to meet demand to one with optimal standard void sizing, and finds modest carbon savings between the two solutions. This shows that structurally logical expression of waffle and filler slab systems can be achieved if desired, but may not be as beneficial when considering the additional complexity that could introduce into fabrication. Furthermore, the design constraint held in this chapter of maintaining a uniform overall structural depth limits the utilization of the slab to a degree that cannot be fully overcome with interior void sizing. Lastly, this chapter shares promising design work done in collaboration with Alexander Curth (MIT) and Twente manufacturing in hopes of enabling additive manufacturing in spanning systems, that also accommodate, code-accepted design practices and conventional construction methods.

6. Conclusions

6.1 Summary of contributions

This dissertation leverages data-driven design methods and shape optimization workflows to provide generalizable and immediately actionable knowledge to increase the carbon efficiency of two-way spanning systems. It highlights the potential computation has to augment current structural design processes without compromising building code requirements, or rigorous structural analysis.

6.1.1 Parametric design and closed form analysis methods of traditional structures reveal new opportunities for efficiency in the early design stage

In Chapter 3, this dissertation demonstrates the utility of parametric design workflows in locating feasible solutions obtained with traditional code-based rule of thumb methods. This is shown across a comprehensive set of spans, load conditions and typology variations, and is accomplished on the length scale of minutes using building code-accepted closed form structural and serviceability analysis vs. temporarily expensive FEA analysis, making this method valuable in early design stage. Perhaps more importantly, this dissertation asks structural engineers to not consider a traditional system a “solved problem” and to rethink what typologies are considered as the obvious solution for a given set of conditions. In fact, this dissertation makes the case throughout that waffle slabs have immense potential at shorter spans, beyond what current rules of thumb dictate. Existing methods for concrete structural design and the resulting rules to ease

difficulty of nonlinear analysis were not created with consideration of the climate crisis and cannot adequately serve modern climate conscious design goals during an intense need for construction.

6.1.2 Filler slabs are a promising solution that now have a computational framework for integrated building energy needs

In addition, this dissertation investigates the potential of filler slabs to be viable solutions in contexts outside of India, and to serve as integrated structural solutions with the incorporation of optimally-sized, insulating lost formwork. This chapter evaluates traditional filler materials as well as emerging agricultural alternatives for insulation that could be manufactured into blocks as filler. Filler slabs, which are structurally equivalent to waffle slabs, have seen huge acceptance in India and have been studied in research most commonly as individual case and field studies. While previous research has reported cost savings of this system and carbon usage for these individual examples, this work makes strides to formalize design methods for filler slabs and quantify the embodied energy and thermal performance of these systems prior to construction, across a variety of spans and material combinations.

Chapter 4 includes several methodological contributions, including a filler material evaluation that can be used to simplify the multi-objective function formulation of minimizing thermal transmittance and embodied energy into a single-objective. While this work looks at materials locally available in India, the analysis required for the filler material evaluation can be adopted for regionally available materials in other contexts. In addition, this chapter extends previous work in optimally shaping apertures in surface structure to allow for the custom sizing of filler slabs voids without an explosion in problem dimensionality.

With respect to typology specific design knowledge, the dissertation shows that the optimal solutions for filler slabs for embodied energy and thermal transmittance reduction do not simply use formwork that removes material up to the neutral axis of an equivalent depth flat slab, but increases the structural depth of the slab as a whole. This is a key revelation not previously reported in research literature of these systems.

6.1.3 Parametric customization of waffle slabs can be achieved but manufacturing tradeoffs limit full carbon savings potential

This dissertation also proposes a hybrid FEA and closed form method to design waffle slabs customized to their varied structural demand. This allows for the incorporation of structural logic in the design of these elements, but also the quantification of the true benefit that customization could provide from an embodied carbon perspective. Chapter 5 ultimately reveals that while there are some scenarios in which a size distribution of filler slabs can be found to outperform a filler slab with voids of the same size, the savings are minimal and may not be worth the added manufacturing complexity. The key variable of structural depth is held constant easing manufacturing of a custom system, but limiting savings. The chapter also shares results from work done in collaboration with Alexander Curth (MIT) and Twente Manufacturing to fabricate custom formwork for these spatially varied void sizes, while still early, the printing of formwork, particularly formwork that references traditional filler formwork geometries of clay pots etc.,

bridges the gap between the use of additive manufacturing for spanning systems, and accommodating conventional concrete molding and reinforcing methods.

6.2 Potential applications and broader impact

The work in this dissertation begins with the broad parametric exploration of the traditional and widely adapted structural typology of the flat slab and the highly efficient, but less utilized waffle slabs system. It highlights the value of a typology switch for carbon efficiency goals and makes the case for the adoption of filler slabs systems, which follow the same structural behavior as waffle slabs but have the potential to address building energy needs in an integrated manner.

6.2.1 In research

The root of this dissertation work is the assembly and application of a variety of data-driven design methods to locate and suggest feasible, efficient, two-way spanning concrete systems. Each chapter not only highlights the utility of the methods, but presents comprehensive results that can serve as benchmarks for future researchers in this field. In particular, Chapter 5 shows the importance of quantification of design performance in conjunction with novel fabrication methods in order to balance desires for aesthetic pursuits with unintentional sacrifices of carbon efficiency performance.

This dissertation also features the first comprehensive multi-objective study of the design of filler slab systems that prioritizes quantifiable thermal performance and embodied energy of the system. The methods for evaluation of filler materials, and structural design of the concrete filler slabs build upon well-accepted and wide-spread material science and structural behavioral analysis that can be leveraged for future work with additional secondary performance objectives that have been reported for the filler slab system but have limited quantification in academic literature such as sound transmittance.

6.2.2 In practice

With a world that is rightfully increasingly worried about the carbon bottom-line in addition to cost, this work provides evidence for the reconsideration of waffle and ribbed slab typologies in a variety of different building programs. Not only would the use of these systems help us reach ambitious carbon targets today, this work introduces two methods—filler slabs with agricultural formwork, 3d printed shell formwork—that can be used to achieve waffle and filler slabs without proprietary formwork, which is a key cost factor limiting the adoption of these systems. Furthermore, this work shows that the greatest savings can be found when geometrically customized for a given span and loading, versus with a preselected catalogued size from formwork manufacturers.

The change to the more efficient typologies in this work is immediately actionable because they are rooted in the American Concrete Institute building code, the standard that has been exported as an analysis knowledge base to many other international building standards. The findings in this dissertation could be used directly as starting points for detailed design and analysis of two-

way concrete systems, or these methods can be coupled with larger building models to investigate downstream impacts and savings on the lateral systems and foundations. Finally, with respect to the broader conclusions that can be drawn from the filler slabs design results, this work encourages the coupling of computational design with vernacular architectural techniques that have proven to be incredibly efficient across multiple metrics of importance. These techniques can be key to achieving high levels of carbon reduction for concrete construction in regions with material cost constraints.

6.3 Remaining questions and future research directions

Remaining questions and future directions for this work can be grouped into expansion of the design methodologies and accessing the necessary economic and manufacturing information to bridge the gap between the desire to deploy waffle and filler slabs more widely, and the context-informed reality

6.3.1 Accommodation of organic and non-orthogonal ribbing and framing

One limitation of this work is that it focusses only on orthogonal ribbing-based load transfer. However, some of the most widely acclaimed structural solutions that feature the use of multidirectional ribbing (e.g. from Nervi) do not adhere to this layout constraint. The next step in this work would be coupling the rigorous concrete structural behavioral methods in this work with more diverse framing layouts in plan. This would allow for the benchmarking and design of more novel statically indeterminate concrete spanning systems.

6.3.2 Economic analysis for implementation of waffle and filler slabs

More location specific information on labor and manufacturing cost for the novel formwork systems proposed would be valuable, especially at scale. For example, for a variety of mold-based fabrication processes, the initial capital investment must be offset by the number of uses. It would be interesting to use a quantitative, rate, quality, cost, flexibility, and sustainability (RQCF + S) framework to evaluate not just the two fabrication methods proposed in this dissertation, but other processes that could be used to achieve a waffle geometry. Essentially, the future work from this dissertation must balance the development of fabrication technologies that allow for a wide spectrum of geometric expression and structural utilization and the impact of these methods.

6.3.3 Repurposing of agricultural waste streams

The use of agricultural waste as formwork, would require another layer of analysis to ensure that again the opportunity that could be provided for low-carbon construction is coupled closely with the location of implementation. For example, when we consider the burning of agricultural byproducts instead of the use of these materials as insulation or with any circular capacity, we know that the biggest culprits are (in order) China, India and the United States. A large portion of that crop is also maize, wheat and rice paddy (Cassou, 2018). Future work could continue examining infrastructure and attitude and acceptance of agricultural formwork in India where

filler slabs are mostly deployed, or could focus on one of these other countries for knowledge transfer.

6.4 Concluding remarks and outlook

The integration of structural performance evaluation that allows for rapid feedback and wide search of the design space is key to designing efficient concrete systems for the future. It is important to understand how concrete can better be utilized as it is a material of choice in so many parts of the world, representing strength and stability in public infrastructure and private residence. Furthermore, there is a missed opportunity for carbon savings in the western world because of the construction economics as well as design simplicity that favor systems where added material is traded for reduced complexity. This dissertation provides several methods to address this issue both from the design side and the manufacturing side, promoting broader use of lost formwork technology which has the potential to impact the labor part of the construction equation.

Ultimately one typology or one method is not enough to address every construction need, but this dissertation emphasizes a context-informed approach that requires consideration of materials used in fabrication, as well as how specific design desires may be limited by reasonable construction constraints. It optimistically proposes computational methods that if implemented by structural engineers in practice can ease the temporal challenge, and analytical burden in the early design stage, which is where the largest difference can be achieved in building embodied energy and carbon performance. Finally, and more broadly, this work challenges structural engineers and designers to inject rigor in their search for structural solutions: the benefits are significant, and just may make the difference in guaranteeing a zero-carbon world for future generations.

References

- Acharya, R. R., Kishore, P., Raghuprem, M., Kini, P., Shetty, S., & Raj, A. (2020). Optimization based feasibility study for filler slabs as a response towards the ECBC roof compliance with respect to thermal transmittance for five climatic zones of India. *Procedia Manufacturing*, 44(2019), 213–220. <https://doi.org/10.1016/j.promfg.2020.02.224>
- ACI Committee 318, ACI Committee 318, ACI Committee 318, & American Concrete Institute. (2016). *Building code requirements for structural concrete (ACI 318-14): An ACI standard ; Commentary on building code requirements for structural concrete (ACI 318R-14) : an ACI report.*
- Al-Homoud, M. S. (2005). Performance characteristics and practical applications of common building thermal insulation materials. *Building and Environment*, 40(3), 353–366. <https://doi.org/10.1016/j.buildenv.2004.05.013>

- Allen, E., & Iano, J. (2004). *Fundamentals of Building Construction: Materials and Methods* (4th ed.). John Wiley & Sons, Inc.
- Allen, E., & Iano, J. (2011). *The Architect's Studio Companion: Rules of Thumb for Preliminary Design* (5th ed.). John Wiley & Sons, Inc.
- Anderson, J., & Moncaster, A. (2020). Embodied carbon of concrete in buildings, Part 1: Analysis of published EPD. *Buildings and Cities*, 1(1), 198–217.
<https://doi.org/10.5334/bc.59>
- Antonsson, E. K., & Cagan, J. (Eds.). (2001). Introduction. In *Formal engineering Design Synthesis* (1st ed.). Cambridge University Press.
- ASCE. (2017). *Minimum Design Loads and Associated Criteria for Buildings and Other Structures*. American Society of Civil Engineers. <https://doi.org/10.1061/9780784414248>
- Ashby, M., Cebon, D., & Ashby, M. F. (1993). Materials selection in mechanical design. *Journal de Physique IV Colloque*, 111(C7), 3.
- Asim, M., Uddin, G., Jamshaid, H., & Raza, A. (2020). Comparative experimental investigation of natural fibers reinforced light weight concrete as thermally efficient building materials Muhammad. *Journal of Building Engineering*, 31, 195–225.
<https://doi.org/10.1080/10643389.2012.728825>
- Bataille, C. (2020). Low and zero emissions in the steel and cement industries: Barriers, technologies and policies. *OECD Green Growth Papers*.
<https://doi.org/10.1787/5ccf8e33-en>
- Beard, A., Rawlinson, S., & Krzyzaniak, A. (2022). *The Arcadis International Construction Costs Index 2022*. Arcadis.

- Besjak, C., Biswas, P., Thewis, A., Sweeney, R., & Chaudhuri, D. (2013). Chhatrapati Shivaji International Airport—Integrated Terminal Building. *Structural Engineering International*, 23(1), 8–13. <https://doi.org/10.2749/101686613X13363929988296>
- Billington, D. P. (1985). *The tower and the bridge*. Princeton University Press.
- Bischoff, P. H., & Gross, S. P. (2011). Equivalent moment of inertia based on integration of curvature. *Journal of Composites for Construction*, 15(3), 263–273. [https://doi.org/10.1061/\(ASCE\)CC.1943-5614.0000164](https://doi.org/10.1061/(ASCE)CC.1943-5614.0000164)
- Block, P., & Ochsendorf, J. (2007). THRUST NETWORK ANALYSIS: A NEW METHODOLOGY FOR THREE-DIMENSIONAL EQUILIBRIUM. *JOURNAL OF THE INTERNATIONAL ASSOCIATION FOR SHELL AND SPATIAL STRUCTURES*, 48(3), 8.
- Block, P., Rippmann, M., & Van Mele, T. (2017). Compressive Assemblies: Bottom-Up Performance for a New Form of Construction. *Architectural Design*, 87(4), 104–109. <https://doi.org/10.1002/ad.2202>
- Bowles, W., Cheslak, K., & Edelson, J. (2022). *Lifecycle GHG Impacts in Building Codes*. New Buildings Institute.
- Branson, D. E. (1977). *Deformation of concrete structures* /. New York ; <http://hdl.handle.net/2027/uc1.b4143901>
- Brown, N. C., Jusiega, V., & Mueller, C. T. (2020). Implementing data-driven parametric building design with a flexible toolbox. *Automation in Construction*, 118(October 2020), 2020–2021. <https://doi.org/10.1016/j.autcon.2020.103252>

- Brown, N. C., & Mueller, C. T. (2016). Design for structural and energy performance of long span buildings using geometric multi-objective optimization. *Energy and Buildings*, *127*, 748–761. <https://doi.org/10.1016/j.enbuild.2016.05.090>
- Broyles, J. M., Hartwell, A. J., Alvarez, E. G., Ismail, M. A., Norford, L. K., Mueller, C. T., & Brown, N. C. (2022, July). Shape optimization of concrete floor systems for sustainability, acoustical, and thermal objectives. *ICSA 2022 Proceedings*. International Conference on Structures and Architecture, Aalborg, Denmark.
- Bureau of Indian Standards. (2000). *IS 456: Plain and Reinforced Concrete—Code of Practice*.
- Caetano, I., & Leitão, A. (2020). Architecture meets computation: An overview of the evolution of computational design approaches in architecture. *Architectural Science Review*, *63*(2), 165–174. <https://doi.org/10.1080/00038628.2019.1680524>
- Calvo-Salve, M. Á. (2018). Influences of the engineer Pier Luigi Nervi on the work of the architect Marcel Breuer. In I. Wouters, S. Van De Voorde, I. Bertels, B. Espion, K. De Jonge, & D. Zastavni (Eds.), *Building Knowledge, Constructing Histories* (1st ed., pp. 417–424). CRC Press. <https://doi.org/10.1201/9780429506208-56>
- Cascone, S., Rapisarda, R., & Cascone, D. (2019). Physical properties of straw bales as a construction material: A review. *Sustainability (Switzerland)*, *11*(12). <https://doi.org/10.3390/SU11123388>
- Chilton, J., & Chuang, C.-C. (2017). Rooted in Nature: Aesthetics, Geometry and Structure in the Shells of Heinz Isler. *Nexus Network Journal*, *19*(3), 763–785. <https://doi.org/10.1007/s00004-017-0357-5>
- Ching, F. D. K., Onouye, B. S., & Zuberbuhler, D. (2014). *Building Structures Illustrated: Patterns Systems and Design* (2nd ed.). John Wiley & Sons, Inc.

- Chougule, A., Mota, M., & Patil, U. (2015). *To Study the Filler Slab As Alternative Construction Technology-a Review*. *14*(2), 975–6744.
- Chudoba, R., van der Woerd, J., Schmerl, M., & Hegger, J. (2014). ORICRETE: Modeling support for design and manufacturing of folded concrete structures. *Advances in Engineering Software*, *72*, 119–127. <https://doi.org/10.1016/j.advengsoft.2013.05.004>
- Crow, J. (2008). The concrete conundrum. *Chemistry World*.
<https://www.chemistryworld.com/features/the-concrete-conundrum/3004823.article>
- Curth, A., Brodesser, T., Sass, L., & Mueller, C. (2021). *Multi-objective optimization of 3D printed shell toolpaths*.
- Curth, A., Hartwell, A., Brodesser, T., & Mueller, C. (2022). *Parametric waffle slabs: Optimal geometry materialized with additive construction*. 12.
- Danhaive, R. (2020). *Structural Design Synthesis Using Machine Learning*. 219.
- Danhaive, R., & Mueller, C. T. (2021). Design subspace learning: Structural design space exploration using performance-conditioned generative modeling. *Automation in Construction*, *127*(November 2020), 103664.
<https://doi.org/10.1016/j.autcon.2021.103664>
- Darwin, D., Dolan, C. W., & Nilson, A. H. (2010). *Design of concrete structures* (14th ed). McGraw-Hill Higher Education.
- Davis, D. (2013). *Modelled on Software Engineering: Flexible Parametric Models in the Practice of Architecture*. Royal Melbourne Institute of Technology.
- De Wolf, C., Hoxha, E., Hollberg, A., Fivet, C., & Ochsendorf, J. (2020). Database of Embodied Quantity Outputs: Lowering Material Impacts Through Engineering. *Journal of Architectural Engineering*, *26*(3), 04020016. <https://doi.org/10/gg55mc>

- De Wolf, C., Yang, F., Cox, D., Charlson, A., Hattan, A. S., & Ochsendorf, J. (2015). Material quantities and embodied carbon dioxide in structures. *Proceedings of the Institution of Civil Engineers - Engineering Sustainability*. <https://doi.org/10/gg55mf>
- Deshmukh, R., & More, A. (2014). Low energy green materials by embodied energy analysis. *International Journal of Civil and Structural Engineering Research*, 2(1), 58–65.
- Dias, W. P. S., & Pooliyadda, S. P. (2004). Quality based energy contents and carbon coefficients for building materials: A systems approach. *Energy*, 29(4), 561–580. <https://doi.org/10.1016/j.energy.2003.10.001>
- Digital Structures, New Story, & Echale. (2022). *Sueños con Fibra/Madera, Tierra/Concreto*. <https://suenos.mit.edu/Dreams-of-concrete>
- Doheny, M. (Ed.). (2022). *Building Construction Costs with RSMeans Data* (80th ed.). Gordian.
- Dolan, C. W., & Nilson, A. H. (2016). *Design of concrete structures*. McGraw Hill. <https://doi.org/10.1201/9781315368221-12>
- Dowrick, D. (1967). Folded Plate Roofs. *The ARUP Journal*, 1(1).
- Eastman, C. (1975). The Use of Computers Instead of Drawings in Building Design. *AIA Journal*, 63(3), 46–50.
- Energy Conservation Building Code*. (2017).
- Fang, D., Brown, N. C., De Wolf, C., & Mueller, C. T. (2023). Strategies for reducing embodied carbon in early-stage structural design: a review. *In Preparation*.
- Fears, R. (2016, September 30). *Bale sizes and shapes—Picking what's right for you*. AG Proud - Progressive Forage. <https://www.agproud.com/articles/32770-bale-sizes-and-shapes-picking-what-s-right-for->

- Gauch, H. L., Hawkins, W., Ibell, T., Allwood, J. M., & Dunant, C. F. (2022). Carbon vs. cost option mapping: A tool for improving early-stage design decisions. *Automation in Construction*, 136, 104178. <https://doi.org/10.1016/j.autcon.2022.104178>
- Gavali, H. R., & Ralegaonkar, R. V. (2019). Design feasibility of load-bearing masonry building for energy-efficient construction. *Proceedings of Institution of Civil Engineers: Energy*, 172(1), 19–25. <https://doi.org/10.1680/jener.18.00013>
- Haftka, R. T., & Grandhi, R. V. (1986). Structural shape optimization—A survey. *Computer Methods in Applied Mechanics and Engineering*, 57(1), 91–106. <https://doi.org/10/bwmn2x>
- Halpern, A. B., Billington, D. P., & Adriaenssens, S. (2013, September). The Ribbed Floor Slab Systems of Pier Luigi Nervi. *Proceedings of IASS Annual Symposia*. International Association for Shell and Spatial Structures (IASS), Wroclaw, Poland.
- Hammond, G. P., & Jones, C. I. (2008). Embodied energy and carbon in construction materials. *Proceedings of the Institution of Civil Engineers - Energy*, 161(2), 87–98. <https://doi.org/10/dj6vsn>
- Hartwell, A. J., & Mueller, C. T. (2021, August). Design optimization of two-way filler slabs: Lightweight concrete floor systems for affordable urban construction. *Proceedings of the IASS Annual Symposium 2020-21 and the 7th International Conference on Spatial Structures*. Proceedings of the IASS Annual Symposium 2020-21 and the 7th International Conference on Spatial Structures, Guilford, UK.
- Hartwell, A., Whalen, E., Ong, B. W. X., & Mueller, C. T. (2023). Visualization of Design Data in the Wild: Interactive Evaluation and Exploration of Combined Performance and

- Geometric Data. In J. S. Gero (Ed.), *Design Computing and Cognition '22*. Springer International Publishing. <https://doi.org/10.1007/978-3-031-20418-0>
- Hawkins, W., Orr, J., Ibell, T., & Shepherd, P. (2020). A design methodology to reduce the embodied carbon of concrete buildings using thin-shell floors. *Engineering Structures*, 207, N.PAG-N.PAG. a9h.
- Herr, C. M. (2019). *The art of collaborative structural design: Structural art in the age of cross-disciplinary collaboration*.
- Hu, M. (2020). A Building Life-Cycle Embodied Performance Index—The Relationship between Embodied Energy, Embodied Carbon and Environmental Impact. *Energies (19961073)*, 13(8), 1905. a9h.
- Hu, N., & Dai, G. (2010, July 2). Structures & Architecture: ICSA 2010 - 1st International Conference on Structures & Architecture, July 21-23 July, 2010 in Guimaraes, Portugal. *Structures and Architecture*. 1st International Conference on Structures & Architecture, ICSA. <https://doi.org/10.1201/b10428>
- Huberman, N., Pearlmutter, D., Gal, E., & Meir, I. A. (2015). Optimizing structural roof form for life-cycle energy efficiency. *Energy and Buildings*, 104, 336–349. <https://doi.org/10.1016/j.enbuild.2015.07.008>
- Iffat, S. (2015). *Relation Between Density and Compressive Strength of Hardened Concrete*. 6, 8.
- Isler, H. (1994). Concrete Shells Derived from Experimental Shapes. *Structural Engineering International*, 4(3), 142–147. <https://doi.org/10/gg549c>

- Ismail, M. (2018). *Computational Structural Design and Fabrication of Hollow-Core Concrete*
Computational Structural Design and Fabrication of Hollow-Core Concrete Beams. July,
0–8.
- Ismail, M. (2019). Materially Efficient Structural Floor Systems for Housing in India_Thesis.
Thesis, 1–139.
- Ismail, M. A. (2023). *Reshaping concrete: Empowering development through low-carbon
structural design*. MIT.
- Ismail, M. A., & Mueller, C. T. (2019). Engineering a New Nation: Mahendra Raj and His
Collaborations Across Disciplines. *107th ACSA Annual Meeting Proceedings, Black Box*,
562–566. <https://doi.org/10.35483/ACSA.AM.107.111>
- Ismail, M. A., & Mueller, C. T. (2021). Minimizing embodied energy of reinforced concrete
floor systems in developing countries through shape optimization. *Engineering
Structures*, 246, N.PAG-N.PAG. a9h.
- Ismail, M. A., & Mueller, C. T. (2022, April 14). Outrage: Colonial legacies of concrete—
Architectural Review. *The Architectural Review*, 1490. [https://www.architectural-
review.com/essays/outrage/outrage-colonial-legacies-of-concrete](https://www.architectural-review.com/essays/outrage/outrage-colonial-legacies-of-concrete)
- Jayasinghe, A., Orr, J., Ibell, T., & Boshoff, W. P. (2022). Minimising embodied carbon in
reinforced concrete flat slabs through parametric design. *Journal of Building
Engineering*, 50, 104136. <https://doi.org/10.1016/j.jobe.2022.104136>
- Jewett, J. (2018). *Design, Fabrication, and Testing of Plain Concrete Beams Using Topology
Optimization*.

- Jipa, A., Bernhard, M., Meibodi, M. A., & Dillenburger, B. (2016). *3D-Printed Stay-in-Place Formwork for Topologically Optimized Concrete Slabs*. <https://doi.org/10.3929/ETHZ-B-000237082>
- Jones, C., & Hammond, G. (2019). *Inventory of Carbon & Energy v3.0*.
<https://www.circularecology.com/embodied-energy-and-carbon-footprint-database.html>
- Karlsson, I., Rootzén, J., Toktarova, A., Odenberger, M., Johnsson, F., & Göransson, L. (2020). Roadmap for Decarbonization of the Building and Construction Industry—A Supply Chain Analysis Including Primary Production of Steel and Cement. *Energies*, *13*(16), 4136. <https://doi.org/10.3390/en13164136>
- Kilian, A., & Ochsendorf, J. (2005). PARTICLE-SPRING SYSTEMS FOR STRUCTURAL FORM FINDING. *JOURNAL OF THE INTERNATIONAL ASSOCIATION FOR SHELL AND SPATIAL STRUCTURES*, *46*(147), 8.
- Kocaturk, T. (2017). Towards an Intelligent Digital Ecosystem—Sustainable Data-driven Design Futures. In P. S. Brandon, P. Lombardi, & G. Q. Shen (Eds.), *Future Challenges in Evaluating and Managing Sustainable Development in the Built Environment* (pp. 164–178). John Wiley & Sons, Ltd. <https://doi.org/10.1002/9781119190691.ch10>
- Lack, A., & Korynta, J. (2020). Changes in the structure of historical consciousness and the perception of architectural style: A case study in the popular perception of Brutalism from 1945 to 2019. *Świat i Słowo*, *34*(1), 179–210.
<https://doi.org/10.5604/01.3001.0014.3074>
- Lebé, A. (2015). From Folds to Structures, a Review. *International Journal of Space Structures*, *30*(2), 55–74. <https://doi.org/10.1260/0266-3511.30.2.55>

- Lee, K. J., & Mueller, C. T. (2023). Geometric analysis of building load demands and structural element capacities. (*In Preparation*).
- Leslie, T. (2017). *Beauty's rigor: Patterns of production in the work of Pier Luigi Nervi*. University of Illinois Press.
- Madurwar, M. V., Mandavgane, S. A., & Ralegaonkar, R. V. (2015). Development and Feasibility Analysis of Bagasse Ash Bricks. *Journal of Energy Engineering*, 141(3), 04014022. [https://doi.org/10.1061/\(asce\)ey.1943-7897.0000200](https://doi.org/10.1061/(asce)ey.1943-7897.0000200)
- Mahananda, R. K., Mendi, V., & Raveesh, R. M. (2020). Design and Analysis of Filler Slab. *IOP Conference Series: Materials Science and Engineering*, 1006(1), 012001. <https://doi.org/10.1088/1757-899X/1006/1/012001>
- Malabi Eberhardt, L. C., van Stijn, A., Kristensen Stranddorf, L., Birkved, M., & Birgisdottir, H. (2021). Environmental Design Guidelines for Circular Building Components: The Case of the Circular Building Structure. *Sustainability*, 13(10), 5621. <https://doi.org/10.3390/su13105621>
- Marks, W. (1997). Multicriteria optimisation of shape of energy-saving buildings. *Building and Environment*, 32(4), 331–339. [https://doi.org/10.1016/S0360-1323\(96\)00065-0](https://doi.org/10.1016/S0360-1323(96)00065-0)
- Mastrucci, A., & Rao, N. D. (2019). Bridging India's housing gap: Lowering costs and CO2 emissions. *Building Research and Information*, 47(1), 8–23. Scopus. <https://doi.org/10.1080/09613218.2018.1483634>
- Mata-Falcón, J., Bischof, P., Huber, T., Anton, A., Burger, J., Ranaudo, F., Jipa, A., Gebhard, L., Reiter, L., Lloret, E., Mele, T., Block, P., Gramazio, F., Kohler, M., Dillenburger, B., Wangler, T., & Kaufmann, W. (2022). *Digitally fabricated ribbed concrete floor slabs: A*

sustainable solution for construction. 7, 68–78.

<https://doi.org/10.21809/rilemtechlett.2022.161>

Mayencourt, P., & Mueller, C. (2020). Hybrid analytical and computational optimization methodology for structural shaping: Material-efficient mass timber beams. *Engineering Structures*, 215, 110532. <https://doi.org/10/ghk58q>

McKinsey & Company. (2020). *The next normal in construction: How disruption is reshaping the world's largest ecosystem*.

Millward-Hopkins, J., Zwirner, O., Purnell, P., Velis, C. A., Iacovidou, E., & Brown, A. (2018). Resource recovery and low carbon transitions: The hidden impacts of substituting cement with imported 'waste' materials from coal and steel production. *Global Environmental Change*, 53, 146–156. <https://doi.org/10.1016/j.gloenvcha.2018.09.003>

Mitchell, W. J. (2001). Vitruvius Redux: Formalized Design Synthesis in Architecture. In E. K. Antonsson & J. Cagan (Eds.), *Formal Engineering Design Synthesis* (1st ed., pp. 1–19). Cambridge University Press. <https://doi.org/10.1017/CBO9780511529627.004>

Mould, O. (2017). Brutalism Redux: Relational Monumentality and the Urban Politics of Brutalist Architecture: Brutalism Redux. *Antipode*, 49(3), 701–720. <https://doi.org/10.1111/anti.12306>

Mueller, C. (2017). Distributed Structures: Digital Tools for Collective Design. *Architectural Design*, 87(4), 94–103. <https://doi.org/10/gctq93>

Mueller, C. T. (2014). *Computational exploration of the structural design space* [Thesis, Massachusetts Institute of Technology]. <https://dspace.mit.edu/handle/1721.1/91293>

- Mueller, C. T., & Ochsendorf, J. A. (2015). Combining structural performance and designer preferences in evolutionary design space exploration. *Automation in Construction*, 52, 70–82. <https://doi.org/10.1016/j.autcon.2015.02.011>
- Nilson, A., & Walters, D. (1975). Deflection of Two-Way Floor Systems by the Equivalent Frame Method. *Journal Proceedings*, 72(5), 210–218.
- Olawale, S., Akintunde, O., Afolabi, M., & Tijani, M. (2020). Design Optimization of Reinforced Concrete Waffle Slab Using Genetic Algorithm. *Journal of Soft Computing in Civil Engineering*, 4(2). <https://doi.org/10.22115/scce.2020.224460.1195>
- Ong, B. W. X., Danhaive, R., & Mueller, C. (2021). Machine learning for human design: Sketch interface for structural morphology ideation using neural networks. *Proceedings of the International Association for Shell and Spatial Structures (IASS) Symposium*, 13.
- Orr, J. J., Darby, A. P., Ibell, T. J., Evernden, M. C., & Otlet, M. (2011). *Concrete structures using fabric formwork*. <https://doi.org/10/gg55d5>
- Panyakaew, S., & Fotios, S. (2008). Agricultural waste materials as thermal insulation for dwellings in Thailand: Preliminary results. *PLEA 2008 - Towards Zero Energy Building: 25th PLEA International Conference on Passive and Low Energy Architecture, Conference Proceedings, October*.
- Panyakaew, S., & Fotios, S. (2011). New thermal insulation boards made from coconut husk and bagasse. *Energy and Buildings*, 43(7), 1732–1739. <https://doi.org/10.1016/j.enbuild.2011.03.015>
- Paolini, A., Kollmannsberger, S., & Rank, E. (2019). Additive manufacturing in construction: A review on processes, applications, and digital planning methods. *Additive Manufacturing*, 30, 100894. <https://doi.org/10.1016/j.addma.2019.100894>

- Pareto, V. (2007). *Considerations on the Fundamental Principles of Pure Political Economy* (F. Mornati & R. Marchionatti, Eds.). Taylor & Francis.
- Petrova, E., Pauwels, P., Svidt, K., & Jensen, R. L. (2019). In Search of Sustainable Design Patterns: Combining Data Mining and Semantic Data Modelling on Disparate Building Data. In I. Mutis & T. Hartmann (Eds.), *Advances in Informatics and Computing in Civil and Construction Engineering* (pp. 19–26). Springer International Publishing.
https://doi.org/10.1007/978-3-030-00220-6_3
- Popescu, M., Reiter, L., Liew, A., Van Mele, T., Flatt, R. J., & Block, P. (2018). Building in Concrete with an Ultra-lightweight Knitted Stay-in-place Formwork: Prototype of a Concrete Shell Bridge. *Structures*, *14*, 322–332. <https://doi.org/10/gg55b6>
- Portland Cement Association. (2018). *Two-Way Joist Concrete Slab Floor (Waffle Slab) System Analysis and Design*. Portland Cement Association -StructurePoint.
<https://structurepoint.org/pdfs/Two-Way-Joist-Concrete-Waffle-Slab-Floor-Design-Detailing.htm>
- Powell, M. J. D. (1994). A Direct Search Optimization Method That Models the Objective and Constraint Functions by Linear Interpolation. *Advances in Optimization and Numerical Analysis*, *1*, 51–67. https://doi.org/10.1007/978-94-015-8330-5_4
- Presinger, C., & Bollinger+Grohmann. (2018). *Karamba* (1.2.2) [Windows].
<http://www.karamba3d.com/>
- Purnell, P. (2013). The carbon footprint of reinforced concrete. *Advances in Cement Research*, *25*(6), 362–368. <https://doi.org/10.1680/adcr.13.00013>
- Radford, A. D., & Gero, J. S. (1980a). On Optimization in Computer Aided Architectural Design. *Building and Environment*, *15*.

- Radford, A. D., & Gero, J. S. (1980b). *Tradeoff Diagrams for the Integrated Design of the Physical Environment in Buildings*.
- Radford, A. D., Hung, P., & Gero, J. S. (1984). New Rules of Thumb from Computer-Aided Structural Design: Acquiring Knowledge for Expert Systems. *CAD64: 6th International Conference and Exhibition on Computers in Design Engineering*, 558–566.
- Ramage, M. H., Ochsendorf, J. A., & Rich, P. (2010). Sustainable shells: New African vaults built with soil-cement tiles. *Journal of the International Association for Shell and Spatial Structures*, 51(166), 255–261. Scopus.
- Rashidi, M., & Sorooshnia, E. (2020). Heuristic Catenary-based Rule of Thumbs to Find Bending Moment Diagrams. *Civil Engineering and Architecture*, 8(4), 557–570.
<https://doi.org/10.13189/cea.2020.080420>
- Reddy, B. V. V. (2009). Sustainable materials for low carbon buildings. *International Journal of Low Carbon Technologies*, 4(3), 175–181. inh. <https://doi.org/10.1093/ijlct/ctp025>
- Rivera, D. A., Danhaive, R. A., & Mueller, C. T. (2020). Adaptive framework for structural pattern optimization. *Journal of the International Association for Shell and Spatial Structures*, 61(4), 296–306. <https://doi.org/10.20898/J.IASS.2020.012>
- Roudsari, M., Pak, M., & Viola, A. (2013, August 28). *Ladybug: A Parametric Environmental Plugin For Grasshopper To Help Designers Create An Environmentally-conscious Design*. 2017 Building Simulation Conference.
<https://doi.org/10.26868/25222708.2013.2499>
- Ryan, M., Camp, P., & Crismond, D. (2001). *Design Rules of Thumb—Connecting Science and Design*. Meetings of the American Educational Research Association.

- Sahab, M. G., Ashour, A. F., & Toropov, V. V. (2005). Cost optimisation of reinforced concrete flat slab buildings. *Engineering Structures*, 27(3), 313–322.
<https://doi.org/10.1016/j.engstruct.2004.10.002>
- Samuelsson, C., & Vestlund, B. (2015). *Structural Folding: A parametric design method for origami architecture* [Master's thesis]. Chalmers University of Technology.
- Scanlon, A., & Lee, Y. H. (2006). Unified Span-to-Depth Ratio Equation for Nonprestressed Concrete Beams and Slabs. *ACI Structural Journal*, 103(1).
<https://doi.org/10.14359/15095>
- Schek, H.-J. (1974). The force density method for form finding and computation of general networks. *Computer Methods in Applied Mechanics and Engineering*, 3(1), 115–134.
<https://doi.org/10/fd89qp>
- Schmit, L. A. (1960, September). Structural design by systematic synthesis. *Proceedings of the Second National Conference on Electronic Computation*.
- Shayegan, D. S., Lork, A., & Hashemi, S. A. H. (2020). A New Hybrid Algorithm for Cost Optimization of Waffle Slab. *Slovak Journal of Civil Engineering*, 28(3), 40–46.
<https://doi.org/10.2478/sjce-2020-0022>
- Sinha, S., Mishra, S., Kumar, P., & Saurabh, S. (2020). Sustainable Low-Cost Housing using Cost Effective Construction Technology “Rat Trap Bond Masonry” and “Filler Roof Slab” in Bihar. *International Journal of Engineering Research and Technology*, 13(7), 1780. <https://doi.org/10.37624/IJERT/13.7.2020.1780-1785>
- Slee, B., & Hyde, R. (2011). Evaluating ‘Rules of Thumb’ for integrating thermal mass into lightweight construction in Australia. *Principles in Architectural Science: 45th Annual Conference of the Architectural Science Association*, 8.

- Sohn, K., Lee, H., & Yan, X. (2015). *Learning Structured Output Representation using Deep Conditional Generative Models*. *Advances in Neural Information Processing Systems* 28 (NIPS 2015).
- Sputo, T. (2012). *Development of Composite Steel Deck*. 30–31.
- Stadler, W. (1977). Natural Structural Shapes of Shallow Arches. *Journal of Applied Mechanics*, 44(2), 291–298. <https://doi.org/10.1115/1.3424040>
- Stiny, G. (1980). Introduction to shape and shape grammars. *Environment and Planning B: Planning and Design*, 7(3), 343–351.
- Stoiber, N., & Kromoser, B. (2021). Topology optimization in concrete construction: A systematic review on numerical and experimental investigations. *Structural and Multidisciplinary Optimization*, 64(4), 1725–1749. <https://doi.org/10.1007/s00158-021-03019-6>
- Sutherland, I. (1963). Sketchpad: A man-machine graphical communication system. *Proceedings of the Spring Joint Computer Conference*.
- Tewari, S., Prabhakar, N., & Popli, S. (2017). A gandhian framework for social design: The work of laurie baker and hunnarshala. *Smart Innovation, Systems and Technologies*, 66, 337–348. https://doi.org/10.1007/978-981-10-3521-0_29
- The Concrete Center. (2022). *Comparison of embodied carbon in concrete structural systems*. <https://www.concretecentre.com/Resources/Publications/Comparison-of-embodied-carbon-in-concrete-structur.aspx>
- Tippey, B. (2018). Historiographies of Technology and Architecture. In E. M. Dudding, C. McDonald, & J. Merwood-Salisbury (Eds.), *Proceedings of the 35th Annual Conference of the Society of Architectural Historians of Australia and New Zealand: 35*.

- United Nations Environment Programme. (2021). *2021 Global Status Report for Buildings and Construction: Towards a Zero-emission, Efficient and Resilient Buildings and Construction Sector*.
- Veenendaal, D. (2017). *Design and Form Finding of Flexibly Formed Concrete Shell Structures* [Doctoral Thesis, ETH Zurich]. <https://doi.org/10.3929/ethz-a-010831669>
- Venkatarama Reddy, B. V. (2004). Sustainable building technologies. *Current Science*, 87(7), 899–907.
- Vijayalaxmi, J. (2023). *Building Thermal Performance and Sustainability* (Vol. 316). Springer Nature Singapore. <https://doi.org/10.1007/978-981-19-9139-4>
- Wang, F. (2013). The Birth and Use of Concrete and Reinforced Concrete. *Advanced Materials Research*, 712–715, 955–960. <https://doi.org/10.4028/www.scientific.net/AMR.712-715.955>
- Ward House. (2023). American Society of Civil Engineers. <https://www.ascemetsection.org/committees/history-and-heritage/landmarks/ward-house>
- Watts, J. (2019, February 25). Concrete: The most destructive material on Earth. *The Guardian*. <https://www.theguardian.com/cities/2019/feb/25/concrete-the-most-destructive-material-on-earth>
- Wight, A. (2019). *Scientists around the world are working to turn agricultural waste into food, packaging and more*. 1–8.
- Wight, J. (2016). *Reinforced Concrete: Mechanics and Design* (7th ed.). Pearson Education.
- Wilde, R. E. (2004). ACI: A Century of Progress. *Concrete International*, 26(3).

Yeo, D., & Potra, F. A. (2015). Sustainable Design of Reinforced Concrete Structures through CO2 Emission Optimization. *Journal of Structural Engineering*, 141(3), B4014002.
[https://doi.org/10.1061/\(ASCE\)ST.1943-541X.0000888](https://doi.org/10.1061/(ASCE)ST.1943-541X.0000888)